

# Receptor-induced redox relay reactions control cytoskeletal dynamics

Inauguraldissertation

zur

Erlangung des akademischen Grades eines  
Doktors der Naturwissenschaft (Dr. rer. nat)

der

Mathematisch-Naturwissenschaftlichen Fakultät

der

Universität Greifswald

vorgelegt von

Clara Ortegón Salas

aus Jerez de la Frontera, Spanien

Greifswald, 16.06.2021

Dekan: Prof. Dr. Gerald Kerth

1. Gutachter: Prof. Dr. Christiane A. Helm

2. Gutachter: PD Dr. Dr. Christopher Horst Lillig

3. Gutachter: Prof. Dr. Tobias P. Dick

4. Gutachter: Prof. Dr. Jan Riemer

Tag der Promotion: 16.12.2021

To my grandmothers, Pepa and Idaly.





## Table of contents

1	Introduction.....	1
1.1	Redox signaling.....	1
1.2	Peroxiredoxins.....	2
1.3	Thioredoxins.....	5
1.4	Glutaredoxins.....	6
1.5	The Semaphorin signaling pathway.....	8
1.6	MICAL proteins.....	9
1.7	CRMP2 and the cytoskeleton.....	14
1.8	Hypothesis.....	16
2	Conclusions.....	17
2.1	Article 1: Signal-regulated oxidation of proteins via MICAL.....	17
2.2	Article 2: Molecular basis for the interactions of human thioredoxins with their respective reductases.....	17
2.3	Manuscript 3: NADPH-dependent oxidation of CRMP2 through a MICAL1-Prx1 redox relay controls neurite outgrowth.....	18
3	Summary.....	20
4	References.....	22
5	Abbreviations.....	36
6	Author contributions.....	38
7	Publications.....	39
7.1	Publications in peer reviewed journals.....	39
7.2	Submitted manuscripts.....	39
7.3	Publications not included in this thesis.....	39
7.4	Submitted manuscripts not included in this thesis.....	39
7.5	Book chapters.....	39
7.6	Further scientific achievements.....	40
7.6.1	Published abstracts.....	40
7.6.2	Invited talks.....	40
7.6.3	Poster presentations.....	41
	Article 1.....	43
	Article 2.....	52
	Manuscript 3.....	70
8	Declaration of originality.....	97
9	Curriculum vitae.....	98
10	Acknowledgments.....	101

# 1 Introduction

The constant exchange and processing of information of cells with and from their environment results in the orchestration of essential cellular mechanisms such as survival, homeostasis, development, and cell death. This information, in form of extra- or intracellular signals, is received by specific receptors, that in turn become activated, enabling the transduction to the effector molecule(s), which eventually will trigger a precise biological response. One effector molecule is not specific for one signal transduction pathway, in consequence a signaling pathway can branch and communicate with other pathways, resulting in the amplification, interconnection, and modulation of signals and responses. Signal transduction depends not only on transducer proteins, *i.e.* enzymes responsible for the production and/or release of second messenger molecules or the introduction of reversible post-translational modifications in other proteins, but also on reaction kinetics and thus enzymatic activity.

## 1.1 Redox signaling

Redox mediated signal transduction occurs by both oxidation and reduction of key molecules as result of the transfer of electrons. In the past, redox modifications were considered to be simply the result of an imbalance on the ratio of pro- and anti-oxidants within the cell; under so-called 'oxidative stress' conditions, the excess of 'pro-oxidants' would favor the oxidation of different effector molecules, resulting in many different pathologies and disorders (1–5). Over the past decade, however, redox-biochemistry has experienced a significant transformation, as these redox modifications have been increasingly shown to be rapid, reversible, physiological, and highly specific key mechanisms in cell signaling (6–8). Moreover, redox signaling was shown to be compartmentalized, *i.e.* localized to a single compartment or even to different regions within a cell at a given time point, which stands in opposition to the view of the overall cellular redox state as a balance (9,10). The major targets of redox modifications are the side chains of the sulfur containing amino acids, *i.e.* cysteine and methionine (Fig. 1). Cysteinylyl and methionyl residues have been identified in numerous signal transduction pathways, highlighting their importance in complex organisms. The specificity of the redox modifications, as well as the low reactivity of most sulfur containing amino acid side chains with hydrogen peroxide, imply that redox signaling requires catalysis by specific enzymes, just like phosphorylation signaling requires kinases and phosphatases. While reducing enzymes of both cysteinyl- and methionyl-derivates have been characterized in great detail

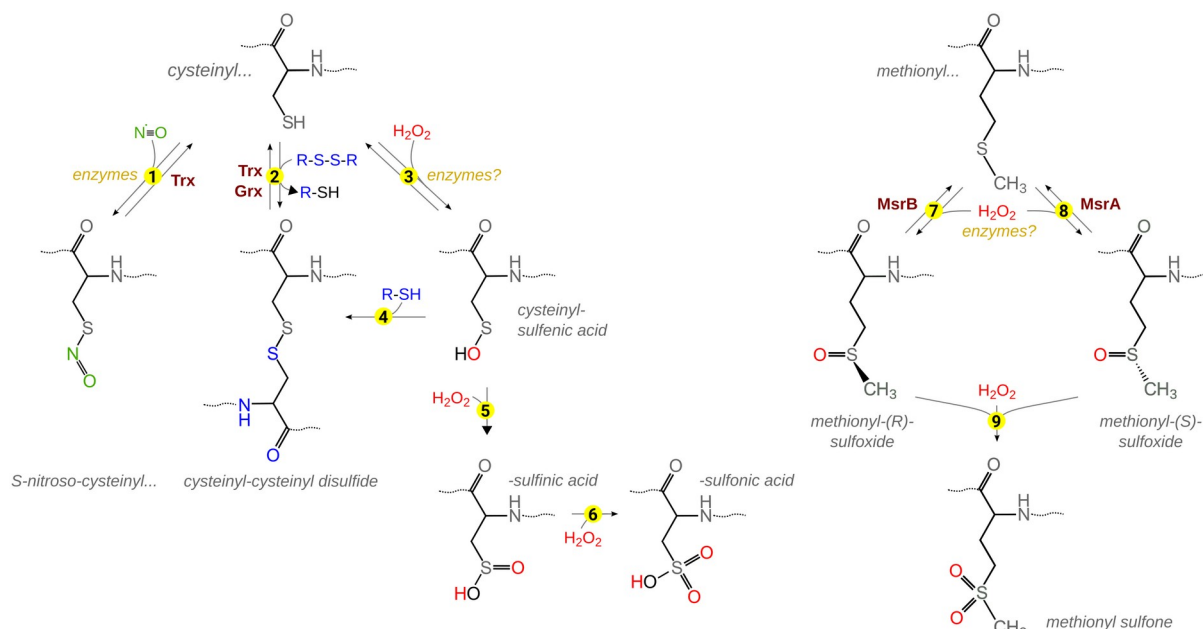


**Figure 1: Redox modifications of cysteinyl and methionyl amino acid side chains.** (1) Nitrosylation of cysteinyl residues requires a catalyst that accepts one electron. De- and trans-nitrosylation are catalyzed by Trxs. (2) Reversible disulfide formation may occur by thiol-disulfide exchange reactions, e.g. with proteins of the Trx family. (3) Reaction with hydrogen peroxide can lead to the formation of sulfenic acids, that can further react to disulfides (4) or, irreversibly, to sulfinic (5) and sulfonic acids (6). Oxidation of methionyl residues, e.g. catalyzed by MICAL enzymes, evinces methionyl-R-sulfoxides that can be reverted by MsrB enzymes (7). Methionyl-S-sulfoxides (8) can be reduced by MsrAs. Methionyl sulfoxides may also be irreversibly oxidized to methionyl sulfone derivatives (9). Adopted from [Article 1](#) (page 43).

before, only little is known about oxidizing enzymes. In this thesis, a new concept of protein oxidation in cell signaling is presented: receptor-induced redox relays.

## 1.2 Peroxiredoxins

Peroxiredoxins (Prxs) belong to the thioredoxin (Trx)-fold family of proteins. Members of this protein family share a common structural motif consisting of three  $\alpha$ -helices surrounding a central core of a four stranded  $\beta$ -sheet (11,12). Among the members of this family of proteins are thioredoxins (Trxs), glutaredoxins (Grxs), and Prxs, on which a major focus of this thesis will lay. Prxs were isolated for the first time from human erythrocytes in 1968 as a result of their high abundance, named as ‘torins’ by then (13); it was more than 25 years later, in 1994, when Rhee *et al.* introduced the term peroxiredoxin (14). Prxs are ubiquitously expressed in all organisms, tissues, cell types, and organelles, and can account for up to 1% of soluble cellular proteins (15,16). Prxs were firstly identified as ‘antioxidant’ due to their enzymatic activity. In contrast to Trxs and Grxs, which are mainly involved in the reduction of protein disulfides, Prxs exhibit peroxidase activity and are therefore able to reduce peroxides

to water in presence of suitable electron donors (17). Despite the difference in the activity and, therefore, in the reaction mechanisms, Prxs, Trxs, and Grxs play a key role as regulators in redox signaling and thus the cellular redox state.

Prxs are proteins of 20-30 kDa expressed in different cellular compartments and different isoforms (18); six Prx isoforms were identified in *Homo sapiens*: Prx1 is mainly localized in the cytosol, nucleus, and peroxisomes; Prx2 is present in the cytosol and nucleus, and has been shown to bind to cell membranes; Prx3 is exclusively targeted to mitochondria; Prx4 is found in the cytosol and endoplasmic reticulum, and is the only Prx isoform that is actively secreted; Prx5 is localized in the cytosol, mitochondria and peroxisomes; Prx6 is present in the cytosol, vesicles, and lysosomes (19). Based on their structure and enzymatic mechanism, the mammalian Prxs are divided into three groups: 2-Cys Prxs (human Prx1-4), atypical 2-Cys Prxs (Prx5), and 1-Cys Prxs (Prx6). All of them contain one conserved, redox-active, peroxidatic cysteine residue ( $C_p$ , Fig. 2). 2-Cys and atypical 2-Cys Prxs contain one addi-

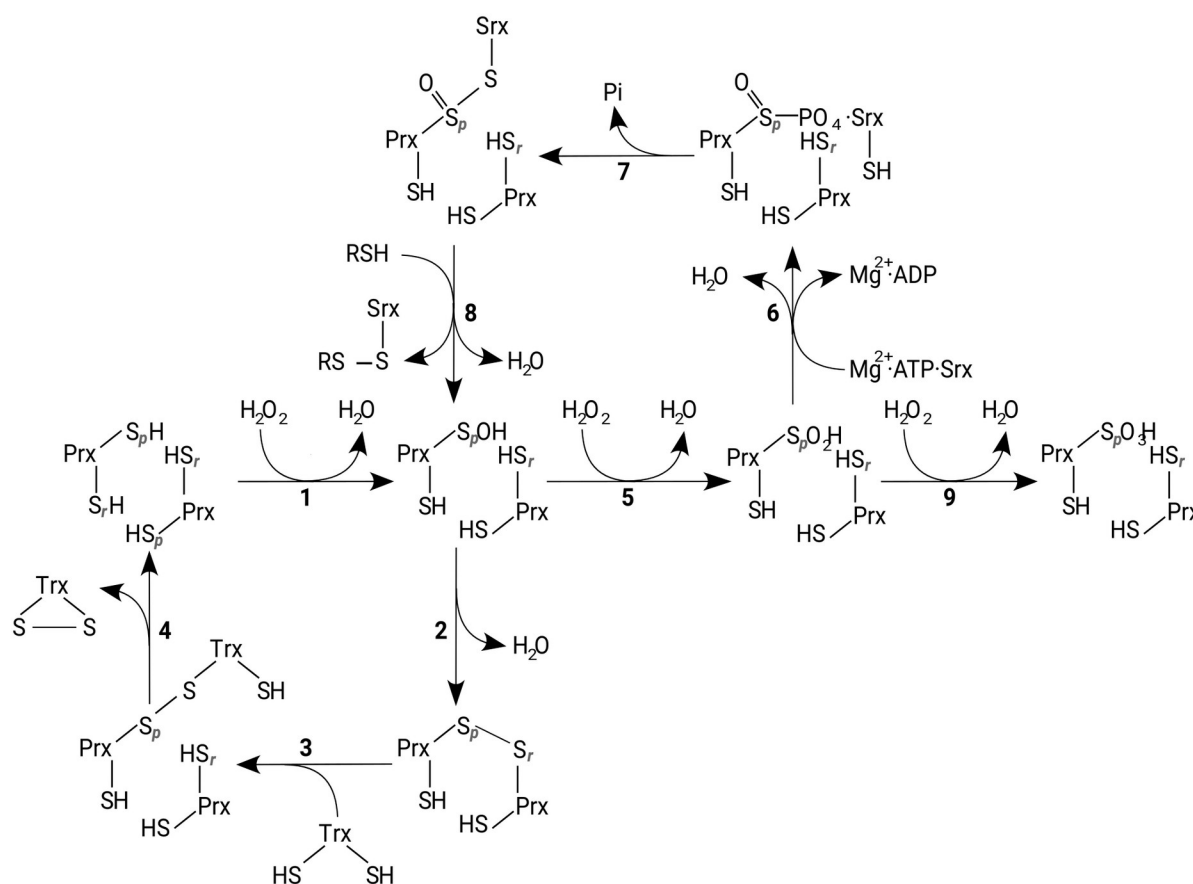


**Figure 2: Reaction mechanism of 2-Cys Prxs.** (1)  $C_p$  (labeled  $S_p$ ) is oxidized by  $H_2O_2$  to sulfenic acid, that is attacked by the  $C_r$  (labeled  $S_r$ ) of other Prx monomer (2), leading to the intermolecular disulfide. The disulfide is reduced by Trx as outlined in (3-4). In the presence of  $H_2O_2$ , the sulfenic acid can be further oxidized (hyper-oxidized) to sulfinic (5) and sulfonic (9) acids. Sulfinic acid modified Prxs can be recovered by the ATP-dependent action of Sr (6-8). Adopted with permission from (12).

tional so-called resolving cysteine residue ( $C_R$ ) located at the C-terminus of the same subunit, while 1-Cys Prx lack this  $C_R$  residue. Most Prxs function as homodimers, although the 2-Cys Prxs also form decamers as result of the association of five dimeric subunits. Depending on different conformations and complex formation, Prxs display different functions. From the catalytical point of view, these three groups slightly differ from each other. During the reduction of  $H_2O_2$  by Prxs, the  $C_P$  is oxidized to sulfenic acid ( $C_P$ -SOH). In the case of 2-Cys Prxs, the  $C_P$ -SOH reacts with the  $C_R$  of the other subunit in the homodimer, leading to an intermolecular disulfide (Fig. 2 and 6); in atypical 2-Cys Prxs, the  $C_P$ -SOH reacts with the  $C_R$  of the same subunit to form an intramolecular disulfide (15,19,20). Both inter- and intramolecular disulfides are eventually reduced by the Trx system (see section 1.3). Due to the absence of a  $C_R$  in 1-Cys Prxs, the sulfenic acid is, in this case, reduced by other small thiol molecules, *e.g.* glutathione (GSH). In the situation of an excess of the substrate, Prxs may be hyper-oxidized to sulfinic or sulfonic acids (see also Fig. 1) on the peroxidatic N-terminal cysteinyl residue, resulting in the inactivation of the enzyme (21). For many years, Prxs hyper-oxidation was thought to be irreversible, but in 2003 Biteau and colleagues identified the ATP-dependent enzyme sulfiredoxin (Srx, Fig. 2) able to restore the peroxidase activity (22,23). So far, Prxs are the only class of proteins for which a specific reductase of the sulfinic acid has been described. The peroxidatic cysteine of Prxs is exceptionally reactive towards peroxides, being thereby oxidized very rapidly with a rate constant in the range of  $1 \cdot 10^6$  to  $1 \cdot 10^8 \text{ M}^{-1} \cdot \text{s}^{-1}$  (24–27), explaining why Prxs are also called peroxide scavengers. This rate constant is 5 to 7 orders of magnitude higher than the rate constant of other small thiol groups or any given protein cysteinyl residue, leaving the Prxs as strong competitors of other target proteins thiol groups. In other words, in order to allow the oxidation of effector proteins with a much slower reactivity towards  $H_2O_2$ , Prxs would have to undergo inactivation, for instance through hyper-oxidation or phosphorylation (21,28). In this way, the produced  $H_2O_2$  could act as second messenger molecule and oxidize the target protein(s) resulting in an appropriate response. Given the high abundance of Prxs and the high sensitivity of the Prxs'  $C_P$  to  $H_2O_2$ , one other possible scenario would be that redox-regulated proteins are not directly oxidized by hydrogen peroxide, instead the oxidation of these proteins could be mediated by Prxs. In this case, Prxs would act as sensors and transducers of  $H_2O_2$  signaling pathways. In Manuscript 3 (page 70) this hypothesis, a new example for this function, is presented and discussed in greater detail.

### 1.3 Thioredoxins

Thioredoxins (Trxs) comprise the first branch and the name-giving proteins of the Trx-fold family of proteins (11,12,29). They were first identified in 1964 as electron donor for ribonucleotide reductase (RNR) (30). Their characteristic dithiol active site motif CGPC, that is conserved throughout all kingdoms of life, facilitates the reduction of the disulfide formed in the catalytic cycle of the RNR. The reaction mechanism by which Trxs reduce protein disulfides is called dithiol mechanism, where both cysteinyl residues in the active site are involved (31,32), see

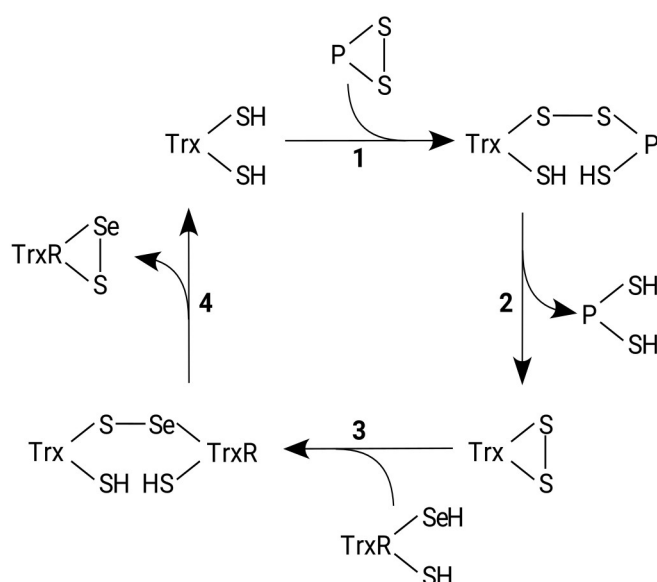


**Figure 3: Reaction mechanism of Trxs.** Trxs reduce protein disulfides via the dithiol mechanism, depending on both active site cysteines. The N-terminal active site Cys forms a covalently bound mixed disulfide intermediate (1), which is reduced by the C-terminal active site Cys, releasing the reduced protein (2). Oxidized Trx is reduced by TrxR in a similar reaction sequence (3-4). Adopted with permission from (12).

Fig. 3 for more details. Briefly, the active site thiol located at the N-terminus initiates the nucleophilic attack on a sulfur atom of the target disulfide, leading to the formation of a mixed disulfide intermediate. This transient intermediate is then reduced by the C-terminal active site thiol of the Trx, releasing the reduced substrate. Oxidized Trx is subsequently regenerated by the flavo- and selenoprotein thioredoxin reductase (TrxR) (33,34), that ultimately receives the reducing equivalents from NADPH. TrxR exists as a 55-60 kDa homodimer, in which every subunit presents a flavin adenine dinucleotide (FAD) domain, a NADPH binding domain, and an interface domain. It contains two active site motifs: one N-terminal active site motif Cys-Val-Asn-Val-Gly-Cys, adjacent to the FAD domain, and one located at the C-terminus with the motif Gly-Cys-Sec-Gly (35,36). The high accessibility and reactivity of the selenocysteine (Sec) residue in the C-terminal active site confers the TrxR a broad substrate specificity (34). The mammalian genome encodes two Trx systems: one cytosolic with Trx1 and TrxR1, and one mitochondrial formed by Trx2 and TrxR2 (37,38). Trx1 is a 12 kDa protein highly conserved in different species, from human to bacteria. The activity and specificity of both human and bacteria Trx1 and TrxR are profoundly discussed in [Article 2](#) (page 52).

## 1.4 Glutaredoxins

Glutaredoxins (Grxs), as the third member of the Trx family of proteins, also contain the well-characterized Trx-fold domain (11). The Grx protein family was first characterized in 1976 as GSH-dependent alternative electron donor for RNR in *E. coli*, after mutants lacking Trx were still viable (39–41). Grxs are classified in two groups attending to their active sites: CxxC/S-type Grxs, with a Cys-Pro-Tyr-Cys/Ser active site motif, and CGFS-type Grxs, with a Cys-Gly-Phe-Ser active site motif (42,43). The key determinant of the Grx function is a unique loop structure consisting of five amino acids directly pre-

ceding the active site, which is present in CGFS-type Grxs and absent in CxxC/S-type Grxs. The latter catalyze the reduction of disulfide bonds in substrates via the so-called dithiol mechanism, similar to the one described above in Fig. 3. In this case, however, the oxidized Grx is regenerated by two GSH molecules (Fig. 4, reaction 1-4), that eventually are reduced by NADPH via glutathione reductase (GR), also at the expense of NADPH (36,44,45). In addition, and as unique feature, Grxs can also reduce glutathionylated proteins in a process called de-glutathionylation via the monothiol mechanism, where only the N-terminal thiol of the active site is involved (Fig. 4, reaction 5-4) (46–48). Human Grx1 and Grx2 belong to this CxxC/S-type Grxs. On the other hand, CGFS-type Grxs do not possess any oxidoreductase activity, with few exceptions (49,50); instead, they are essential in cellular iron metabolism (42,51,52). Human Grx3 and Grx5 belong to this group of proteins (53–55). Iron is an essential element for the survival of almost all living organisms, it can be incorporated in heme or iron-sulfur (FeS) cluster in proteins that are essential for life (56–58). These proteins participate in the transfer of electrons, are cofactors in enzymatic catalysis, control the stability of biomolecules, and act as regulatory elements (42). The first two FeS-Grxs described were *Arabidopsis thaliana* GrxC1 (59) and human Grx2 (54,60), with the CGYC and CSYC con-

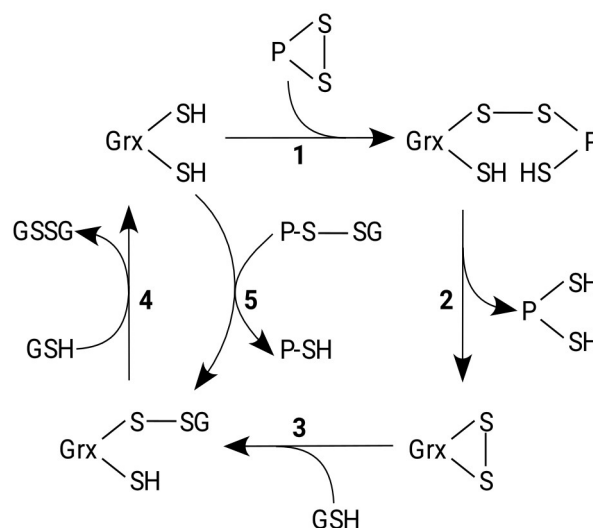


Figure 4: **Reaction mechanism of Grxs.** Grxs reduce protein disulfides via the dithiol mechanism, being reduced by two GSH molecules (1-4). In addition, they reduce glutathionylated proteins via the monothiol mechanism only depending on the N-terminal active site Cys, that attacks the GSH moiety and forms a GSH-mixed disulfide intermediate (5), which is reduced by another GSH molecule (4). Adopted with permission from (12).

sensus active site, respectively, sufficient to allow cluster ligation. The clusters are bridged in a dimeric holo-complex at the interface of two hardly interacting Grx monomers, where the N-terminal active site cysteinyl residue of each Grx and also the thiol groups of two non-covalently bound GSH molecules are involved (61,62). Since the discovery of these two proteins, all CGFS-type Grxs have been characterized as Fe<sub>2</sub>S<sub>2</sub>-proteins that bind the FeS cluster in a very similar way, including the co-ligation by GSH. Because cellular iron levels need to be tightly controlled, organisms have developed effective regulatory mechanisms, *e.g.* iron regulatory proteins (IRPs) (51,63,64). For instance, in case of iron deficiency, cytosolic IRP1 and IRP2 bind to specific mRNA structures, called iron responsive elements (IRE), that promote the synthesis of proteins involved in iron homeostasis such as transferrin receptor (TfR), ferritin, and ferroportin (65). In eukaryotic cells, once the Fe<sub>2</sub>S<sub>2</sub> cluster is synthesized in the mitochondria by the iron-sulfur cluster assembly machinery (ISC), it is transferred to Grx5 by the heat shock protein HSP70 chaperone system (58). Subsequently, the cluster is either transferred directly to Fe<sub>2</sub>S<sub>2</sub> target proteins or to protein complexes involved in Fe<sub>4</sub>S<sub>4</sub> clusters assembly (66,67). Independent of their enzymatic activity, all Grxs use GSH as substrate that binds to an evolutionary conserved GSH binding site. Among the four different Grxs identified in mammals, Grx2 merits special mention in this thesis. The human Grx2 gene (GLRX2) encodes three different protein isoforms by alternative splicing: mitochondrial Grx2a, and nuclear and cytosolic Grx2b and Grx2c (68,69). Grx2 contains the uncommon active site motif CSYC, while its cytosolic counterpart Grx1 contains the conserved CPYC motif. The exchange of the prolyl residue at the second position in the active site sequence for a seryl residue in Grx2 has two consequences: first, Grx2 is able to bridge a FeS cluster, resulting in a dimeric holo-Grx2 inactive as reductase. Certain conditions, for instance a more oxidized GSH pool, lead to the degradation of the cluster and the activation of the Grx2 monomers, suggesting a function for Grx2 as sensor *in vivo* (54). And second, the CSYC sequence results in an increased affinity for glutathionylated substrates, giving Grx2 the ability to (de-)glutathionylate target proteins, as well as to reduce protein disulfides (70–72). In this regard, Grx2c has been identified as specific reductase of the regulatory disulfide in collapsin response mediator protein 2 (CRMP2) (72,73) and is therefore included in the model of a specific redox signaling pathway proposed in [Manuscript 3](#) (page 70). In addition, several studies have shown the importance of the isoform Grx2c, as it is essential for brain development as



well as heart functionality in zebrafish, and it is specifically induced in many cancer cell lines, promoting cell motility and invasiveness (74,75).

## 1.5 The Semaphorin signaling pathway

Semaphorins (Sems) are expressed in most – if not all – tissues, although they were initially characterized in the nervous system (76–78). Semaphorins act via a hetero-dimeric transmembrane receptor formed by neuropilin (NP)-1 or -2 proteins, and plexin (Plex) proteins of the classes A to D (79,80). The semaphorin signaling pathways are part of the regulatory networks controlling the processes that shape the developing nervous system, *i.e.* axon guidance, synaptic plasticity, and neuronal migration (80–82). Among all members of the semaphorin family, Semaphorin 3A (Sem3A) is a prototypical secreted semaphorin present in neurons, where it is involved in axon repulsion, dendritic branching, and synapse formation (83–85). For Sem3A in particular, the receptor NP1/PlexA is necessary to mediate the signal transduction (86–88). Activation of the Sem3A pathway induces growth cone collapse and retraction of the outgrowths by controlling the de-polymerization of the cytoskeleton. Effector proteins include Ser/Thr kinases like cyclin dependent kinase 5 (Cdk5) and glycogen synthase kinase 3  $\beta$  (GSK3 $\beta$ ) that sequentially phosphorylate CRMP2 (89,90). Terman and colleagues showed that MICAL proteins (see section 1.6) directly interact with PlexA (91), supporting the idea that these proteins are involved in the semaphorin-mediated axon repulsion through the regulation of cytoskeletal dynamics (see Fig. 5, page 17, for an overview of MICALs-Sem3A receptor interactions). Furthermore, MICALs directly oxidize actin and promote growth cone collapse and cellular repulsion (91–95).

Both MICAL and CRMP2 interact with the cytosolic domain of PlexA and both are required for the Sem signaling pathway (91,96). The activity of the MICAL monooxygenases is required for their function in the pathway, for instance MICALs can produce H<sub>2</sub>O<sub>2</sub> upon activation of the Sem3A pathway (97). In this thesis, the following pathway and mechanism of CRMP2 oxidation is proposed: MICAL1 is activated in response to Sem3A signaling, presumably by direct interaction with the Sem3A receptor. Next, reduced MICAL1 (FADH<sub>2</sub>) reacts fast with molecular oxygen yielding a peroxy-flavin intermediate (FAD-OO $\cdot$ ). This immediately decays to H<sub>2</sub>O<sub>2</sub> and oxidized MICAL (FAD). This H<sub>2</sub>O<sub>2</sub> oxidizes transducer proteins, *i.e.* Prxs, that in turn oxidize CRMP2 (see [Manuscript 3](#), page 70).

## 1.6 MICAL proteins

MICAL proteins acquired their name after a study that identified a novel ‘molecule interacting with CasL’ in 2002 (98). CasL belongs to the p130 Cas family of proteins (99), it contains an N-terminal SH3 domain followed by a substrate domain, both motifs responsible for its interaction with many molecules and, thus, for its functions (100). A couple of months later in 2002, Terman *et al.* identified MICALs in *Drosophila melanogaster* as proteins binding to the cytoplasmic domain of the semaphorin receptor PlexA (91), suggesting that MICALs are involved in the semaphorin signaling pathway (see section 1.5). MICALs are cytosolic proteins expressed in specific neuronal as well as non-neuronal tissues, such as spleen, thymus, lung, and testis (98,101). They are highly conserved from vertebrates to invertebrates. The human genome contains three different MICAL genes (MICAL1, MICAL2, MICAL3), and two MICAL-like genes (MICAL-L1, MICAL-L2) also found in mice. In contrast, *Drosophila* has only one MICAL gene and one MICAL-like gene (91,98,102). All MICAL proteins contain a flavin-dependent monooxygenase (MO) domain located at the N-terminus, followed by a calponin homology (CH) domain and a LIM domain. Additionally, a C-terminal Rab-binding domain (RBD) can be found in some MICALs, *i.e.* human MICAL1 and MICAL3 (103,104). Presumably the most interesting feature of MICAL proteins is the presence of the N-terminal FAD-containing MO domain. Since MICAL-L proteins lack this domain, they have been excluded from this thesis, in which the main focus resides particularly on the oxidase activity. Nevertheless, it shall be mentioned that some studies point to the involvement of MICAL-L proteins in processes such as the regulation of cell surface receptors recycling, actin remodeling, or neurite outgrowth (105–107). The MO domain confers the ability of MICALs to function as oxygenases, *i.e.* oxidize targets using molecular oxygen and NADPH as substrates. The CH domain is typical for actin-binding proteins. There are three types of CH domains (1-3) (108–110), type 2 is present in MICALs. This type of CH domain is not sufficient by itself to bind F-actin, however, it is important for the MO domain to function, as it enhances the binding to actin as well as its catalytic activity (111). The LIM domain consisting of small cysteine-rich zinc-finger structures is involved in cytoarchitecture and protein-protein interactions (112–115). The RBD domain includes binding sites for small GTPases of the Rab family, for instance Rab8, Rab1, or Rab35 (102,116–120). This domain has been suggested to auto-inhibit the oxidase activity of the MO domain, as the C-term-truncated MICAL1 resulted in a constitutively active enzyme *in vivo*, in contrast to full-length

MICAL1 (121). This domain was formerly named C-terminal domain (CTD), with a proline-rich region, a glutamic acid repeat, and a coiled coil (CC) motif. The motif PPKPP (Pro-Pro-Lys-Pro-Pro) present in the proline-rich region interacts with the SH3 domain of CasL, as mentioned above (98). It is also through this C-terminal domain that MICAL interacts with vimentin, a protein that is present in intermediate filaments of the cytoskeleton (98). This association supports the idea that MICAL may function as regulator of the cytoskeleton.

As a flavoprotein, MICAL has been compared to other FAD-containing proteins. Based on a high similarity of the MICAL MO domain to the aromatic hydroxylase *p*-hydroxybenzoate (pHBH) from *Pseudomonas fluorescens* (91,122,123), the MO domain of mouse MICAL (mMICAL) was characterized in great detail (124). From a structural point of view, the domain is folded in two subdomains connected by two  $\beta$ -strands. The large subdomain, also called domain-1 or FAD-binding domain, contains the two consensus sequence motifs required for the FAD binding. The first motif is the GxGxxG sequence, commonly found in FAD-dependent oxidoreductases; the second motif is the GD sequence, conserved among the hydroxylases. The FAD molecule seats in between the two subdomains and binds to one side of mMICAL via a hydrogen bond network (123). In pHBH, the flavin ring can switch between the so-called “out” and “in” conformation depending on its oxidized and reduced states, respectively. (125–127). Briefly, in the “out” conformation, the ring occupies a more solvent-exposed position, away from the substrate; upon NADPH binding, the flavin ring is reduced and pulled inward into a more buried position (“in”) facing the active site and favoring the catalysis. According to this nomenclature, the flavin ring in the crystal mMICAL structure was found to adopt the “out” position (123). In the same study they also showed that mMICAL binds NADPH, which likewise triggers a similar change in the FAD conformation. In contrast to other hydroxylases and uniquely to mMICAL1, the shift from the “out” to the “in” conformation leads to the opening of a channel directly connecting the molecular surface with its active site. This channel opens out on the opposite side of the NADPH binding site, and it is sufficient in length and width to permit the access of a potential substrate amino acid side chain (123). A representation of both “in” and “out” conformations of the FAD in mMICAL, as well as the surface open channel can be found in [Article 1](#) (page 43). In [Manuscript 3](#) (page 70) of this thesis, the following reaction mechanism of human MICAL is proposed (Fig. 6, page 18): firstly, FAD is reduced to FADH<sub>2</sub> at the expense of NADPH (Fig. 6, reaction 1). In presence of molecular oxygen, reduced FADH<sub>2</sub> is extremely rapid oxidized to the

transient C4a-hydroperoxide intermediate form of the enzyme (FAD-OO<sup>•</sup>) (Fig. 6, reaction 2), which decomposes to H<sub>2</sub>O<sub>2</sub> and the oxidized flavin (FAD) (Fig. 6, reaction 3). The shift of the flavin ring from the “out” to the “in” conformation is crucial for MICAL to act as oxidase, as well as the rate limiting step of the whole mechanism. Generated H<sub>2</sub>O<sub>2</sub> is responsible for the substrate oxidation, in this case Prxs (Fig. 6, reaction 4). This model mechanism, including the kinetic characterization of every step, is shown in [Manuscript 3](#) (page 70). Additionally, *in vitro* experiments included in this manuscript show that indeed MICAL oxidizes Prxs, noteworthy even in presence of catalase, indicating that the produced H<sub>2</sub>O<sub>2</sub> is not released, but locally produced instead. This observation suggests that Prxs must bind to MICAL in very close proximity to the open channel in order to be oxidized. Once oxidized, Prxs would transfer the oxidizing equivalents to a dedicated effector protein, *e.g.* CRMP2 as proposed in this thesis. According to this model, a quite low reactive thiol group such as CRMP2 Cys504 thiol (128) could be efficiently oxidized by other highly sensitive thiol groups such as Prxs thiols, that are rapidly oxidized by H<sub>2</sub>O<sub>2</sub>, as discussed above. It has been published recently that Prxs, upon oxidation by H<sub>2</sub>O<sub>2</sub>, transfer disulfides to redox-regulated proteins, introducing the concept of a “redox relay” (129). Such redox relays have been known for more than 15 years only in fungi. For instance, *S. cerevisiae* glutathione peroxidase-like 3 (GPx3), later named oxidant receptor peroxidase 1 (Orp1), acts as H<sub>2</sub>O<sub>2</sub> receptor and mediates the oxidation of the transcription factor Yap1 (130), and when *S. cerevisiae* lacks all eight thiol peroxidases sensing H<sub>2</sub>O<sub>2</sub>, cells are unable to regulate gene expression in response to H<sub>2</sub>O<sub>2</sub> (131). Evidence of similar Prx-based redox relays has been reported in mammalian cells, with few well-documented reports in which deletion or depletion of human 2-Cys Prxs compromises H<sub>2</sub>O<sub>2</sub>-dependent thiol oxidation (129,132,133).

Following the identification of MICALs as flavin-dependent enzymes that specifically produce H<sub>2</sub>O<sub>2</sub> by Nadella *et al.* (124), the function of MICAL proteins as potential oxidases has been a subject of great interest. Back in 2002, although Terman and colleagues’ study did not characterize MICAL as oxygenase, they yet showed growth cone repulsion upon inhibition of flavo-monooxygenases *in vitro*, suggesting that MICALs are involved in axon guidance, and thus semaphorin signaling (91). The collapse of the growth cone induced by semaphorins requires localized de-polymerization of actin. The actin cytoskeleton is crucial for many, if not all, cellular events, and as such, actin is a meticulously regulated protein. This regulation is mediated not only by actin binding proteins, but also by post-translational modifications.

Actin is susceptible to redox modifications including oxidation, nitrosylation, glutathionylation and carbonylation (134–136). As they are widely variable, the effects of the redox modifications cannot be grouped together (135). In general, redox mediated alterations have been found to regulate the polymerization/de-polymerization dynamics of actin, but they are specific to the cell type, the redox environment, and the crosstalk to other signaling pathways. Additionally, these redox mediated alterations are critically dependent on the monomeric, globular (G) or polymeric, filamentous (F) state of actin, as well as the particular amino acid residues modified, *i.e.* cysteinyl or methionyl residues. Unlike cysteine, methionyl residues do not react rapidly with hydrogen peroxide at physiological pH (137). However, it has been shown that methionyl residues at position 44 (M44) and 47 (M47) of actin are post-translationally modified by MICAL (92). In this study, Hung *et al.* generated mutants of actin where either single or both methionyl residues were replaced by leucine (M44L, M47L and M44/47L, respectively). All three mutants showed similar polymerization to the wild-type actin, and all of them were found to bind MICAL. In contrast, actin filaments of wild-type and M47L de-polymerized in presence of MICAL and NADPH, while actin filaments of M44L and M44/47L were resistant to de-polymerization under the same conditions, indicating that the specific oxidation of M44 is sufficient to cause F-actin disassembly and decreased G-actin polymerization. Both M44 and M47 residues are located within the D-loop, a region that is essential for actin subunits contact (138). Upon oxidation, the side chain of the sulfoxide derivative is no longer flexible and negatively charged, that directly affects the monomer-monomer interaction region, thus leading to de-polymerization. Already in 1948, after the identification of actin (139), Straub and colleagues suggested that the presence of an oxidizing agent not only dismantled polymerized F-actin, but also inhibited the polymerization of G-actin, an observation that was much later confirmed after the failure of MICAL-treated actin to re-polymerize *in vitro* (92). Binding to F-actin, but not G-actin, stimulates the enzymatic activity of MICAL, resulting in the modification of the actin cytoskeleton in a redox dependent manner, both *in vitro* and *in vivo* (92,140–142).

Methionine is a sulfur-containing amino acid susceptible to oxidation in a unique pattern (Fig. 1). The addition of an oxygen group on its sulfur atom generates a chiral center and results in a mixture of two diastereoisomers, *i.e.* R- and S-methionine sulfoxide (R-MetO and S-MetO, respectively) (143). Virtually all aerobic organisms have two distinct types of stereospecific methionine sulfoxide reductases (Msr) that catalyze the reduction of MetO back to

Met: MsrA specifically reduces S-MetO, while MsrB is specific for the reduction of R-MetO (144,145). Both Msrs are thioredoxin-dependent enzymes, the oxidized form of Trx produced in the reduction of MetO to Met is regenerated by TrxR at the expense of NADPH (146). Actin M44 was found to be stereospecifically oxidized to the R-MetO isomer by MICAL, that is reduced specifically by MsrB resulting in restored actin polymerization properties (147). For this reason, we focus here on the MsrB family. It shall be mentioned, however, that substantial evidence has been presented that highlight the importance of MsrA *in vivo* in a number of events, for instance Alzheimer's disease (148), cells sensitivity to hydrogen peroxide (149), or lifespan regulation (150,151). MsrB structural genes are highly conserved among almost all free-living organisms, and as such they have been identified and characterized in bacteria (145,152,153), yeast (154), fly (155), and mammals (154,156,157). Human and mouse genomes encode three MsrB genes, designated MsrB1, MsrB2, and MsrB3. MsrB1 is a selenocysteine (Sec)-containing protein, also called selenoprotein R (SelR). Out of the three orthologs, MsrB1 is the main form in mammals, located in both the cytosol and nucleus. It possesses the highest catalytic activity ( $2280 \text{ M}^{-1}\cdot\text{s}^{-1}$ ) due to the presence of Sec on its active site; the MsrB1 cysteine mutant exhibits an 800- to 1000-fold lower specific activity (158). MsrB2 contains a cysteinyl residue on its active site instead, and it is around 2-fold less catalytically efficient than MsrB1. MsrB2 is present in mitochondria of muscle tissues, mainly heart and skeletal muscle (157). Similar to MsrB2, MsrB3 also has a conserved catalytic cysteinyl residue and a 3-fold lower catalytic efficiency compared to MsrB1. The human MsrB3 gene generates two protein variants by alternative splicing, *i.e.* MsrB3A and MsrB3B, present in endoplasmic reticulum and mitochondria, respectively (158). The reaction mechanism as well as the substrates specificity of these three (seleno)cysteine-containing proteins are depicted in detail in references (159,160). Considering the functions and cellular locations, MsrB genes, together with MsrA, comprise a system with an enzyme- and stereo-specific function to repair oxidized methionyl residues (161). In particular, MICAL and SelR constitute a reversible cellular redox signaling system that controls actin cytoskeletal organization (135). MICAL's ability to destabilize actin cytoskeleton also plays an important role downstream of repulsive guidance cues like semaphorins, which have been well characterized for their disruptive effects on the F-actin cytoskeleton.

## 1.7 CRMP2 and the cytoskeleton

Collapsin response mediator protein 2 (CRMP2), also named dihydropyrimidinase like 2 (DPYSL2, gene name: DPYL2), is one of the five members of the putative intracellular CRMP family, which are expressed, among others, in the developing nervous system (94). Among the 5 homologous cytosolic proteins of the family (CRMP1 to CRMP5), CRMP2 is the most abundant, as well as the most studied, and it was the first one to be discovered in *C. elegans* (162). In addition, CRMP1, 2 and 4 give rise to two different isoforms derived from alternative splicing, called isoforms A and B, resulting in an alternative N-terminus (163). The more C-terminal regions, however, are conserved among the CRMP family members, and contain the binding sites for the two major proteins of the cytoskeleton, *i.e.* tubulin and actin, suggesting that this region determines the main function of the proteins (164,165). In case of CRMP2, CRMP2B is considered as the canonical isoform, herein referred to as CRMP2, unless otherwise stated. CRMP2 has been implied in semaphorin-mediated growth cone collapse, hence this protein has a strong impact on cytoskeleton rearrangements (166,167). CRMP2 is present in the cytosol as a homo- as well as heterotetramer (168,169), which is extensively regulated by phosphorylation, *e.g.* through Cdk5 and GSK3 $\beta$  (89,90,170,171). Briefly, following stimulation of neurons with Sem3A, the CRMP2 tetramer is recruited to the Sem3A receptor, where it undergoes a conformational change that enables Cdk5 to phosphorylate CRMP2's seryl residue at position 522 (Ser522), that allows the subsequent phosphorylation of Thr509, Thr514, and Ser518 mediated by GSK3 $\beta$ , resulting in microtubuli disassembly and growth cone collapse (94). In contrast, in absence of Sem3A, CRMP2 associates with  $\alpha/\beta$ -tubulin heterodimers and stimulates microtubules assembly (172). CRMP2 has also been characterized as promising drug target in the treatment of neurodegenerative pathologies. Lanthionine ketimine and the cell penetrating lanthione ketimine esters bind to CRMP2 and effect it in a way that improves neuronal plasticity and thus neuroregeneration, for instance in animal models of multiple sclerosis, Parkinson's disease, and spinal cord injury (173–176).

The study of Morinaka *et al.* revealed that MICALs produce H<sub>2</sub>O<sub>2</sub> *in vivo* upon activation by Sem3A (97). Schmidt *et al.* (121) have demonstrated that members of the CRMP family interact with MICALs when promoted by Sem3A signaling. Together, this points to a common role of both proteins in the regulation of the cytoskeleton. Even more, CRMP2 has also been reported to be subject to redox regulation (74). Grx2c (see section 1.4) controls axonal

outgrowth, survival of neurons, and development of a functional brain via redox regulation of CRMP2 *in vivo*. Apparently, at least some functions of CRMP2 are controlled by a thiol-disulfide switch characterized in (73). Human CRMP2 contains eight cysteinyl residues at positions 132, 133, 179, 248, 323, 334, 439 and 504. Treatment with hydrogen peroxide leads to the oxidation of two adjacent cysteinyl 504 thiol groups and the subsequent formation of an intermolecular disulfide in the homotetrameric CRMP2 complex. This reversible intermolecular thiol switch involves two distinct conformations of the complex (73): the formation of the disulfide brings the C-terminal regions of two CRMP2 subunits in close proximity, whereas the reduced CRMP2 tetramer adopts a more open conformation with hydrophobic regions exposed. Oxidized CRMP2 is a target of Grx2c, resulting in the reduction of the CRMP2 disulfide via the dithiol reaction mechanism (Fig. 4). Interestingly, also Trx1 is able to reduce CRMP2 disulfide *in vitro*. Morinaka and colleagues (97) have even proposed a stable mixed disulfide between Trx1 and CRMP2. However, their study was misled by the use of mutant protein. No stable mixed Trx1-CRMP2 disulfide complex could be detected neither *in vitro* nor *in vivo*. The different  $pK_a$  values of the active site cysteines and the resulting reaction mechanism and kinetics of Trx1 make a stable complex with CRMP2 highly unlikely to occur, or rather excluded (31,177).

The CRMP2 thiol switch has been well characterized *in silico* and *in vitro* (128). It was confirmed that the transition between oxidized and reduced CRMP2 involves a profound structural and conformational change in the tetramer, that adopts a more “relaxed” conformation upon reduction. In this conformation, the phosphorylation sites of CRMP2 are more solvent exposed and favor their phosphorylation by protein kinases as mentioned above, indicating the tightly connected regulation of CRMP2 by redox and phosphorylation modifications. The second order rate constant of CRMP2 thiol oxidation by  $H_2O_2$  was determined to be  $k = 0.82 M^{-1}\cdot s^{-1}$  (128). This rate constant is seven to eight orders of magnitude lower than the rate constant of the most  $H_2O_2$  reactive proteins in the cell, *i.e.* Prxs, which indicates that the CRMP2 thiol group is very unlikely to be oxidized by  $H_2O_2$  directly in competition with these highly abundant peroxidases. Instead, this thesis supports the idea that the CRMP2 thiol switch is specifically oxidized by dedicated enzymes, *i.e.* a specific Prx. The potential oxidation of CRMP2 by Prxs has been suggested before (129,178). Noteworthy, MICAL proteins have also been identified as interaction partners of CRMP2 (121). Co-immunoprecipitation assays showed that full-length MICAL1 failed to interact with CRMPs. In contrast, a trun-



cated version of MICAL1 lacking the C-terminal region does interact, suggesting that CRMPs bind rather to the N-terminal region including the MO and LIM domains. No direct interaction of CRMP with the LIM domain or MO domain alone was detected, which suggests that multiple residues located at the N-terminal region may be involved in CRMP binding, rather than a specific linear chain of amino acids (121). Despite the described interaction between CRMP2 and MICAL, no study has linked the oxidation of the CRMP2 thiol switch to the MICALs. As a proof of concept, *in vitro* experiments included in the supplementary material of [Manuscript 3](#) (page 70) failed to show a direct CRMP2 oxidation by MICALs. Hence, at least one more protein must be involved in this oxidation mechanism.

## 1.8 Hypothesis

The main hypothesis of this paper was: *CRMP2 thiol switch is oxidized via a receptor-induced redox relay that involves MICAL and Prx proteins*. As discussed above, Prxs are extremely reactive towards  $H_2O_2$  and possess the ability to transfer the oxidizing equivalents to redox-regulated target proteins (129,130,179–181). In addition, we identified Prxs as interaction partners of both MICAL and CRMP2. Together, these findings made the Prxs strong candidates for the proposed redox relay, facilitating the transmission of the oxidation from a receptor-induced MICAL protein to CRMP2. Such a relay would ideally fulfill the requirements for a specific redox signaling pathway as introduced above (section 1.1). The primary aim of this thesis was to identify and characterize the components of this redox relay ([Article 1](#), page 43, and [Manuscript 3](#), page 70).

Specificity in (redox) signaling must be mediated through specific protein-protein interactions. *We also propose that the basis for the specific protein-protein interactions is compatible electrostatic surface potentials* that mediate recognition and the formation of an encounter complex between the two proteins. The second aim of this thesis was to analyze the importance of electrostatic complementarity using the Trx1/TrxR1 system as model ([Article 2](#), page 52).

## 2 Conclusions

### 2.1 Article 1: Signal-regulated oxidation of proteins via MICAL

In this review, MICAL proteins and their role as specific oxidases in signal transduction were presented and discussed. MICALs structure, reaction mechanism as well as reactivities were summarized. The human genome encodes three different MICAL isoforms (MICAL1-3), while only one gene has been identified in *Drosophila melanogaster*. Virtually all MICAL proteins contain a monooxygenase (MO) domain with FAD as prosthetic group. Similarly to aromatic hydroxylases and amine oxidases, they reduce molecular oxygen to hydrogen peroxide in presence of NADPH. The produced hydrogen peroxide might act as signaling molecule (Fig. 5). So far, only methionyl residues of actin filaments, *i.e.* F-actin, have been identified as MICAL substrates. MICAL proteins bind to F-actin and oxidize methionyl residues M44 and M47 in a stereospecific manner, yielding the R diastereoisomer of the methionine sulfoxide (R-MetO), which is eventually reduced back to methionine by methionine sulfoxide reductase B (MsrB). The oxidation of actin M44 and M47 leads to filaments de-polymerization, thus affecting cytoskeletal dynamics, and explaining why MICALs have been also linked to semaphorin signaling pathways. This paper was the basis for the main hypothesis of this thesis (see 1.8)

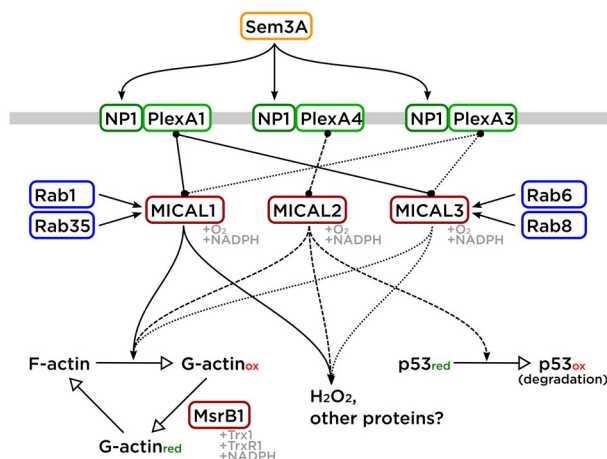


Figure 5: **Signaling networks with mammalian MICAL proteins as transducers.** Semaphorin acts via NP1/PlexA receptors activating MICAL transducer proteins, that are also regulated by small GTPases of the Rab family. MICALs' monooxygenase activities lead to the oxidation of actin and potentially other cysteine-containing effector proteins. Adopted from [Article 1](#) (page 43).

### 2.2 Article 2: Molecular basis for the interactions of human thioredoxins with their respective reductases

In general, thioredoxins (Trxs) are characterized by their highly conserved active site with two cysteinyl residues (CPGC), which are crucial for the reversible catalysis of thiol-disulfide exchange reactions. After the release of the reduced substrate, oxidized Trx is eventually re-

duced by its reductase TrxR at the expense of NADPH. The interaction between human thioredoxin 1 (hTrx1) and its counterpart, the NADPH-dependent seleno-enzyme thioredoxin reductase 1 (hTrxR1), was proposed to be controlled by electrostatic complementarity. In this work we demonstrated that hTrx1 binds to its reductase independent of its redox state, as the redox inactive hTrx1 mutant C32/35S still binds to the reductase, *i.e.* the redox state of the substrate does not seem to have a major influence on the recognition and formation of the complex with its reductase. The study of engineered mutants of hTrx1 with electrostatic changes within and outside the contact area with hTrxR1 gives insight in the electrostatic complementarity as a key force for the formation of an encounter complex between the proteins. The change of potential in hTrx1 within the contact area with the reductase decreased the affinity of the enzyme for its substrate, while electrostatic potential changes outside the immediate contact area may have a strong influence on the catalytic efficiency.

### 2.3 Manuscript 3: NADPH-dependent oxidation of CRMP2 through a MICAL1-Prx1 redox relay controls neurite outgrowth

Fine balanced cell-cell communication and signal transduction pathways control cytoskeletal dynamics ensuring, among others, neuronal development and plasticity. Changes of the intracellular redox milieu have been associated with various stages of these processes. CRMP2/DPYL2 is an effector protein in the semaphorin signaling pathway that effects both actin and tubulin dynamics, thus linking cell surface signal reception to processes such as neuronal development and cell migration. CRMP2 is subject to a complex network of post-translational modifications including a regulatory dithiol-disulfide switch. The mechanisms of reduction of this redox switch were established, the signal-induced oxidation of the

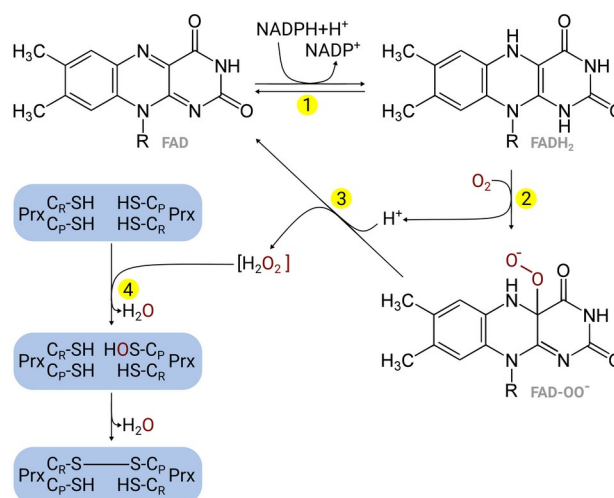


**Figure 6: Proposed reaction mechanism of MICAL-catalyzed Prx oxidation.** (1) The FAD in MICAL is reduced by NADPH. (2) FADH<sub>2</sub> reacts with molecular oxygen yielding peroxy-flavin. (3) Fast decay of the peroxy-flavin to H<sub>2</sub>O<sub>2</sub> and FAD. (4) H<sub>2</sub>O<sub>2</sub> is not released, but directly channeled to the peroxidatic cysteine (C<sub>P</sub>) of a MICAL-bound Prx dimer. The resulting sulfenic acid is attacked by the resolving cysteine (C<sub>R</sub>) yielding the intermolecular disulfide between two Prx monomers. Adopted from *Manuscript 3* (page 70)

mechanisms of reduction of this redox switch were established, the signal-induced oxidation of the

switch, however, remained unclear. Here, we report the oxidation of CRMP2 through a redox relay in the semaphorin pathway that involves the signal-regulated flavin monooxygenase MICAL1 and the peroxidase Prx1 as specific signal transducers. Using molecular oxygen and electrons provided by NADPH, MICAL produces hydrogen peroxide and specifically oxidizes Prx1 (Fig. 6). This reaction does not require hydrogen peroxide to be released into the surrounding, *i.e.* it occurs through direct interaction between the two proteins. Subsequently, Prx1 is responsible for the oxidation of the CRMP2 redox switch, thus modulating its biological activity. The lack of any component of this proposed redox relay causes the same dysregulation of neurite outgrowth in a cellular model of neuronal differentiation. An intriguing consequence of our findings is that both the oxidation and the reduction of the CRMP2 thiol switch require reducing equivalents in the form of NADPH (Fig. 7).

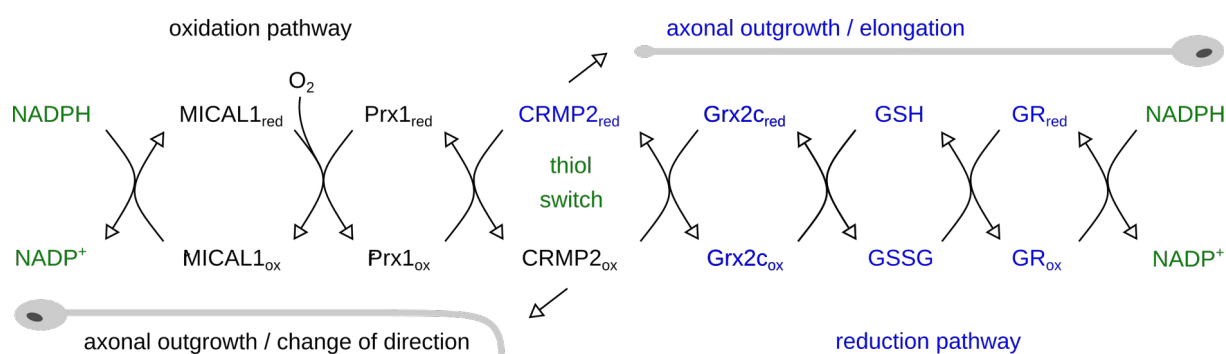


**Figure 7: NADPH-dependent redox relays in both the oxidation and reduction of the CRMP2 thiol switch control axonal outgrowth.** Adopted from *Manuscript 3* (page 70)

### 3 Summary

Survival, development, and function of cells depend on numerous signaling pathways orchestrating the response to external and internal stimuli. Besides the well-established signaling through reversible phosphorylation, the concept of specific, spatio-temporal redox modifications of protein cysteinyl and methionyl side chains that regulate the biological function of these proteins is supported by an overwhelming amount of data. Members of the thioredoxin fold family of proteins, *e.g.* glutaredoxins (Grxs), thioredoxins (Trxs), and peroxiredoxins (Prxs), are widely characterized to catalyze thiol-disulfide exchange reactions. One of the most studied proteins of this family is mammalian Trx1, that, together with its reductase, the NADPH-dependent seleno-enzyme thioredoxin reductase (TrxR) 1, forms the cytosolic Trx system. This Trx system is required as electron donor *e.g.* in DNA synthesis, proliferation, and protection against apoptosis. In [Article 2], we analyzed the interactions between Trx1 and TrxR1 using a combination of molecular dynamics simulations and *in vitro* analysis with recombinant proteins. *In vitro* analysis using numerous Trx1 mutants confirmed that the transient protein-protein interactions during the formation of the encounter complex are independent of the subsequent redox reaction, but are controlled by electrostatic compatibility within the interaction area. Electrostatic complementarity outside of this contact area can have an influence on the catalytic efficiency.

Although the specific reduction of protein redox modifications has been studied intensively, the oxidation of protein side chains was thought to be a result of so-called ‘oxidative stress’. However, this term has been increasingly challenged, since signaling pathways depend on specific, spatio-temporal oxidation of target proteins, most likely catalyzed by specific enzymes. The discovery of MICAL (molecule interacting with CasL) proteins evinced the first examples of specific oxidases in signal transduction in the redox regulation of cellular functions. In [Article 1], we discuss the signal regulated oxidation of proteins by MICAL, taking recent discoveries into account. As part of the semaphorin signaling pathway, MICAL proteins were characterized to stereo-specifically oxidize methionyl residues in actin, thereby regulating actin de-polymerization, a process important in neurogenesis and cell migration. This oxidation can be reversed by the specific methionine-R-sulfoxide reductase B1. Besides the regulation of actin dynamics, MICALs are involved in the regulation of cell proliferation and apoptosis, and the production of hydrogen peroxide may qualify them as specific oxidases also for cysteinyl residues.

In [Manuscript 3], we identified and characterized the NADPH-dependent oxidation of collapsin response mediator protein (CRMP) 2 through a MICAL1-Prx1 redox relay. The monooxygenase MICAL1 is able to produce hydrogen peroxide, in a NADPH and oxygen dependent manner. MICALs are involved in the semaphorin signaling pathway, and therefore important for the regulation of axonal outgrowth, guidance, and repulsion. CRMP2, also an effector in the semaphorin signaling pathway, is regulated by reversible phosphorylation and the formation of an intermolecular disulfide between two adjacent cysteinyl 504 residues in the tetrameric complex. Based on molecular dynamics simulations, *in vitro* and *in vivo* analysis, we confirmed the specific oxidation of Prx1 by MICAL1, most likely through the local production of hydrogen peroxide, that is directly channeled to Prx1's active site cysteinyl residue, and the subsequent transfer of the oxidizing equivalents to the effector protein CRMP2. CRMP2's thiol-disulfide switch is efficiently reduced by cytosolic Grx2 or Trx1, oxidoreductases that are reduced by glutathione and glutathione reductase or TrxR1, respectively, also at the expense of NADPH.

In synopsis, the results presented and discussed in these papers support the concept of specific redox signaling through specific protein-protein interactions and the importance of electrostatic complementarity for these. With MICAL1, so far only known for the oxidation of methionyl residues, and Prx1, we demonstrated the first redox relay that oxidizes CRMP2's thiol-disulfide switch, that in turn can be re-reduced by Grx2c. One of the most surprising results of this thesis is that both the reductive and oxidative pathways of this redox switch rely on electrons provided by NADPH. Misinterpretations or errors in specific redox regulated signaling pathways may contribute to pathological alterations, *i.e.* CRMP2's redox switch is essential for neuronal development and the progression of cell migration and invasiveness. Identification of further target proteins of MICAL as well as the identification and analysis of other potential specific oxidases will be subject of future investigations.

## 4 References

1. Cadenas E, Sies H. Oxidative stress: excited oxygen species and enzyme activity. *Adv Enzyme Regul.* 1985;23:217–37.
2. Sies H. Oxidative stress: from basic research to clinical application. *Am J Med.* 1991 Sep 30;91(3C):31S-38S.
3. Sies H, Cadenas E. Oxidative stress: damage to intact cells and organs. *Philos Trans R Soc Lond B Biol Sci.* 1985 Dec 17;311(1152):617–31.
4. Bellomo G, Mirabelli F. Oxidative stress and cytoskeletal alterations. *Ann N Y Acad Sci.* 1992 Nov 21;663:97–109.
5. Pizzino G, Irrera N, Cucinotta M, Pallio G, Mannino F, Arcoraci V, et al. Oxidative Stress: Harms and Benefits for Human Health. *Oxid Med Cell Longev.* 2017;2017(8416763).
6. Jones DP. Redefining oxidative stress. *Antioxid Redox Signal.* 2006 Oct;8(9–10):1865–79.
7. Ghezzi P, Bonetto V, Fratelli M. Thiol-disulfide balance: from the concept of oxidative stress to that of redox regulation. *Antioxid Redox Signal.* 2005 Aug;7(7–8):964–72.
8. Winterbourn CC, Hampton MB. Thiol chemistry and specificity in redox signaling. *Free Radic Biol Med.* 2008 Sep 1;45(5):549–61.
9. Go Y-M, Jones DP. Redox compartmentalization in eukaryotic cells. *Biochim Biophys Acta.* 2008 Nov;1780(11):1273–90.
10. Halvey PJ, Watson WH, Hansen JM, Go Y-M, Samali A, Jones DP. Compartmental oxidation of thiol–disulphide redox couples during epidermal growth factor signalling. *Biochem J.* 2005 Mar 1;386(2):215.
11. Martin JL. Thioredoxin--a fold for all reasons. *Struct Lond Engl* 1993. 1995 Mar 15;3(3):245–50.
12. Hanschmann E-M, Godoy JR, Berndt C, Hudemann C, Lillig CH. Thioredoxins, glutaredoxins, and peroxiredoxins--molecular mechanisms and health significance: from cofactors to antioxidants to redox signaling. *Antioxid Redox Signal.* 2013 Nov 1;19(13):1539–605.
13. Harris JR. Release of a macromolecular protein component from human erythrocyte ghosts. *Biochim Biophys Acta.* 1968 Apr 29;150(3):534–7.
14. Chae HZ, Robison K, Poole LB, Church G, Storz G, Rhee SG. Cloning and sequencing of thiol-specific antioxidant from mammalian brain: alkyl hydroperoxide reductase and thiol-specific antioxidant define a large family of antioxidant enzymes. *Proc Natl Acad Sci U S A.* 1994 Jul 19;91(15):7017–21.

15. Wood ZA, Schröder E, Robin Harris J, Poole LB. Structure, mechanism and regulation of peroxiredoxins. *Trends Biochem Sci.* 2003 Jan;28(1):32–40.
16. Hofmann B, Hecht H-J, Flohé L. Peroxiredoxins. *Biol Chem.* 2002 Apr;383(3–4):347–64.
17. Chae HZ, Kim HJ, Kang SW, Rhee SG. Characterization of three isoforms of mammalian peroxiredoxin that reduce peroxides in the presence of thioredoxin. *Diabetes Res Clin Pract.* 1999 Sep;45(2–3):101–12.
18. Rhee SG, Kang SW, Chang TS, Jeong W, Kim K. Peroxiredoxin, a novel family of peroxidases. *IUBMB Life.* 2001 Jul;52(1–2):35–41.
19. Rhee SG, Kil IS. Multiple Functions and Regulation of Mammalian Peroxiredoxins. *Annu Rev Biochem.* 2017;86(1):749–75.
20. Rhee SG, Chae HZ, Kim K. Peroxiredoxins: a historical overview and speculative preview of novel mechanisms and emerging concepts in cell signaling. *Free Radic Biol Med.* 2005 Jun 15;38(12):1543–52.
21. Yang K-S, Kang SW, Woo HA, Hwang SC, Chae HZ, Kim K, et al. Inactivation of human peroxiredoxin I during catalysis as the result of the oxidation of the catalytic site cysteine to cysteine-sulfinic acid. *J Biol Chem.* 2002 Oct 11;277(41):38029–36.
22. Biteau B, Labarre J, Toledano MB. ATP-dependent reduction of cysteine-sulphinic acid by *S. cerevisiae* sulphiredoxin. *Nature.* 2003 Oct 30;425(6961):980–4.
23. Jeong W, Park SJ, Chang T-S, Lee D-Y, Rhee SG. Molecular mechanism of the reduction of cysteine sulfinic acid of peroxiredoxin to cysteine by mammalian sulfiredoxin. *J Biol Chem.* 2006 May 19;281(20):14400–7.
24. Peskin AV, Low FM, Paton LN, Maghzal GJ, Hampton MB, Winterbourn CC. The high reactivity of peroxiredoxin 2 with H<sub>2</sub>O<sub>2</sub> is not reflected in its reaction with other oxidants and thiol reagents. *J Biol Chem.* 2007 Apr 20;282(16):11885–92.
25. Cox A, Peskin A, Paton L, Winterbourn C, Hampton M. Redox Potential and Peroxide Reactivity of Human Peroxiredoxin 3. *Biochemistry.* 2009 Jul 1;48:6495–501.
26. Parsonage D, Karplus PA, Poole LB. Substrate specificity and redox potential of AhpC, a bacterial peroxiredoxin. *Proc Natl Acad Sci.* 2008 Jun 17;105(24):8209–14.
27. Nagy P, Karton A, Betz A, Peskin AV, Pace P, O'Reilly RJ, et al. Model for the Exceptional Reactivity of Peroxiredoxins 2 and 3 with Hydrogen Peroxide: A KINETIC AND COMPUTATIONAL STUDY \*. *J Biol Chem.* 2011 May 20;286(20):18048–55.
28. Woo HA, Yim SH, Shin DH, Kang D, Yu D-Y, Rhee SG. Inactivation of peroxiredoxin I by phosphorylation allows localized H<sub>2</sub>O<sub>2</sub> accumulation for cell signaling. *Cell.* 2010 Feb 19;140(4):517–28.



29. Holmgren A. Thioredoxin. *Annu Rev Biochem.* 1985;54:237–71.
30. Laurent TC, Moore EC, Reichard P. Enzymatic synthesis of deoxyribonucleotides. iv. isolation and characterization of thioredoxin, the hydrogen donor from *Escherichia coli* B. *J Biol Chem.* 1964 Oct;239:3436–44.
31. Berndt C, Lillig CH, Holmgren A. Thiol-based mechanisms of the thioredoxin and glutaredoxin systems: implications for diseases in the cardiovascular system. *Am J Physiol Heart Circ Physiol.* 2007;292(3):H1227-1236.
32. Carvalho ATP, Swart M, van Stralen JNP, Fernandes PA, Ramos MJ, Bickelhaupt FM. Mechanism of Thioredoxin-Catalyzed Disulfide Reduction. Activation of the Buried Thiol and Role of the Variable Active-Site Residues. *J Phys Chem B.* 2008 Feb 1;112(8):2511–23.
33. Luthman M, Holmgren A. Rat liver thioredoxin and thioredoxin reductase: purification and characterization. *Biochemistry.* 1982 Dec 21;21(26):6628–33.
34. Zhong L, Arnér ESJ, Holmgren A. Structure and mechanism of mammalian thioredoxin reductase: The active site is a redox-active selenolthiol/selenenylsulfide formed from the conserved cysteine-selenocysteine sequence. *Proc Natl Acad Sci U S A.* 2000 May 23;97(11):5854–9.
35. Arnér ES, Holmgren A. Physiological functions of thioredoxin and thioredoxin reductase. *Eur J Biochem FEBS.* 2000 Oct;267(20):6102–9.
36. Arnér ESJ. Focus on mammalian thioredoxin reductases - Important selenoproteins with versatile functions. *Biochim Biophys Acta.* 2009 Jun;1790(6):495–526.
37. Nordberg J, Arnér ES. Reactive oxygen species, antioxidants, and the mammalian thioredoxin system. *Free Radic Biol Med.* 2001 Dec 1;31(11):1287–312.
38. Miranda-Vizuete A, Sadek CM, Jiménez A, Krause WJ, Sutovsky P, Oko R. The mammalian testis-specific thioredoxin system. *Antioxid Redox Signal.* 2004 Feb;6(1):25–40.
39. Holmgren A. Hydrogen donor system for *Escherichia coli* ribonucleoside-diphosphate reductase dependent upon glutathione. *Proc Natl Acad Sci U S A.* 1976 Jul;73(7):2275–9.
40. Holmgren A. Glutathione-dependent synthesis of deoxyribonucleotides. Characterization of the enzymatic mechanism of *Escherichia coli* glutaredoxin. *J Biol Chem.* 1979 May 10;254(9):3672–8.
41. Holmgren A. Glutathione-dependent synthesis of deoxyribonucleotides. Purification and characterization of glutaredoxin from *Escherichia coli*. *J Biol Chem.* 1979 May 10;254(9):3664–71.
42. Trnka D, Hossain MF, Jordt LM, Gellert M, Lillig CH. Role of GSH and Iron-Sulfur

- Glutaredoxins in Iron Metabolism—Review. *Molecules*. 2020 Aug 25;25(17).
43. Gellert M, Hossain MF, Berens FJF, Bruhn LW, Urbainsky C, Liebscher V, et al. Substrate specificity of thioredoxins and glutaredoxins - towards a functional classification. *Heliyon*. 2019 Dec;5(12):e02943.
  44. Prast-Nielsen S, Huang H-H, Williams DL. Thioredoxin glutathione reductase: its role in redox biology and potential as a target for drugs against neglected diseases. *Biochim Biophys Acta*. 2011 Dec;1810(12):1262–71.
  45. Sun Q-A, Su D, Novoselov SV, Carlson BA, Hatfield DL, Gladyshev VN. Reaction mechanism and regulation of mammalian thioredoxin/glutathione reductase. *Biochemistry*. 2005 Nov 8;44(44):14528–37.
  46. Lillig CH. Glutaredoxin systems. *Biochim Biophys Acta*. 2008;1780:1304–17.
  47. Mieyal JJ, Gallogly MM, Qanungo S, Sabens EA, Shelton MD. Molecular mechanisms and clinical implications of reversible protein S-glutathionylation. *Antioxid Redox Signal*. 2008 Nov;10(11):1941–88.
  48. Lillig CH, Berndt C. Glutaredoxins in Thiol/Disulfide Exchange. *Antioxid Redox Signal*. 2012 Dec 11;18(13):1654–65.
  49. Mesecke N, Spang A, Deponte M, Herrmann JM. A Novel Group of Glutaredoxins in the cis-Golgi Critical for Oxidative Stress Resistance. *Mol Biol Cell*. 2008 Jun;19(6):2673–80.
  50. Ströher E, Millar AH. The biological roles of glutaredoxins. *Biochem J*. 2012 Sep 15;446(3):333–48.
  51. Hentze MW, Muckenthaler MU, Galy B, Camaschella C. Two to tango: regulation of Mammalian iron metabolism. *Cell*. 2010 Jul 9;142(1):24–38.
  52. Berndt C, Lillig CH. Glutathione, Glutaredoxins, and Iron. *Antioxid Redox Signal*. 2017 Nov 20;27(15):1235–51.
  53. Rodríguez-Manzaneque MT, Tamarit J, Bellí G, Ros J, Herrero E. Grx5 is a mitochondrial glutaredoxin required for the activity of iron/sulfur enzymes. *Mol Biol Cell*. 2002 Apr;13(4):1109–21.
  54. Lillig CH, Berndt C, Vergnolle O, Lönn ME, Hudemann C, Bill E, et al. Characterization of human glutaredoxin 2 as iron-sulfur protein: a possible role as redox sensor. *Proc Natl Acad Sci U S A*. 2005 Jun 7;102(23):8168–73.
  55. Mühlhoff U, Molik S, Godoy JR, Uzarska MA, Richter N, Seubert A, et al. Cytosolic monothiol glutaredoxins function in intracellular iron sensing and trafficking via their bound iron-sulfur cluster. *Cell Metab*. 2010 Oct 6;12(4):373–85.
  56. Rouhier N, Couturier J, Johnson MK, Jacquot J-P. Glutaredoxins: roles in iron homeostasis. *Trends Biochem Sci*. 2010 Jan;35(1):43–52.

57. Bandyopadhyay S, Chandramouli K, Johnson MK. Iron-sulfur cluster biosynthesis. *Biochem Soc Trans.* 2008 Dec;36(Pt 6):1112–9.
58. Braymer JJ, Lill R. Iron-sulfur cluster biogenesis and trafficking in mitochondria. *J Biol Chem.* 2017 04;292(31):12754–63.
59. Feng Y, Zhong N, Rouhier N, Hase T, Kusunoki M, Jacquot J-P, et al. Structural insight into poplar glutaredoxin C1 with a bridging iron-sulfur cluster at the active site. *Biochemistry.* 2006 Jul 4;45(26):7998–8008.
60. Berndt C, Hudemann C, Hanschmann E-M, Axelsson R, Holmgren A, Lillig CH. How does iron-sulfur cluster coordination regulate the activity of human glutaredoxin 2? *Antioxid Redox Signal.* 2007 Jan;9(1):151–7.
61. Rouhier N, Unno H, Bandyopadhyay S, Masip L, Kim S-K, Hirasawa M, et al. Functional, structural, and spectroscopic characterization of a glutathione-ligated [2Fe-2S] cluster in poplar glutaredoxin C1. *Proc Natl Acad Sci U S A.* 2007 May 1;104(18):7379–84.
62. Sipos K, Lange H, Fekete Z, Ullmann P, Lill R, Kispal G. Maturation of cytosolic iron-sulfur proteins requires glutathione. *J Biol Chem.* 2002 Jul 26;277(30):26944–9.
63. Mackenzie EL, Iwasaki K, Tsuji Y. Intracellular Iron Transport and Storage: From Molecular Mechanisms to Health Implications. *Antioxid Redox Signal.* 2008 Jun;10(6):997–1030.
64. Müllner EW, Neupert B, Kühn LC. A specific mRNA binding factor regulates the iron-dependent stability of cytoplasmic transferrin receptor mRNA. *Cell.* 1989 Jul;58(2):373–82.
65. Volz K. The functional duality of iron regulatory protein 1. *Curr Opin Struct Biol.* 2008 Feb;18(1):106–11.
66. Sheftel AD, Wilbrecht C, Stehling O, Niggemeyer B, Elsässer H-P, Mühlenhoff U, et al. The human mitochondrial ISCA1, ISCA2, and IBA57 proteins are required for [4Fe-4S] protein maturation. *Mol Biol Cell.* 2012 Apr;23(7):1157–66.
67. Weiler BD, Brück M-C, Kothe I, Bill E, Lill R, Mühlenhoff U. Mitochondrial [4Fe-4S] protein assembly involves reductive [2Fe-2S] cluster fusion on ISCA1–ISCA2 by electron flow from ferredoxin FDX2. *Proc Natl Acad Sci.* 2020 Aug 25;117(34):20555–65.
68. Hudemann C, Lönn ME, Godoy JR, Zahedi Avval F, Capani F, Holmgren A, et al. Identification, expression pattern, and characterization of mouse glutaredoxin 2 isoforms. *Antioxid Redox Signal.* 2009 Jan;11(1):1–14.
69. Lundberg M, Johansson C, Chandra J, Enoksson M, Jacobsson G, Ljung J, et al. Cloning and expression of a novel human glutaredoxin (Grx2) with mitochondrial and nuclear isoforms. *J Biol Chem.* 2001 Jul 13;276(28):26269–75.

70. Johansson C, Lillig CH, Holmgren A. Human Mitochondrial Glutaredoxin Reduces S-Glutathionylated Proteins with High Affinity Accepting Electrons from Either Glutathione or Thioredoxin Reductase. *J Biol Chem.* 2004;279(9):7537–43.
71. Gladyshev VN, Liu A, Novoselov SV, Krysan K, Sun QA, Kryukov VM, et al. Identification and characterization of a new mammalian glutaredoxin (thioltransferase), Grx2. *J Biol Chem.* 2001 Aug 10;276(32):30374–80.
72. Schütte LD, Baumeister S, Weis B, Hudemann C, Hanschmann E-M, Lillig CH. Identification of potential protein dithiol-disulfide substrates of mammalian Grx2. *Biochim Biophys Acta.* 2013 Nov;1830(11):4999–5005.
73. Gellert M, Venz S, Mitlöhner J, Cott C, Hanschmann E-M, Lillig CH. Identification of a dithiol-disulfide switch in collapsin response mediator protein 2 (CRMP2) that is toggled in a model of neuronal differentiation. *J Biol Chem.* 2013 Dec 6;288(49):35117–25.
74. Bräutigam L, Schütte LD, Godoy JR, Prozorovski T, Gellert M, Hauptmann G, et al. Vertebrate-specific glutaredoxin is essential for brain development. *Proc Natl Acad Sci U S A.* 2011 Dec 20;108(51):20532–7.
75. Gellert M, Richter E, Mostertz J, Kantz L, Masur K, Hanschmann E-M, et al. The cytosolic isoform of glutaredoxin 2 promotes cell migration and invasion. *Biochim Biophys Acta - Gen Subj.* 2020;1864(7):129599.
76. Roth L, Koncina E, Satkauskas S, Crémel G, Aunis D, Bagnard D. The many faces of semaphorins: from development to pathology. *Cell Mol Life Sci.* 2008 Oct 27;66(4):649.
77. Epstein JA, Aghajanian H, Singh MK. Semaphorin signaling in cardiovascular development. *Cell Metab.* 2015 Feb 3;21(2):163–73.
78. Lu Q, Zhu L. The Role of Semaphorins in Metabolic Disorders. *Int J Mol Sci.* 2020 Jan;21(16):5641.
79. Neufeld G, Kessler O. The semaphorins: versatile regulators of tumour progression and tumour angiogenesis. *Nat Rev Cancer.* 2008 Aug;8(8):632–45.
80. Jongbloets BC, Pasterkamp RJ. Semaphorin signalling during development. *Dev Camb Engl.* 2014 Sep;141(17):3292–7.
81. Behar O, Golden JA, Mashimo H, Schoen FJ, Fishman MC. Semaphorin III is needed for normal patterning and growth of nerves, bones and heart. *Nature.* 1996 Oct 10;383(6600):525–8.
82. Uesaka N, Uchigashima M, Mikuni T, Nakazawa T, Nakao H, Hirai H, et al. Retrograde semaphorin signaling regulates synapse elimination in the developing mouse brain. *Science.* 2014 May 30;344(6187):1020–3.

83. Pasterkamp RJ. Getting neural circuits into shape with semaphorins. *Nat Rev Neurosci*. 2012 Sep;13(9):605–18.
84. Morita A, Yamashita N, Sasaki Y, Uchida Y, Nakajima O, Nakamura F, et al. Regulation of Dendritic Branching and Spine Maturation by Semaphorin3A-Fyn Signaling. *J Neurosci*. 2006 Mar 15;26(11):2971–80.
85. Fenstermaker V, Chen Y, Ghosh A, Yuste R. Regulation of dendritic length and branching by semaphorin 3A. *J Neurobiol*. 2004;58(3):403–12.
86. Fujisawa H. Discovery of semaphorin receptors, neuropilin and plexin, and their functions in neural development. *J Neurobiol*. 2004;59(1):24–33.
87. He Z, Tessier-Lavigne M. Neuropilin Is a Receptor for the Axonal Chemorepellent Semaphorin III. *Cell*. 1997 Aug 22;90(4):739–51.
88. Takahashi T, Fournier A, Nakamura F, Wang L-H, Murakami Y, Kalb RG, et al. Plexin-Neuropilin-1 Complexes Form Functional Semaphorin-3A Receptors. *Cell*. 1999 Oct 1;99(1):59–69.
89. Sasaki Y, Cheng C, Uchida Y, Nakajima O, Ohshima T, Yagi T, et al. Fyn and Cdk5 mediate Semaphorin-3A signaling, which is involved in regulation of dendrite orientation in cerebral cortex. *Neuron*. 2002 Aug 29;35(5):907–20.
90. Eickholt BJ, Walsh FS, Doherty P. An inactive pool of GSK-3 at the leading edge of growth cones is implicated in Semaphorin 3A signaling. *J Cell Biol*. 2002 Apr 15;157(2):211–7.
91. Terman JR, Mao T, Pasterkamp RJ, Yu H-H, Kolodkin AL. MICALs, a family of conserved flavoprotein oxidoreductases, function in Plexin-mediated axonal repulsion. *Cell*. 2002 Jun 28;109(7):887–900.
92. Hung R-J, Pak CW, Terman JR. Direct redox regulation of F-actin assembly and disassembly by Mical. *Science*. 2011 Dec 23;334(6063):1710–3.
93. Hung R-J, Yazdani U, Yoon J, Wu H, Yang T, Gupta N, et al. Mical links semaphorins to F-actin disassembly. *Nature*. 2010 Feb 11;463(7282):823–7.
94. Schmidt EF, Strittmatter SM. The CRMP family of proteins and their role in Sema3A signaling. *Adv Exp Med Biol*. 2007;600:1–11.
95. Arimura N, Menager C, Fukata Y, Kaibuchi K. Role of CRMP-2 in neuronal polarity. *J Neurobiol*. 2004 Jan;58(1):34–47.
96. Jiang T, Zhang G, Liang Y, Cai Z, Liang Z, Lin H, et al. PlexinA3 interacts with CRMP2 to mediate Sema3A signalling during dendritic growth in cultured cerebellar granule neurons. *Neuroscience*. 2020 May 10;434:83–92.
97. Morinaka A, Yamada M, Itofusa R, Funato Y, Yoshimura Y, Nakamura F, et al. Thioredoxin mediates oxidation-dependent phosphorylation of CRMP2 and growth

- cone collapse. *Sci Signal*. 2011;4(170):ra26.
98. Suzuki T, Nakamoto T, Ogawa S, Seo S, Matsumura T, Tachibana K, et al. MICAL, a novel CasL interacting molecule, associates with Vimentin\*. *J Biol Chem*. 2002 Apr 26;277(17):14933–41.
  99. Sakai R, Iwamatsu A, Hirano N, Ogawa S, Tanaka T, Mano H, et al. A novel signaling molecule, p130, forms stable complexes in vivo with v-Crk and v-Src in a tyrosine phosphorylation-dependent manner. *EMBO J*. 1994 Aug 1;13(16):3748–56.
  100. Sattler M, Salgia R, Shrikhande G, Verma S, Uemura N, Law SF, et al. Differential signaling after  $\beta$ 1 Integrin ligation is mediated through binding of CRKL to p120CBL and p110HEF1\*. *J Biol Chem*. 1997 May 30;272(22):14320–6.
  101. Giridharan SSP, Caplan S. MICAL-family proteins: Complex regulators of the actin cytoskeleton. *Antioxid Redox Signal*. 2014 May 1;20(13):2059–73.
  102. Weide T, Teuber J, Bayer M, Barnekow A. MICAL-1 isoforms, novel Rab1 interacting proteins. *Biochem Biophys Res Commun*. 2003 Jun 20;306(1):79–86.
  103. Kolk SM, Pasterkamp RJ. MICAL flavoprotein monooxygenases: structure, function and role in semaphorin signaling. *Adv Exp Med Biol*. 2007;600:38–51.
  104. Pasterkamp RJ, Dai H, Terman JR, Wahlin KJ, Kim B, Bregman BS, et al. MICAL flavoprotein monooxygenases: Expression during neural development and following spinal cord injuries in the rat. *Mol Cell Neurosci*. 2006 Jan 1;31(1):52–69.
  105. Sharma M, Giridharan SSP, Rahajeng J, Naslavsky N, Caplan S. MICAL-L1 links EHD1 to tubular recycling endosomes and regulates receptor recycling. *Mol Biol Cell*. 2009 Dec;20(24):5181–94.
  106. Nakatsuji H, Nishimura N, Yamamura R, Kanayama H-O, Sasaki T. Involvement of actinin-4 in the recruitment of JRAB/MICAL-L2 to cell-cell junctions and the formation of functional tight junctions. *Mol Cell Biol*. 2008 May;28(10):3324–35.
  107. Sakane A, Honda K, Sasaki T. Rab13 regulates neurite outgrowth in PC12 cells through its effector protein, JRAB/MICAL-L2. *Mol Cell Biol*. 2010 Feb;30(4):1077–87.
  108. Bañuelos S, Saraste M, Djinović Carugo K. Structural comparisons of calponin homology domains: implications for actin binding. *Struct Lond Engl* 1993. 1998 Nov 15;6(11):1419–31.
  109. Gimona M, Djinovic-Carugo K, Kranewitter WJ, Winder SJ. Functional plasticity of CH domains. *FEBS Lett*. 2002 Feb 20;513(1):98–106.
  110. Korenbaum E, Rivero F. Calponin homology domains at a glance. *J Cell Sci*. 2002 Sep 15;115(18):3543–5.
  111. Kim J, Lee H, Roh YJ, Kim H, Shin D, Kim S, et al. Structural and kinetic insights

- into flavin-containing monooxygenase and calponin-homology domains in human MICAL3. *IUCrJ*. 2020 Jan 1;7(Pt 1):90–9.
112. Freyd G, Kim SK, Horvitz HR. Novel cysteine-rich motif and homeodomain in the product of the *Caenorhabditis elegans* cell lineage gene *lin-II*. *Nature*. 1990 Apr;344(6269):876–9.
  113. Kadrmas JL, Beckerle MC. The LIM domain: from the cytoskeleton to the nucleus. *Nat Rev Mol Cell Biol*. 2004 Nov;5(11):920–31.
  114. Bach I. The LIM domain: regulation by association. *Mech Dev*. 2000 Mar 1;91(1–2):5–17.
  115. Zheng Q, Zhao Y. The diverse biofunctions of LIM domain proteins: determined by subcellular localization and protein-protein interaction. *Biol Cell*. 2007 Sep;99(9):489–502.
  116. Esposito A, Ventura V, Petoukhov MV, Rai A, Svergun DI, Vanoni MA. Human MICAL1: Activation by the small GTPase Rab8 and small-angle X-ray scattering studies on the oligomerization state of MICAL1 and its complex with Rab8. *Protein Sci Publ Protein Soc*. 2019;28(1):150–66.
  117. Fischer J, Weide T, Barnekow A. The MICAL proteins and Rab1: a possible link to the cytoskeleton? *Biochem Biophys Res Commun*. 2005 Mar 11;328(2):415–23.
  118. Kobayashi H, Etoh K, Ohbayashi N, Fukuda M. Rab35 promotes the recruitment of Rab8, Rab13 and Rab36 to recycling endosomes through MICAL-L1 during neurite outgrowth. *Biol Open*. 2014 Sep 15;3(9):803–14.
  119. Fukuda M, Kanno E, Ishibashi K, Itoh T. Large scale screening for novel Rab effectors reveals unexpected broad Rab binding specificity. *Mol Cell Proteomics*. 2008 Jul 1;7:1031–42.
  120. Rahajeng J, Giridharan SSP, Cai B, Naslavsky N, Caplan S. Important relationships between Rab and MICAL proteins in endocytic trafficking. *World J Biol Chem*. 2010 Aug 26;1(8):254–64.
  121. Schmidt EF, Shim S-O, Strittmatter SM. Release of MICAL autoinhibition by semaphorin-plexin signaling promotes interaction with collapsin response mediator protein. *J Neurosci Off J Soc Neurosci*. 2008 Feb 27;28(9):2287–97.
  122. Wierenga RK, de Jong RJ, Kalk KH, Hol WGJ, Drenth J. Crystal structure of p-hydroxybenzoate hydroxylase. *J Mol Biol*. 1979 Jun 15;131(1):55–73.
  123. Siebold C, Berrow N, Walter TS, Harlos K, Owens RJ, Stuart DI, et al. High-resolution structure of the catalytic region of MICAL (molecule interacting with CasL), a multidomain flavoenzyme-signaling molecule. *Proc Natl Acad Sci U S A*. 2005 Nov 15;102(46):16836–41.

124. Nadella M, Bianchet MA, Gabelli SB, Barrila J, Amzel LM. Structure and activity of the axon guidance protein MICAL. *Proc Natl Acad Sci U S A*. 2005 Nov 15;102(46):16830–5.
125. Wang J, Ortiz-Maldonado M, Entsch B, Massey V, Ballou D, Gatti DL. Protein and ligand dynamics in 4-hydroxybenzoate hydroxylase. *Proc Natl Acad Sci*. 2002 Jan 22;99(2):608–13.
126. Gatti DL, Palfey BA, Lah MS, Entsch B, Massey V, Ballou DP, et al. The mobile flavin of 4-OH benzoate hydroxylase. *Science*. 1994 Oct 7;266(5182):110–4.
127. Brender J, Dertouzos J, Ballou D, Massey V, Palfey B, Entsch B, et al. Conformational dynamics of the isoalloxazine in substrate-free p -hydroxybenzoate hydroxylase: single-molecule studies. *J Am Chem Soc*. 2006 Jan 1;127:18171–8.
128. Möller D, Gellert M, Langel W, Lillig CH. Molecular dynamics simulations and in vitro analysis of the CRMP2 thiol switch. *Mol Biosyst*. 2017 Aug 22;13(9):1744–53.
129. Stöcker S, Maurer M, Ruppert T, Dick TP. A role for 2-Cys peroxiredoxins in facilitating cytosolic protein thiol oxidation. *Nat Chem Biol*. 2018 Feb;14(2):148–55.
130. Delaunay A, Pflieger D, Barrault MB, Vinh J, Toledano MB. A thiol peroxidase is an H<sub>2</sub>O<sub>2</sub> receptor and redox-transducer in gene activation. *Cell*. 2002 Nov 15;111(4):471–81.
131. Fomenko DE, Koc A, Agisheva N, Jacobsen M, Kaya A, Malinouski M, et al. Thiol peroxidases mediate specific genome-wide regulation of gene expression in response to hydrogen peroxide. *Proc Natl Acad Sci U S A*. 2011 Feb 15;108(7):2729–34.
132. Jarvis RM, Hughes SM, Ledgerwood EC. Peroxiredoxin 1 functions as a signal peroxidase to receive, transduce, and transmit peroxide signals in mammalian cells. *Free Radic Biol Med*. 2012 Oct 1;53(7):1522–30.
133. Sobotta MC, Liou W, Stöcker S, Talwar D, Oehler M, Ruppert T, et al. Peroxiredoxin-2 and STAT3 form a redox relay for H<sub>2</sub>O<sub>2</sub> signaling. *Nat Chem Biol*. 2015 Jan;11(1):64–70.
134. Terman JR, Kashina A. Post-translational modification and regulation of actin. *Curr Opin Cell Biol*. 2013 Feb;25(1):30–8.
135. Wilson C, Terman JR, González-Billault C, Ahmed G. Actin filaments-A target for redox regulation. *Cytoskelet Hoboken NJ*. 2016 Oct;73(10):577–95.
136. Dalle-Donne I, Rossi R, Giustarini D, Gagliano N, Di Simplicio P, Colombo R, et al. Methionine oxidation as a major cause of the functional impairment of oxidized actin. *Free Radic Biol Med*. 2002 May 1;32(9):927–37.
137. Richardson DE, Regino CAS, Yao H, Johnson JV. Methionine oxidation by peroxydicarbonate, a reactive oxygen species formed from CO<sub>2</sub>/bicarbonate and



- hydrogen peroxide. *Free Radic Biol Med*. 2003 Dec 15;35(12):1538–50.
138. Dominguez R, Holmes KC. Actin Structure and Function. *Annu Rev Biophys*. 2011 May 5;40(1):169–86.
  139. Feuer G, Molnár F, Pettkó E, Straub F. Studies on the composition and polymerization of actin. *Hung Acta Physiol*. 1948;1:150.
  140. Zucchini D, Caprini G, Pasterkamp RJ, Tedeschi G, Vanoni MA. Kinetic and spectroscopic characterization of the putative monooxygenase domain of human MICAL-1. *Arch Biochem Biophys*. 2011 Nov;515(1–2):1–13.
  141. McDonald CA, Liu YY, Palfey BA. Actin stimulates reduction of the MICAL-2 monooxygenase domain. *Biochemistry*. 2013 Sep 3;52(35):6076–84.
  142. Wu H, Yesilyurt HG, Yoon J, Terman JR. The MICALs are a family of F-actin dismantling oxidoreductases conserved from *Drosophila* to humans. *Sci Rep*. 2018 Jan 17;8(1):937.
  143. Lavine TF. The formation, resolution, and optical properties of the diastereoisomeric sulfoxides derived from L-methionine. *J Biol Chem*. 1947 Aug 1;169(3):477–91.
  144. Sharov VS, Schöneich C. Diastereoselective protein methionine oxidation by reactive oxygen species and diastereoselective repair by methionine sulfoxide reductase. *Free Radic Biol Med*. 2000 Nov 15;29(10):986–94.
  145. Grimaud R, Ezraty B, Mitchell JK, Lafitte D, Briand C, Derrick PJ, et al. Repair of Oxidized Proteins: IDENTIFICATION OF A NEW METHIONINE SULFOXIDE REDUCTASE\*. *J Biol Chem*. 2001 Dec 28;276(52):48915–20.
  146. Moskovitz J, Singh VK, Requena J, Wilkinson BJ, Jayaswal RK, Stadtman ER. Purification and characterization of methionine sulfoxide reductases from mouse and *Staphylococcus aureus* and their substrate stereospecificity. *Biochem Biophys Res Commun*. 2002 Jan 11;290(1):62–5.
  147. Lee BC, Péterfi Z, Hoffmann FW, Moore RE, Kaya A, Avanesov A, et al. MsrB1 and MICALs regulate actin assembly and macrophage function via reversible stereoselective methionine oxidation. *Mol Cell*. 2013 Aug 8;51(3):397–404.
  148. Gabbita SP, Aksenov MY, Lovell MA, Markesbery WR. Decrease in peptide methionine sulfoxide reductase in Alzheimer's disease brain. *J Neurochem*. 1999 Oct;73(4):1660–6.
  149. Moskovitz J, Flescher E, Berlett BS, Azare J, Poston JM, Stadtman ER. Overexpression of peptide-methionine sulfoxide reductase in *Saccharomyces cerevisiae* and human T cells provides them with high resistance to oxidative stress. *Proc Natl Acad Sci*. 1998 Nov 24;95(24):14071–5.
  150. Ruan H, Tang XD, Chen M-L, Joiner MA, Sun G, Brot N, et al. High-quality life

- extension by the enzyme peptide methionine sulfoxide reductase. *Proc Natl Acad Sci.* 2002 Mar 5;99(5):2748–53.
151. Moskovitz J, Bar-Noy S, Williams WM, Requena J, Berlett BS, Stadtman ER. Methionine sulfoxide reductase (MsrA) is a regulator of antioxidant defense and lifespan in mammals. *Proc Natl Acad Sci.* 2001 Nov 6;98(23):12920–5.
  152. Olry A, Boschi-Muller S, Marraud M, Sanglier-Cianferani S, Dorsselear AV, Branlant G. Characterization of the Methionine Sulfoxide Reductase Activities of PILB, a Probable Virulence Factor from *Neisseria meningitidis* \*. *J Biol Chem.* 2002 Apr 5;277(14):12016–22.
  153. Etienne F, Spector D, Brot N, Weissbach H. A methionine sulfoxide reductase in *Escherichia coli* that reduces the R enantiomer of methionine sulfoxide. *Biochem Biophys Res Commun.* 2003 Jan 10;300(2):378–82.
  154. Kryukov GV, Kumar RA, Koc A, Sun Z, Gladyshev VN. Selenoprotein R is a zinc-containing stereo-specific methionine sulfoxide reductase. *Proc Natl Acad Sci.* 2002 Apr 2;99(7):4245–50.
  155. Kumar RA, Koc A, Cerny RL, Gladyshev VN. Reaction Mechanism, Evolutionary Analysis, and Role of Zinc in *Drosophila* Methionine-R-sulfoxide Reductase \*. *J Biol Chem.* 2002 Oct 4;277(40):37527–35.
  156. Moskovitz J, Stadtman ER. Selenium-deficient diet enhances protein oxidation and affects methionine sulfoxide reductase (MsrB) protein level in certain mouse tissues. *Proc Natl Acad Sci.* 2003 Jun 24;100(13):7486–90.
  157. Jung S, Hansel A, Kasperczyk H, Hoshi T, Heinemann SH. Activity, tissue distribution and site-directed mutagenesis of a human peptide methionine sulfoxide reductase of type B: hCBS1. *FEBS Lett.* 2002;527(1–3):91–4.
  158. Kim H-Y, Gladyshev VN. Methionine sulfoxide reduction in mammals: characterization of methionine-R-sulfoxide reductases. *Mol Biol Cell.* 2003 Dec 29;15(3):1055–64.
  159. Boschi-Muller S, Gand A, Branlant G. The methionine sulfoxide reductases: Catalysis and substrate specificities. *Arch Biochem Biophys.* 2008 Jun 15;474(2):266–73.
  160. Tarrago L, Gladyshev VN. Recharging oxidative protein repair: catalysis by methionine sulfoxide reductases towards their amino acid, protein, and model substrates. *Biochem Biokhimiia.* 2012 Oct;77(10):1097–107.
  161. Lourenço dos Santos S, Petropoulos I, Friguet B. The oxidized protein repair enzymes methionine sulfoxide reductases and their roles in protecting against oxidative stress, in ageing and in regulating protein function. *Antioxidants.* 2018 Dec 12;7(12).
  162. Li W, Herman RK, Shaw JE. Analysis of the *Caenorhabditis elegans* axonal guidance and outgrowth gene *unc-33*. *Genetics.* 1992 Nov;132(3):675–89.

163. Quinn CC, Chen E, Kinjo TG, Kelly G, Bell AW, Elliott RC, et al. TUC-4b, a novel TUC family variant, regulates neurite outgrowth and associates with vesicles in the growth cone. *J Neurosci Off J Soc Neurosci*. 2003 Apr 1;23(7):2815–23.
164. Tan M, Cha C, Ye Y, Zhang J, Li S, Wu F, et al. CRMP4 and CRMP2 Interact to Coordinate Cytoskeleton Dynamics, Regulating Growth Cone Development and Axon Elongation. *Neural Plast*. 2015;2015:1–13.
165. Nagai J, Baba R, Ohshima T. CRMPs Function in Neurons and Glial Cells: Potential Therapeutic Targets for Neurodegenerative Diseases and CNS Injury. *Mol Neurobiol*. 2017 Aug 1;54(6):4243–56.
166. Goshima Y, Nakamura F, Strittmatter P, Strittmatter SM. Collapsin-induced growth cone collapse mediated by an intracellular protein related to UNC-33. *Nature*. 1995 Aug 10;376(6540):509–14.
167. Nakamura F, Ohshima T, Goshima Y. Collapsin Response Mediator Proteins: Their Biological Functions and Pathophysiology in Neuronal Development and Regeneration. *Front Cell Neurosci*. 2020;14.
168. Wang LH, Strittmatter SM. Brain CRMP forms heterotetramers similar to liver dihydropyrimidinase. *J Neurochem*. 1997 Dec;69(6):2261–9.
169. Stenmark P, Ogg D, Flodin S, Flores A, Kotenyova T, Nyman T, et al. The structure of human collapsin response mediator protein 2, a regulator of axonal growth. *J Neurochem*. 2007 May;101(4):906–17.
170. Ahmed A, Eickholt BJ. Intracellular kinases in semaphorin signaling. *Adv Exp Med Biol*. 2007;600:24–37.
171. Yoshimura T, Kawano Y, Arimura N, Kawabata S, Kikuchi A, Kaibuchi K. GSK-3 $\beta$  Regulates Phosphorylation of CRMP-2 and Neuronal Polarity. *Cell*. 2005 Jan 14;120(1):137–49.
172. Fukata Y, Itoh TJ, Kimura T, Ménager C, Nishimura T, Shiromizu T, et al. CRMP-2 binds to tubulin heterodimers to promote microtubule assembly. *Nat Cell Biol*. 2002 Aug;4(8):583–91.
173. Hensley K, Venkova K, Christov A, Gunning W, Park J. Collapsin response mediator protein-2: an emerging pathologic feature and therapeutic target for neurodegeneration. *Mol Neurobiol*. 2011 Jun;43(3):180–91.
174. Togashi K, Hasegawa M, Nagai J, Kotaka K, Yazawa A, Takahashi M, et al. Lanthionine ketimine ester improves outcome in an MPTP-induced mouse model of Parkinson's disease via suppressions of CRMP2 phosphorylation and microglial activation. *J Neurol Sci*. 2020 15;413:116802.
175. Dupree JL, Polak PE, Hensley K, Pelligrino D, Feinstein DL. Lanthionine ketimine ester provides benefit in a mouse model of multiple sclerosis. *J Neurochem*. 2015

- Jul;134(2):302–14.
176. Kotaka K, Nagai J, Hensley K, Ohshima T. Lanthionine ketimine ester promotes locomotor recovery after spinal cord injury by reducing neuroinflammation and promoting axon growth. *Biochem Biophys Res Commun.* 2017 Jan 29;483(1):759–64.
  177. Kallis GB, Holmgren A. Differential reactivity of the functional sulfhydryl groups of cysteine-32 and cysteine-35 present in the reduced form of thioredoxin from *Escherichia coli*. *J Biol Chem.* 1980 Nov 10;255(21):10261–5.
  178. Pace PE, Peskin AV, Konigstorfer A, Jasoni CJ, Winterbourn CC, Hampton MB. Peroxiredoxin interaction with the cytoskeletal-regulatory protein CRMP2: Investigation of a putative redox relay. *Free Radic Biol Med.* 2018 Dec;129:383–93.
  179. Perkins A, Nelson KJ, Parsonage D, Poole LB, Karplus PA. Peroxiredoxins: Guardians Against Oxidative Stress and Modulators of Peroxide Signaling. *Trends Biochem Sci.* 2015 Aug;40(8):435–45.
  180. Winterbourn CC, Hampton MB. Signaling via a peroxiredoxin sensor. *Nat Chem Biol.* 2015 Jan;11(1):5–6.
  181. Netto LES, Antunes F. The Roles of Peroxiredoxin and Thioredoxin in Hydrogen Peroxide Sensing and in Signal Transduction. *Mol Cells.* 2016 Jan 31;39(1):65–71.

## 5 Abbreviations

CC	Coiled coil (motif)
Cdk5	Cyclin dependent kinase 5
CH	Calponin homology (domain)
C <sub>P</sub>	Peroxidatic cysteinyl residue
C <sub>R</sub>	Resolving cysteinyl residue
CRMP	Collapsin response mediator protein
CTD	C-terminal domain
D-loop	Deoxyribonuclease I binding loop
DNA	Deoxyribonucleic acid
DPYSL2	Dihydropyrimidinase like 2
F-actin	Filamentous actin
FAD	Flavin adenine dinucleotide
FeS	Iron-sulfur cluster
G-actin	Globular actin
GR	Glutathione reductase
GPx	Glutathione peroxidase
Grx	Glutaredoxin
GSH	Glutathione
GSK3 $\beta$	Glycogen synthase kinase 3 beta
GTPase	Guanosine triphosphate hydrolase
hTrx1	Human thioredoxin 1
hTrx1R	Human thioredoxin reductase 1
HSP70	Heat shock protein 70
IRE	Iron responsive elements
IRP	Iron regulatory protein
ISC	Iron-sulfur cluster assembly machinery
LIM	LIN-11, Isl-1, and MEC-3 like (domain)
MICAL	Molecule interacting with CasL
MICAL-L	MICAL-like
mMICAL	Mouse MICAL
MO	Monooxygenase (domain)
mRNA	Messenger ribonucleic acid
Msr	Methionyl sulfoxide reductase

---

NADPH	Nicotinamide adenine dinucleotide phosphate
NP	Neuropilin
Orp1	Oxidant receptor peroxidase 1
pHBH	<i>para</i> -hydroxybenzoate hydroxylase
PlexA	Plexin A
Prx	Peroxiredoxin
R-MetO	R-methionyl sulfoxide
RBD	Rab binding domain
RNR	Ribonucleotide reductase
S-MetO	S-methionyl sulfoxide
Sec	Selenocysteine
SelR	Selenoprotein R
Sem	Semaphorin
SH3	Sarcoma homology 3 (domain)
Srx	Sulfiredoxin
TfR	Transferrin receptor
Trx	Thioredoxin
TrxR	Thioredoxin reductase
Yap1	Yes-associated protein 1

## 6 Author contributions

1. **Ortegón Salas C**, Schneider K, Lillig CH, Gellert M. Signal-regulated oxidation of proteins via MICAL. *Biochem Soc Trans.* 2020 Apr 29;48(2): 613-620. doi: [10.1042/BST20190866](https://doi.org/10.1042/BST20190866)  
COS, KS, CHL and MG conceived and designed this review article. COS did the literature research for this review, COS and CHL wrote the text and prepare all the figures. MG reviewed the article.
2. Hossain MD, Bodnar Y, Klein K, **Ortegón Salas C**, Arnér ESJ, Gellert M, Lillig CH. Molecular basis for the interactions of human thioredoxins with their respective reductases. *Oxid Med Cell Longev.* 2021. doi: [10.1155/2021/6621292](https://doi.org/10.1155/2021/6621292)  
EA, MG and CHL conceptualized the study and analyzed the data. MFH, YB, EA, MG and CHL wrote the paper, and COS reviewed the article. MFH, YB, CK, COS and MG performed and analyzed the experiments. In particular, COS performed complementation assays of human and *E. coli* Trx1 with TrxR1, purified human thioredoxin wild-type and mutants, performed kinetics assays, and analyzed the results. She prepared supplementary Fig. 5.
3. **Ortegón Salas C**, Bodnar Y, Uhlenkamp D, Schneider K, Knaup L, Deponte M, Berndt C, Lillig CH, Gellert M. NADPH-dependent oxidation of CRMP2 through a MICAL1-Prx1 redox relay controls neurite outgrowth. Submitted to *Science*. Manuscript number: abj9997  
CB, CHL, MD and MG conceived the study and designed the experiments. COS, DU, KS, LK and MG performed the experiments, YB the molecular dynamics analysis. All authors analyzed the data. CB, CHL, COS and MG wrote the paper. In particular, COS performed and analyzed all *in vitro* and cell based experiments (Fig. 1, 2, 3, 5, and supplementary material except supplementary Fig. 8).

Greifswald, 16.06.2021

## 7 Publications

### 7.1 Publications in peer reviewed journals

- I. **Ortegón Salas C**, Schneider K, Lillig CH, Gellert M. Signal-regulated oxidation of proteins via MICAL. *Biochemical Society Transactions* 48 (2), 613-620, 2020. doi: [10.1042/BST20190866](https://doi.org/10.1042/BST20190866)
- II. Hossain MD, Bodnar Y, Klein K, **Ortegón Salas C**, Arnér ESJ, Gellert M, Lillig CH. Molecular basis for the interactions of human thioredoxins with their respective reductases. *Oxidative Medicine and Cellular Longevity*, 2021. doi: [10.1155/2021/6621292](https://doi.org/10.1155/2021/6621292)

### 7.2 Submitted manuscripts

- III. **Ortegón Salas C**, Bodnar Y, Uhlenkamp D, Schneider K, Knaup L, Deponte M, Berndt C, Lillig CH, Gellert M. NADPH-dependent oxidation of CRMP2 through a MICAL1-Prx1 redox relay controls neurite outgrowth. Submitted to *Science*. Manuscript number: abj9997

### 7.3 Publications not included in this thesis

- IV. García Hernández M, **Ortegón Salas C**, Oset Gasque MJ. Protein etiology of Alzheimer's disease. *Reduca*, 6 (1), 312-316, 2014. [reduca/article1719/1736](https://doi.org/10.1007/s12017-014-0173-6)

### 7.4 Submitted manuscripts not included in this thesis

- V. Berndt C, Hanschmann EM, Urbainsky C, Jordt LM, Müller CS, Bodnar Y, Schipper S, Handorf O, Nowack R, **Ortegón Salas C**, Gellert M, Moulis JM, Schulzke C, Schünemann V, Lillig CH. FeS-cluster coordination of vertebrate thioredoxins regulates suppression of hypoxia-induced factor 2 $\alpha$  through iron regulatory protein 1. Submitted to *Proc. Natl. Acad. Sci. USA*, under revision, 2020

### 7.5 Book chapters

- VI. **Ortegón Salas C**, Gellert M, Lillig CH. Redox regulation of cytoskeletal dynamics. Chapter in book *Redox regulation of differentiation and de-differentiation*. CRC Press Taylor & Francis Group, in press, 2021. ISBN 9780367895662



## 7.6 Further scientific achievements

### 7.6.1 Published abstracts

- VII. **Ortegón Salas C**, Knaup LK, Schneider K, Scharf C, Berndt C, Deponte M, Lillig CH, Gellert M. Receptor-induced Redox Signalling Relay - From Signal to Effector. *Free Radical Biology and Medicine*, 159 (1), S118, 2020. doi: [10.1016/j.freeradbiomed.2020.10.298](https://doi.org/10.1016/j.freeradbiomed.2020.10.298)

### 7.6.2 Invited talks

- VIII. **Ortegón Salas C**, Uhlenkamp D, Gellert M, Deponte M, Berndt C, Lillig CH. Signal-regulated oxidation of proteins in the cytosol via a flavo-monooxygenase-disulfide relay at the cell membrane. 3<sup>rd</sup> Annual Workshop of the Research Training Group 1947-BiOx, 5<sup>th</sup>-6<sup>th</sup> October 2017, Greifswald, Germany
- IX. **Ortegón Salas C**, Uhlenkamp D, Gellert M, Deponte M, Berndt C, Lillig CH. Signal-regulated oxidation of proteins in the cytosol via a flavo-monooxygenase-disulfide relay at the cell membrane. 1<sup>st</sup> Symposium of the DFG Priority Program 1710 “Dynamics of Thiol-based Redox Switches in Cellular Physiology”, 12<sup>th</sup>-14<sup>th</sup> March 2018, Rauischholzhausen, Germany
- X. **Ortegón Salas C**, Uhlenkamp D, Gellert M, Deponte M, Berndt C, Lillig CH. Signal-regulated oxidation of proteins in the cytosol via a flavo-monooxygenase-disulfide relay at the cell membrane. 4<sup>th</sup> Annual Workshop of the Research Training Group 1947-BiOx, 1<sup>st</sup>-2<sup>nd</sup> October 2018, Greifswald, Germany
- XI. **Ortegón Salas C**, Knaup LK, Schneider K, Scharf, C, Berndt C, Deponte M, Lillig CH, Gellert M. Receptor-induced redox signaling relay – from signal to effector. Biochemical Society scientific meeting “Redox signalling in physiology, ageing and disease”, 1<sup>st</sup>-3<sup>rd</sup> July 2019, Newcastle, UK  
*Awarded with the short talk price*
- XII. **Ortegón Salas C**, Knaup LK, Schneider K, Scharf, C, Berndt C, Deponte M, Lillig CH, Gellert M. Receptor-induced redox signaling relay – from signal to effector. 5<sup>th</sup> Annual Workshop of the Research Training Group 1947-BiOx, 30<sup>th</sup> September-1<sup>st</sup> October 2019, Greifswald, Germany

- XIII. **Ortegón Salas C**, Knaup LK, Schneider K, Uhlenkamp D, Gellert M, Deponte M, Berndt C, Lillig CH. Signal-regulated oxidation of proteins via MICAL. “Baltic redox workshop”, joint meeting of the Study Group Redox Biology of the German Society for Biochemistry and Molecular Biology (GBM) and the DFG Research Training Group 1947-BiOx, held virtually on 14<sup>th</sup>-16<sup>th</sup> September 2020, Greifswald, Germany

### 7.6.3 Poster presentations

- XIV. **Ortegón Salas C**, Schneider K, Uhlenkamp D, Berndt C, Deponte M, Lillig CH, Gellert M. Signal-regulated oxidation of proteins via MICAL. “The Berlin redox sessions”, common meeting of the DFG Priority Program 1710 and the Study Group Redox Biology of the GBM, 26<sup>th</sup>-28<sup>th</sup> September 2018, Berlin, Germany
- XV. **Ortegón Salas C**, Schneider K, Uhlenkamp D, Berndt C, Deponte M, Lillig CH, Gellert M. Signal-regulated oxidation of proteins via MICAL. 2<sup>nd</sup> Symposium of the DFG Priority Program 1710 “Dynamics of Thiol-based Redox Switches in Cellular Physiology”, 18<sup>th</sup>-19<sup>th</sup> March 2019, Rauischholzhausen, Germany  
*Awarded with the best poster price*
- XVI. **Ortegón Salas C**, Knaup LK, Schneider K, Scharf, C, Berndt C, Deponte M, Lillig CH, Gellert M. Receptor-induced redox signaling relay – from signal to effector. Biochemical Society scientific meeting “Redox signalling in physiology, ageing and disease”, 1<sup>st</sup>-3<sup>rd</sup> July 2019, Newcastle, UK
- XVII. **Ortegón Salas C**, Knaup LK, Schneider K, Scharf, C, Berndt C, Deponte M, Lillig CH, Gellert M. Receptor-induced redox signaling relay – from signal to effector. 3<sup>rd</sup> Symposium of the SPP1710 “Thiol-based switches and redox regulation – from microbes to men”, 15<sup>th</sup>-20<sup>th</sup> September 2019, Sant Feliu de Guixols, Spain
- XVIII. **Ortegón Salas C**, Knaup LK, Schneider K, Scharf, C, Berndt C, Deponte M, Lillig CH, Gellert M. Receptor-induced redox signaling relay – from signal to effector. 5<sup>th</sup> Annual Workshop of the Research Training Group 1947-BiOx, 30<sup>th</sup> September-1<sup>st</sup> October 2019, Greifswald, Germany
- XIX. **Ortegón Salas C**, Knaup LK, Schneider K, Scharf, C, Berndt C, Deponte M, Lillig CH, Gellert M. Receptor-induced redox signaling relay – from signal to effector. 27<sup>th</sup>

Annual Conference of the Society for Redox Biology and Medicine (SfRBM), held virtually on 18<sup>th</sup>-20<sup>th</sup> November 2020, Indianapolis, IN, USA

- XX. **Ortegón Salas C**, Uhlenkamp D, Bodnar Y, Berndt C, Deponte M, Lillig CH, Gellert M. Specific protein oxidation. Final Symposium of the SPP1710 “Dynamics of Thiol-based Redox Switches in Cellular Physiology”, held virtually on 29<sup>th</sup>-31<sup>st</sup> March 2021, Greifswald, Germany

**Article 1****Signal-regulated oxidation of proteins via MICAL**

**Clara Ortegón Salas, Katharina Schneider, Christopher Horst Lillig and Manuela Gellert**

*Biochemical Society Transactions*

Vol 48 Issue 2 (613-620)

Published: 27 March 2020

This review was originally published in the journal of Biochemical Society Transactions, Ortégón Salas C, Schneider K, Lillig CH, Gellert M. Signal-regulated oxidation of proteins via MICAL. © 2020 The Author(s). Published by Portland Press Limited on behalf of the Biochemical Society.

Link to the publication on Portland Press: <https://doi.org/10.1042/BST20190866>

Portland Press allows the authors to include their article in whole or in part in their own dissertation or thesis. The original article must be properly cited and linked to the original publication.

Biochemical Society Transactions (2020)  
<https://doi.org/10.1042/BST20190866>



## Review Article

# Signal-regulated oxidation of proteins via MICAL

Clara Ortegón Salas, Katharina Schneider, Christopher Horst Lillig and Manuela Gellert

Institute for Medical Biochemistry and Molecular Biology, University Medicine Greifswald, University of Greifswald, Greifswald, Germany

Correspondence: Manuela Gellert ([manuela@gellert.org](mailto:manuela@gellert.org))

Processing of and responding to various signals is an essential cellular function that influences survival, homeostasis, development, and cell death. Extra- or intracellular signals are perceived via specific receptors and transduced in a particular signalling pathway that results in a precise response. Reversible post-translational redox modifications of cysteinyl and methionyl residues have been characterised in countless signal transduction pathways. Due to the low reactivity of most sulfur-containing amino acid side chains with hydrogen peroxide, for instance, and also to ensure specificity, redox signalling requires catalysis, just like phosphorylation signalling requires kinases and phosphatases. While reducing enzymes of both cysteinyl- and methionyl-derivates have been characterised in great detail before, the discovery and characterisation of MICAL proteins evinced the first examples of specific oxidases in signal transduction. This article provides an overview of the functions of MICAL proteins in the redox regulation of cellular functions.

## Redox signalling

In the past, redox-dependent modifications were supposed to be the result of a global cellular redox state, which is determined by the ratio of pro- and anti-oxidants within the cell. This concept defined 'oxidative stress' as excess of the 'pro-oxidant' molecules or decreased levels of 'anti-oxidant' molecules [1]. Over the past decade, however, redox-biochemistry experienced a dramatic shift in paradigm as redox modifications were more and more shown to be specific, rapid, physiological, and reversible signalling events, see for instance [2–4], and [5–9] for in-depth discussions. Redox mediated signal transduction occurs in different cellular compartments, often at the same time, both by oxidation and reduction of key molecules. Signal transduction depends on the reaction kinetics and thus enzymatic activity [2,5,6,10].

## Redox modifications of cysteinyl and methionyl side chains

The sulfur moieties of cysteinyl and methionyl side chains are prime targets for reversible redox modifications (Figure 1) summarised, e.g. in [7]. The oxidation of thiols groups can lead to the formation of inter- or intramolecular disulfides and thus the generation of e.g. hetero- or homo-dimers of proteins (Figure 1, reaction 2). Such intra- or intermolecular disulfides can be reduced by specific thiol-containing reductases such as glutaredoxins (Grx) or thioredoxins (Trx). In addition, cysteinyl residues may also form disulfides with other thiol-containing molecules such as glutathione (GSH), the most abundant cellular thiol component. The oxidation of thiol groups by hydrogen peroxide evinces sulphenic acids (Figure 1, reaction 3). Cysteinyl sulphenic acid derivatives are rather unstable and will readily react with thiols yielding disulfides (Figure 1, reaction 4). If these derivatives react with further hydrogen peroxide molecules, sulphinic and sulphonic acids may form, reactions that are considered irreversible (Figure 1, reactions 5 and 6). Another form of post-translational redox modification is the reaction of thiol groups and nitric oxide (NO), resulting in S-nitroso-thiols (Figure 1, reaction 1).

The thiol-ether groups of methionine or methionyl residues can be reversibly oxidised by hydrogen peroxide to methionine or methionyl sulfoxide (Figure 1, reactions 7 and 8), i.e. to a mixture of two diastereomers, methionine-S-sulfoxide, and methionine-R-sulfoxide. This reaction is today also recognised as a redox signalling mechanism [11]. Methionine/methionyl-S-sulfoxide is specifically reduced

Received: 18 December 2019  
 Revised: 9 March 2020  
 Accepted: 11 March 2020

Version of Record published:  
 27 March 2020

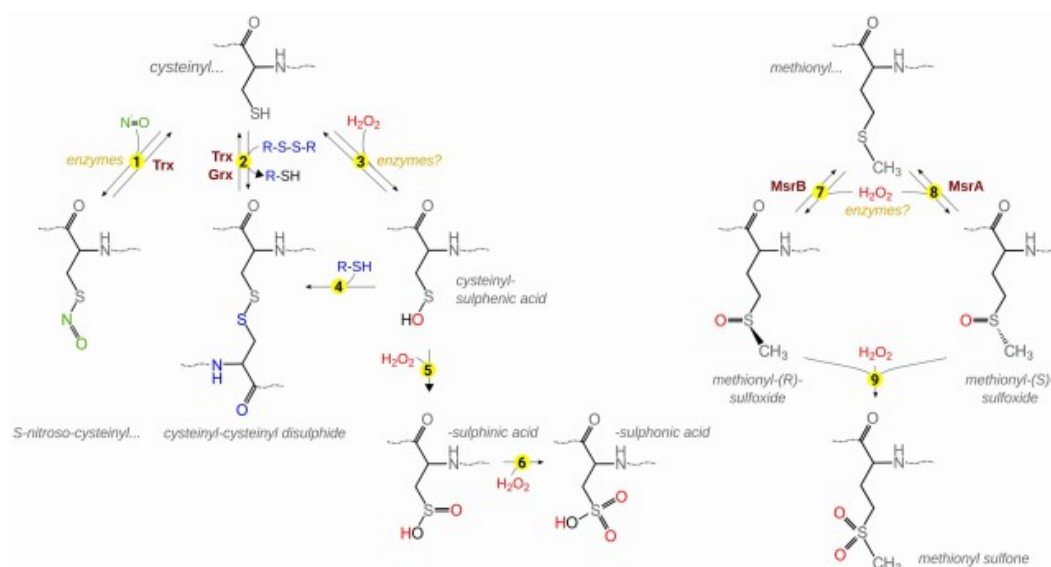


**Figure 1. Redox modifications of cysteinyl and methionyl amino acid side chains.**

(1) Nitrosylation of cysteinyl residues requires a catalyst that accepts one electron. De- and trans-nitrosylation are catalysed by Trxs. (2) Reversible disulfide formation may occur by thiol disulfide exchange reactions, e.g. with proteins of the Trx family. (3) Reaction with hydrogen peroxide can lead to the formation of sulphenic acids, that can further react to disulfides (4) or, irreversibly, to sulphinic (5) and sulphonic acids (6). Oxidation of methionyl residues, e.g. catalysed by MICAL enzymes, evinces methionyl-R-sulfoxides that can be reverted by MsrB enzymes (7). Methionine-S-sulfoxides (8) can be reduced by MsrAs. Methionyl sulfoxides may also be irreversibly oxidised to methionyl sulfone derivatives (9).

by methionine sulfoxide reductase (Msr) A, methionine/methionyl-R-sulfoxide by MsrB [12]. Human MsrA is expressed in various isoforms from a single gene, giving rise to mitochondrial, cytosolic, and nuclear variants [13–15]. Oxidised Msrs form an intramolecular disulfide that is reduced by Trxs or Grxs [12,16]. Most mammalian genomes possess three MsrB genes. MsrB1 is a seleno-protein. MsrB2 and 3 contain cysteinyl residues only and are catalytically less efficient [17,18].

Signal transduction depends on specificity and reversibility. In fact, redox modifications do not occur randomly at any given cysteinyl or methionyl side chain. Today, we see more and more evidence that many — if not most — reactions outlined above are catalysed by enzymes (see Figure 1). This ensures not only a fine tuned, enzymatically catalysed activation and inactivation of protein functions, but also allows for spatio-temporal control of these events through cell signalling, see for instance [11]. In this model, the specificity of the redox modification does not depend on the accessibility or reactivity/nucleophilicity of the modified residue, but arises primarily from the specificity of the protein–protein interactions between catalyst and target proteins. These interactions may be influenced by conformational changes of the proteins induced by other signalling events as, for instance, seen in phosphorylation cascades or G-protein-coupled receptor signalling pathways.

### Hydrogen peroxide production, reactivity, and reduction

Outside the endoplasmic reticulum and peroxisomes,  $H_2O_2$  is primarily the product of superoxide dismutases (SOD). Mammalian cells contain two SOD isoforms: the cytosolic SOD1 that is Cu/Zn-dependent, and the mitochondrial SOD2 that is Mn-dependent. These enzymes catalyse the alternate reduction and oxidation of superoxide yielding hydrogen peroxide and molecular oxygen [19–21]. Superoxide is produced by numerous enzymes in the cell, for instance: mitochondrial complexes I [22] and III [23], NADPH oxidases [24], cyclooxygenases [25], xanthine oxidoreductase [26], and cytochrome p450 enzymes [27].



In principle, hydrogen peroxide readily reacts with cysteinyl and also methionyl groups (see above). However, the second-order rate constant of hydrogen peroxide with free cysteine is  $\sim k = 2.9 \text{ M}^{-1} \text{ s}^{-1}$ , with GSH  $\sim 0.9 \text{ M}^{-1} \text{ s}^{-1}$  [28], and with the active site motif of Trx  $\sim 1 \text{ M}^{-1} \text{ s}^{-1}$  [29]. The rate constants of hydrogen peroxide with methionine and methionyl residues in peptides and proteins were determined to be as low as  $7 \times 10^{-4}$ – $8 \times 10^{-3} \text{ M}^{-1} \text{ s}^{-1}$  [30]. Not only are these rate constants really low, these reactions also compete for hydrogen peroxide with some of the most abundant proteins of all cells, i.e. peroxiredoxins (Prxs) and glutathione peroxidases (Gpxs). The rate constant of the reaction of hydrogen peroxide with the peroxidatic cysteinyl residue at the active site of Prxs and the cysteinyl or selenocysteinyl residue in the active sites of Gpxs ranges from  $3 \times 10^5$  to  $10^7 \text{ M}^{-1} \text{ s}^{-1}$  [29,31]. Peroxynitrite may also react with the sulfur moieties of cysteinyl and methionyl residues at considerably higher rate, however, Prxs are also highly reactive with this reactive nitrogen species [32,32,33]. We can thus conclude that by far most hydrogen peroxide (and also peroxynitrite) *in vivo* will react with dedicated peroxidases, for detailed quantitative calculations see also [34]. The low rate constants of regulatory methionyl or cysteinyl residues with these species compared with the dedicated peroxidases makes a direct reaction highly unlikely. This, in turn, necessitates enzymatic catalysis of the modifications in physiological redox signalling. Most cysteinyl and methionyl residues modified in signalling pathways may only be oxidised in the presence of a catalyst or when tethered to a site of peroxide production. For more comprehensive discussions on this topic, see also [5,10,35–37].

## Flavin monooxygenases of the MICAL family

MICALs (molecule(s) interacting with CasL) are a family of multidomain proteins that participate in cellular processes such as axonal growth cone repulsion, membrane trafficking, and actin dynamics [38–41]. MICALs were first described in 2002 as regulators of axon repulsion [42]. The human MICAL family consists of three isoforms (MICAL 1–3) that differ in their domain composition (Figure 2a). All genuine MICAL proteins contain an N-terminal monooxygenase (MO) domain with FAD as prosthetic group. Subsequently, calponin homology (CH) and LIM domains follow. An additional C-terminal Rab-binding domain (RBD) was identified for some MICAL family proteins, e.g. human MICAL1 and MICAL3. The MO domain enables MICAL proteins to function as flavin MO and oxidise substrates using oxygen and NADPH as substrates. The CH domains are important to facilitate the actin binding by the MO domain [43–45]. LIM domains have been shown to play roles in cytoskeletal organisation and mediate protein–protein interactions [46]. The RBD incorporates two distinct binding sites for small GTPases of the Rab family with different affinities and was initially proposed to form a coiled-coil domain, thus sometimes termed CC domain.

### Reactivity, kinetics, and mechanism

MICALs are FAD-containing MO structurally similar to aromatic hydroxylases and amine oxidases [47]. In the presence of NADPH, the proteins reduce molecular oxygen to hydrogen peroxide via a peroxyflavin intermediate ( $k_{\text{cat}} = 77 \text{ s}^{-1}$ ). It was thus proposed that the proteins may produce hydrogen peroxide as signalling molecules [47]. When methionyl residues in actin were identified as MICAL substrates (see below), it was shown that F-actin, but not G-actin, nor free methionine, stimulates NADPH oxidation by increasing  $k_{\text{cat}}$  [4]. Moreover, an apparent  $K_m$  for actin of  $4.7 \mu\text{M}$  could be determined, suggesting a direct oxidation of methionyl residues to methionyl sulfoxides [9,48]. The reductive half-reaction of the MICAL2 hydroxylase domain is stimulated by F-actin. In the absence of actin, NADPH reduces the flavin relatively slowly; the presence of actin increases the velocity of this reaction significantly. Hence, MICAL2 has the classic behaviour of class A MO, i.e. slow reduction in the flavin when the substrate to be oxygenated is absent [49]. Under physiological conditions, this may attenuate the production of hydrogen peroxide released from the enzyme. The comparison of the structures before and after reaction with NADPH revealed that the flavin ring can or even must switch between two discrete positions (Figure 2b) [50]. Most notably, this conformational switch is coupled to the opening of a channel to the active site (Figure 2c). In this structure, a water molecule is placed in close proximity to the carbon C4a (arrow in Figure 2c). Thus, this oxygen molecule is in exactly the same position as the expected peroxy group of the peroxyflavin intermediate. Being placed only 0.2 nm from the surface of the protein, it might well be available for an attack by an amino acid side chain. Alternatively, hydrogen peroxide could be released at this position and presented directly to target proteins bound in close proximity to the channel.

In all MICALS, the MO domain is followed by a type-2 CH domain (Figure 2a). A recent study on the structure of a fragment of MICAL1 containing the MO and the CH domains suggests that the MICAL redox activity

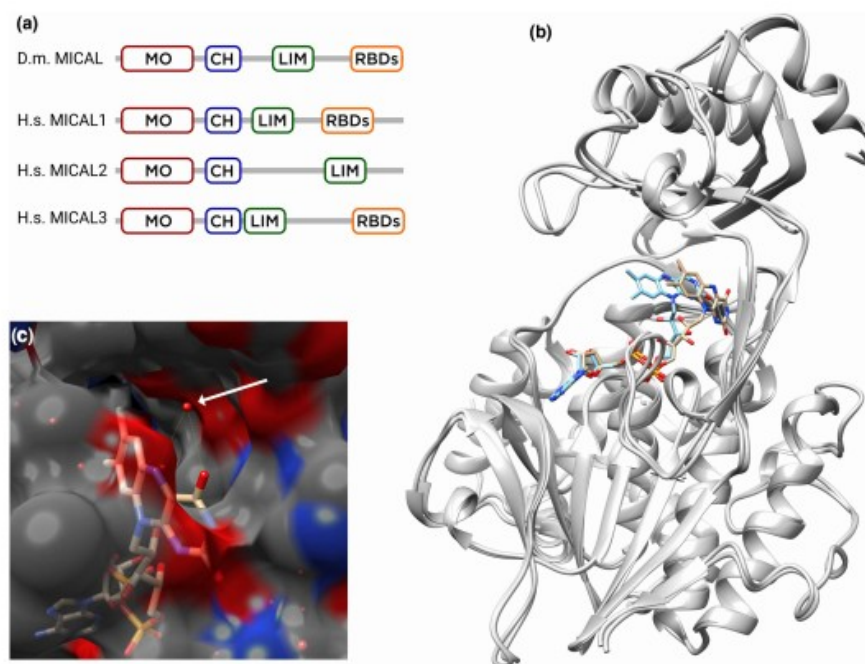


**Figure 2. MICAL structure.**

(a) Domain structures of human (H.s.) and for comparison *Drosophila melanogaster* (D.m.) MICALs. MO, monooxygenase domain; CH, calponin homology domain; LIM, LIM domain; RBDs, Rab-binding domains. (b) Structure of the monooxygenase domain of mouse MICAL1 (pdb code 2c4c) with the two conformations of the oxidised (blue, chain B) and reduced (brown, chain A) FAD indicated. (c) Tunnel opening in the reduced FAD conformation with a water molecule (arrow) in the proposed position of the peroxyflavin (pdb code 2c4c, chain A).

is controlled by a cooperative mechanism between the domains [43]. For a more detailed discussion on the structure–function relations of MICALs catalytic mechanisms, we refer to Vanoni [51].

### MICAL proteins as signal transducers

Redox control of protein function involves the specific oxidation and reduction in amino acid side chains and, as discussed above, kinetic constraints require catalysis of both oxidation and reduction. Various specific reductases have been described in great detail, most of them belong to the Trx family of proteins [7]. To the best of our knowledge, MICALs are the first examples of signal-induced specific oxidases. Two methionyl residues (M44 and M47) in F-actin are specifically converted to methionyl-R-sulfoxides by MICALs regulating actin filament dynamics [4,52]. The re-reduction back to methionyl residues is specifically catalysed by MsrB selenoproteins, representing an example for a fully catalysed reversible site- and stereo-specific methionyl oxidation [53–55]. So, what signalling pathways lead to the activation of MICALs?

Semaphorins (Sema) are a large family of secreted signalling proteins involved in many cellular processes [42]. Cellular and genetic work using the model organism *Drosophila* indicates that Semaphorins regulate the activity of MICALs and their interaction with target molecules including their F-actin substrate [39,42], see [41] for a review. In mammals, a role for MICALs in Semaphorin signalling has also begun to emerge, e.g. [56–59]. For example, Sema3A, which is one of the most widely studied Sema, influences many cellular processes including kidney development and polarisation [60], as well as the migration of T-lymphocytes [38]. Neuropilin-1 (NP1) and plexin A (PlexA) form a heterodimeric transmembrane protein which acts as a Sema3A receptor. Sema3A binds to its ligand partner NP1 leading to PlexA activation and further signal transduction, summarised in [38]. MICAL1 was shown to directly interact with PlexA1 and A3, MICAL2 with



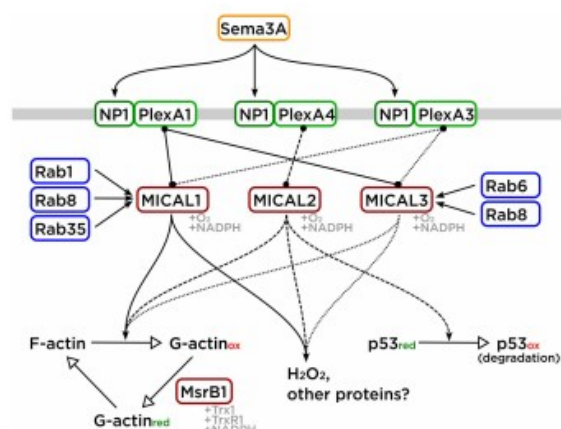


**Figure 3. Signalling networks with mammalian MICAL proteins as transducers.**

For details, see the text. Black arrow head: activation; point-to-point line: direct interaction; white arrow head: transformation. The straight, dashed, and pointed lines were used for clarity only.

PlexA4 via their C-terminal domains, overview in [42]. As in *Drosophila*, results indicate that these interactions regulate the activity of MICALs and their interaction with target molecules (Figure 3).

The C-termini of some MICALs (in human 1 and 3) contain a RBD, suggesting their regulation by small GTPase signalling. Redox-active MICAL1 was shown to be inhibited by its C-terminal domain. This inhibition can be released by a direct interaction of MICAL1 with Rab35. This interaction activates the MO domain and/or allows the interaction with actin filaments and thus the regulation of their dynamics [61] (Figure 3). The interaction of MICAL1 with Rab8 in the active GTP-bound state stabilises the active MICAL1 conformation causing a specific four-fold increase in  $k_{cat}$  of the NADPH oxidase reaction [62]. The interaction of MICAL3 with Rab8 was suggested to play an important role in vesicle docking and fusion contributing to the receptor and channel membrane trafficking mechanisms disturbed in human ciliopathies [63]. Moreover, Rab1, involved in vesicle trafficking, was also identified as an interaction partner of MICAL1 [64]. Rab6, Rab8, and MICAL3 were suggested to co-operate in controlling docking and fusion of exocytotic carriers [65]. Interestingly, interactions of Rab proteins (Rab8, 13, and 15) with MICAL-like proteins, that lack the MO domain, have also been characterised [66,67].

MICALs functions regulate actin dynamics in various processes, for overviews see [41,51,54,68,69]. In addition, MICALs might also act on other proteins as oxidase of specific amino acid side chains. Depletion of MICAL1 markedly reduced cell proliferation in breast cancer cells likely by reduction in hydrogen peroxide production, presumably via maintaining cyclin D expression through the hydrogen peroxide-sensitive PI3K/Akt/ERK signalling pathway [70]. MICAL1 and 3 may also be involved in the formation of a regulatory disulfide in the collapsin response mediator protein 2 through the production of hydrogen peroxide [71]. MICAL1 is a binding partner of nuclear Dbf2-related (NDR) kinases. MICAL1 was suggested to compete with mammalian Ste-20-like kinase (MST1) for NDR binding and thereby to antagonise MST1-induced NDR activation that would otherwise lead to pro-apoptotic signalling [72]. MICAL2 was demonstrated to bind to p53 and oxidises it at M40 and M160, thus promoting ubiquitination, degradation, and inactivation of p53 [73]. MICAL2 was also reported to promote breast cancer cell migration by inhibiting endothelial growth factor receptor degradation in a Rac1-dependent manner [74].

## Perspectives

- Importance of the field — The identification and characterisation of MICAL proteins as specific oxidases in signal transduction was a major breakthrough in our understanding of reversible redox signalling. MICALs fulfil all requirements for the proposed catalysts in redox signalling.

- Summary of the current thinking — The proteins act in specific signalling events and as specific oxidases of methionyl residues and maybe also as generators of hydrogen peroxide and thereby as oxidases of cysteinyl residues [70,75]. One of the major functions is the regulation of actin dynamics.
- Comments on future directions — While our knowledge on MICALs is steadily increasing (see also [41,51,54,68,69] for more comprehensive coverage), various questions have to be addressed in the future: Do MICAL proteins oxidise more target proteins? Why do mammalian genomes encode three MICAL isoforms? The results outlined above imply that they might act, at least in part, on different targets and are activated by different mechanisms. What are the molecular mechanisms for MICAL activation? Especially the activation by the semaphorin receptors were not addressed yet. And, what is/are the molecular mechanism(s) of target oxidation? Do MICALs produce hydrogen peroxide *in vivo*, or do they act on protein targets exclusively?

### Competing Interests

The authors declare that there are no competing interests associated with the manuscript.

### Acknowledgements

We gratefully acknowledge the financial support by the Deutsche Forschungsgemeinschaft (DFG, German Research Foundation), grants (to CHL) LI 984/3-2 (SPP 1710) and GRK1947-A1.

### Abbreviations

CH, calponin homology; Gpxs, glutathione peroxidases; Grx, glutaredoxins; MO, monooxygenase; Msr, methionine sulfoxide reductase; NDR, nuclear Dbf2-related; NP1, Neuropilin-1; PlexA, plexin A; Prxs, peroxiredoxins; RBD, Rab-binding domain; SOD, superoxide dismutases; Trx, thioredoxins.

### References

- 1 Sies, H., Berndt, C. and Jones, D.P. (2017) Oxidative stress. *Annu. Rev. Biochem.* **86**, 715–748 <https://doi.org/10.1146/annurev-biochem-061516-045037>
- 2 Delaunay, A., Pflieger, D., Barrault, M.B., Vinh, J. and Toledano, M.B. (2002) A thiol peroxidase is an H<sub>2</sub>O<sub>2</sub> receptor and redox-transducer in gene activation. *Cell* **111**, 471–481 [https://doi.org/10.1016/S0092-8674\(02\)01048-6](https://doi.org/10.1016/S0092-8674(02)01048-6)
- 3 Fourquet, S., Huang, M.-E., D'Autreaux, B. and Toledano, M.B. (2008) The dual functions of thiol-based peroxidases in H<sub>2</sub>O<sub>2</sub> scavenging and signaling. *Antioxid. Redox Signal.* **10**, 1565–1576 <https://doi.org/10.1089/ars.2008.2049>
- 4 Hung, R.-J., Pak, C.W. and Terman, J.R. (2011) Direct redox regulation of F-actin assembly and disassembly by Mical. *Science* **334**, 1710–1713 <https://doi.org/10.1126/science.1211956>
- 5 Berndt, C., Lillig, C.H. and Flohé, L. (2014) Redox regulation by glutathione needs enzymes. *Front. Pharmacol.* **5**, 168 <https://doi.org/10.3389/fphar.2014.00168>
- 6 Deponte, M. and Lillig, C.H. (2015) Enzymatic control of cysteinyl thiol switches in proteins. *Biol. Chem.* **396**, 401–413 <https://doi.org/10.1515/hsz-2014-0280>
- 7 Hanschmann, E.-M., Godoy, J.R., Berndt, C., Hudemann, C. and Lillig, C.H. (2013) Thioredoxins, glutaredoxins, and peroxiredoxins-molecular mechanisms and health significance: from cofactors to antioxidants to redox signaling. *Antioxid. Redox Signal.* **19**, 1539–1605 <https://doi.org/10.1089/ars.2012.4599>
- 8 Jones, D.P. (2006) Redefining oxidative stress. *Antioxid. Redox Signal.* **8**, 1865–1879 <https://doi.org/10.1089/ars.2006.8.1865>
- 9 Vanoni, M.A., Vitall, T. and Zucchini, D. (2013) MICAL, the flavoenzyme participating in cytoskeleton dynamics. *Int. J. Mol. Sci.* **14**, 6920–6959 <https://doi.org/10.3390/ijms14046920>
- 10 Flohé, L. (2013) The fairytale of the GSSG/GSH redox potential. *Biochim. Biophys. Acta* **1830**, 3139–3142 <https://doi.org/10.1016/j.bbagen.2012.10.020>
- 11 Drazic, A. and Winter, J. (2014) The physiological role of reversible methionine oxidation. *Biochim. Biophys. Acta* **1844**, 1367–1382 <https://doi.org/10.1016/j.bbapap.2014.01.001>
- 12 Boschi-Muller, S., Gand, A. and Branlant, G. (2008) The methionine sulfoxide reductases: catalysis and substrate specificities. *Arch. Biochem. Biophys.* **474**, 266–273 <https://doi.org/10.1016/j.abb.2008.02.007>
- 13 Hansel, A., Kuschel, L., Hehl, S., Lemke, C., Agrícola, H.-J., Hoshi, T. et al. (2002) Mitochondrial targeting of the human peptide methionine sulfoxide reductase (MSRA), an enzyme involved in the repair of oxidized proteins. *FASEB J.* **16**, 911–913 <https://doi.org/10.1096/fj.01-0737je>



Biochemical Society Transactions (2020)  
<https://doi.org/10.1042/BST20190866>



- 14 Hansel, A., Heinemann, S.H. and Hoshi, T. (2005) Heterogeneity and function of mammalian MSRs: enzymes for repair, protection and regulation. *Biochim. Biophys. Acta* **1703**, 239–247 <https://doi.org/10.1016/j.bbapap.2004.09.010>
- 15 Lee, J.W., Gordiyenko, N.V., Marchetti, M., Tserentsoodol, N., Sagher, D., Alam, S. et al. (2006) Gene structure, localization and role in oxidative stress of methionine sulfoxide reductase A (MSRA) in the monkey retina. *Exp. Eye Res.* **82**, 816–827 <https://doi.org/10.1016/j.exer.2005.10.003>
- 16 Kim, H.-Y. (2012) Glutaredoxin serves as a reductant for methionine sulfoxide reductases with or without resolving cysteine. *Acta Biochim. Biophys. Sin.* **44**, 623–627 <https://doi.org/10.1093/abbs/gms038>
- 17 Kim, H.-Y. and Gladyshev, V.N. (2004) Methionine sulfoxide reduction in mammals: characterization of methionine-R-sulfoxide reductases. *Mol. Biol. Cell.* **15**, 1055–1064 <https://doi.org/10.1091/mbc.e03-08-0629>
- 18 Lee, B.C., Dikly, A., Kim, H.-Y. and Gladyshev, V.N. (2009) Functions and evolution of selenoprotein methionine sulfoxide reductases. *Biochim. Biophys. Acta* **1790**, 1471–1477 <https://doi.org/10.1016/j.bbagen.2009.04.014>
- 19 McCord, J.M. and Fridovich, I. (1969) The utility of superoxide dismutase in studying free radical reactions. I. radicals generated by the interaction of sulfite, dimethyl sulfoxide, and oxygen. *J. Biol. Chem.* **244**, 6056–6063 PMID:4981789
- 20 Fukui, T. and Ushio-Fukai, M. (2011) Superoxide dismutases: role in redox signaling, vascular function, and diseases. *Antioxid. Redox Signal.* **15**, 1583–1606 <https://doi.org/10.1089/ars.2011.3999>
- 21 Zelko, I.N., Mariani, T.J. and Folz, R.J. (2002) Superoxide dismutase multigene family: a comparison of the CuZn-SOD (SOD1), Mn-SOD (SOD2), and EC-SOD (SOD3) gene structures, evolution, and expression. *Free Radic. Biol. Med.* **33**, 337–349 [https://doi.org/10.1016/S0891-5849\(02\)00905-X](https://doi.org/10.1016/S0891-5849(02)00905-X)
- 22 McCord, J.M. and Fridovich, I. (1970) The utility of superoxide dismutase in studying free radical reactions. II. The mechanism of the mediation of cytochrome c reduction by a variety of electron carriers. *J. Biol. Chem.* **245**, 1374–1377 PMID:5462997
- 23 Fridovich, I. (1970) Quantitative aspects of the production of superoxide anion radical by milk xanthine oxidase. *J. Biol. Chem.* **245**, 4053–4057 PMID:5496991
- 24 Wolin, M.S., Ahmad, M. and Gupta, S.A. (2005) The sources of oxidative stress in the vessel wall. *Kidney Int.* **67**, 1659–1661 <https://doi.org/10.1111/j.1523-1755.2005.00257.x>
- 25 Nishino, T., Okamoto, K., Eger, B.T., Pai, E.F. and Nishino, T. (2008) Mammalian xanthine oxidoreductase - mechanism of transition from xanthine dehydrogenase to xanthine oxidase. *FEBS J.* **275**, 3278–3289 <https://doi.org/10.1111/j.1742-4658.2008.06489.x>
- 26 Brand, M.D. (2010) The sites and topology of mitochondrial superoxide production. *Exp. Gerontol.* **45**, 466–472 <https://doi.org/10.1016/j.exger.2010.01.003>
- 27 Bylund, J., Brown, K.L., Movitz, C., Dahlgren, C. and Karlsson, A. (2010) Intracellular generation of superoxide by the phagocyte NADPH oxidase: how, where, and what for? *Free Radic. Biol. Med.* **49**, 1834–1845 <https://doi.org/10.1016/j.freeradbiomed.2010.09.016>
- 28 Winterbourn, C.C. and Metodiewa, D. (1999) Reactivity of biologically important thiol compounds with superoxide and hydrogen peroxide. *Free Radic. Biol. Med.* **27**, 322–328 [https://doi.org/10.1016/S0891-5849\(99\)00051-9](https://doi.org/10.1016/S0891-5849(99)00051-9)
- 29 Borisenko, G., Kagan, V.E., Bayir, H.A., Belikova, N.A., Kapralov, O., Tyurina, Y.Y. et al. (2009) Cytochrome c/cardioplin relations in mitochondria: a kiss of death. *Free Radic. Biol. Med.* **46**, 1439–1453 <https://doi.org/10.1016/j.freeradbiomed.2009.03.004>
- 30 Sjöberg, B., Foley, S., Cardey, B., Fromm, M. and Enescu, M. (2018) Methionine oxidation by hydrogen peroxide in peptides and proteins: a theoretical and Raman spectroscopy study. *J. Photochem. Photobiol. B. Biol.* **188**, 95–99 <https://doi.org/10.1016/j.jphotobiol.2018.09.009>
- 31 Trujillo, M., Clippe, A., Manta, B., Ferrer-Sueta, G., Smeets, A., Declercq, J.-P. et al. (2007) Pre-steady state kinetic characterization of human peroxiredoxin 5: taking advantage of Trp84 fluorescence increase upon oxidation. *Arch. Biochem. Biophys.* **467**, 95–106 <https://doi.org/10.1016/j.abb.2007.08.008>
- 32 Briviba, K., Kissner, R., Koppenol, W.H. and Sies, H. (1998) Kinetic study of the reaction of glutathione peroxidase with peroxynitrite. *Chem. Res. Toxicol.* **11**, 1398–1401 <https://doi.org/10.1021/bx980086y>
- 33 Trujillo, M., Ferrer-Sueta, G., Thomson, L., Flohé, L. and Radi, R. (2007) Kinetics of peroxiredoxins and their role in the decomposition of peroxynitrite. *Subcell. Biochem.* **44**, 83–113 [https://doi.org/10.1007/978-1-4020-6051-9\\_5](https://doi.org/10.1007/978-1-4020-6051-9_5)
- 34 Antunes, F. and Brito, P.M. (2017) Quantitative biology of hydrogen peroxide signaling. *Redox Biol.* **13**, 1–7 <https://doi.org/10.1016/j.redox.2017.04.039>
- 35 Flohé, L. (2010) Changing paradigms in thiology from antioxidant defense toward redox regulation. *Methods Enzymol.* **473**, 1–39 [https://doi.org/10.1016/S0076-6879\(10\)73001-9](https://doi.org/10.1016/S0076-6879(10)73001-9)
- 36 Marinho, H.S., Real, C., Cyme, L., Soares, H. and Antunes, F. (2014) Hydrogen peroxide sensing, signaling and regulation of transcription factors. *Redox Biol.* **2**, 535–562 <https://doi.org/10.1016/j.redox.2014.02.006>
- 37 Forman, H.J., Ursini, F. and Maiorino, M. (2014) An overview of mechanisms of redox signaling. *J. Mol. Cell. Cardiol.* **73**, 2–9 <https://doi.org/10.1016/j.yjmcc.2014.01.018>
- 38 Schmidt, E.F. and Strittmatter, S.M. (2007) The CRMP family of proteins and their role in Semaphorin 3A signaling. *Adv. Exp. Med. Biol.* **600**, 1–11 [https://doi.org/10.1007/978-0-387-70956-7\\_1](https://doi.org/10.1007/978-0-387-70956-7_1)
- 39 Hung, R.-J., Yazdani, U., Yoon, J., Wu, H., Yang, T., Gupta, N. et al. (2010) Mical links semaphorins to F-actin disassembly. *Nature* **463**, 823–827 <https://doi.org/10.1038/nature08724>
- 40 Giridharan, S.S.P., Rohn, J.L., Naslavsky, N. and Caplan, S. (2012) Differential regulation of actin microfilaments by human MICAL proteins. *J. Cell. Sci.* **125**, 614–624 <https://doi.org/10.1242/jcs.089367>
- 41 Alto, L.T. and Terman, J.R. (2018) MICALs. *Curr. Biol.* **28**, R538–R541 <https://doi.org/10.1016/j.cub.2018.01.025>
- 42 Terman, J.R., Mao, T., Pasterkamp, R.J., Yu, H.-H. and Kolodkin, A.L. (2002) MICALs, a family of conserved flavoprotein oxidoreductases, function in plexin-mediated axonal repulsion. *Cell* **109**, 887–900 [https://doi.org/10.1016/S0092-8674\(02\)00794-8](https://doi.org/10.1016/S0092-8674(02)00794-8)
- 43 Alqassim, S.S., Urquiza, M., Borgnia, E., Nagib, M., Amzel, L.M. and Blanchet, M.A. (2016) Modulation of MICAL monooxygenase activity by its calponin homology domain: structural and mechanistic insights. *Sci Rep.* **6**, 22176 <https://doi.org/10.1038/srep22176>
- 44 Kim, J., Lee, H., Roh, Y.J., Kim, H.-U., Shin, D., Kim, S. et al. (2020) Structural and kinetic insights into flavin-containing monooxygenase and calponin-homology domains in human MICAL3. *IUCr.* **7**, 90–99 <https://doi.org/10.1107/S2052252519015409>
- 45 Hartwig, J.H. (1995) Actin-binding proteins. 1: spectrin super family. *Protein Profile* **2**, 703–800 PMID:7584474
- 46 Bach, I. (2000) The LIM domain: regulation by association. *Mech. Dev.* **91**, 5–17 [https://doi.org/10.1016/S0925-4773\(99\)00314-7](https://doi.org/10.1016/S0925-4773(99)00314-7)

Downloaded from https://portlandpress.com/biochemical-transaction/pdf/doi/10.1042/BST20190866/7584474 by guest on 29 April 2020



- 47 Nadella, M., Blanchet, M.A., Gabelli, S.B., Barrila, J. and Amzel, L.M. (2005) Structure and activity of the axon guidance protein MICAL. *Proc. Natl. Acad. Sci. U.S.A.* **102**, 16830–16835 <https://doi.org/10.1073/pnas.0504838102>
- 48 Zucchini, D., Caprini, G., Pasterkamp, R.J., Tedeschi, G. and Vanoni, M.A. (2011) Kinetic and spectroscopic characterization of the putative monooxygenase domain of human MICAL-1. *Arch. Biochem. Biophys.* **515**, 1–13 <https://doi.org/10.1016/j.abb.2011.08.004>
- 49 McDonald, C.A., Liu, Y.Y. and Paley, B.A. (2013) Actin stimulates reduction of the MICAL-2 monooxygenase domain. *Biochemistry* **52**, 6076–6084 <https://doi.org/10.1021/bi4008462>
- 50 Siebold, C., Berrow, N., Walter, T.S., Harlos, K., Owens, R.J., Stuart, D.I. et al. (2005) High-resolution structure of the catalytic region of MICAL (molecule interacting with CasL), a multidomain flavoenzyme-signaling molecule. *Proc. Natl. Acad. Sci. U.S.A.* **102**, 16836–16841 <https://doi.org/10.1073/pnas.0504997102>
- 51 Vanoni, M.A. (2017) Structure-function studies of MICAL, the unusual multidomain flavoenzyme involved in actin cytoskeleton dynamics. *Arch. Biochem. Biophys.* **632**, 118–141 <https://doi.org/10.1016/j.abb.2017.06.004>
- 52 Grintsevich, E.E., Ge, P., Sawaya, M.R., Yesilyurt, H.G., Terman, J.R., Zhou, Z.H. et al. (2017) Catastrophic disassembly of actin filaments via Mical-mediated oxidation. *Nat. Commun.* **8**, 2183 <https://doi.org/10.1038/s41467-017-02357-8>
- 53 Lee, B.C., Péterfi, Z., Hoffmann, F.W., Moore, R.E., Kaya, A., Avanesov, A. et al. (2013) Msr1 and MICALs regulate actin assembly and macrophage function via reversible stereoselective methionine oxidation. *Mol. Cell* **51**, 397–404 <https://doi.org/10.1016/j.molcel.2013.06.019>
- 54 Manta, B. and Gladyshev, V.N. (2017) Regulated methionine oxidation by monooxygenases. *Free Radic. Biol. Med.* **109**, 141–155 <https://doi.org/10.1016/j.freeradbiomed.2017.02.010>
- 55 Hung, R.-J., Spaeth, C.S., Yesilyurt, H.G. and Terman, J.R. (2013) Seir reverses Mical-mediated oxidation of actin to regulate F-actin dynamics. *Nat. Cell Biol.* **15**, 1445–1454 <https://doi.org/10.1038/ncb2871>
- 56 Schmidt, E.F., Shim, S.-O. and Strittmatter, S.M. (2008) Release of MICAL autoinhibition by semaphorin-plexin signaling promotes interaction with collapsin response mediator protein. *J. Neurosci.* **28**, 2287–2297 <https://doi.org/10.1523/JNEUROSCI.5646-07.2008>
- 57 Aggarwal, P.K., Veron, D., Thomas, D.B., Siegel, D., Moeckel, G., Kashgarian, M. et al. (2015) Semaphorin3a promotes advanced diabetic nephropathy. *Diabetes* **64**, 1743–1759 <https://doi.org/10.2337/db14-0719>
- 58 Hou, S.T., Milchi, L., Li, X., Gangaraju, S., Jiang, S.X., Aylsworth, A. et al. (2015) Semaphorin3a elevates vascular permeability and contributes to cerebral ischemia-induced brain damage. *Sci. Rep.* **5**, 7890 <https://doi.org/10.1038/srep07890>
- 59 Tominaga, K., Minato, H., Murayama, T., Sasahara, A., Nishimura, T., Kiyokawa, E. et al. (2019) Semaphorin signaling via MICAL3 induces symmetric cell division to expand breast cancer stem-like cells. *Proc. Natl. Acad. Sci. U.S.A.* **116**, 625–630 <https://doi.org/10.1073/pnas.1806851116>
- 60 Reidy, K. and Tufro, A. (2011) Semaphorins in kidney development and disease: modulators of ureteric bud branching, vascular morphogenesis, and podocyte-endothelial crosstalk. *Pediatr. Nephrol.* **26**, 1407–1412 <https://doi.org/10.1007/s00467-011-1769-1>
- 61 Frémont, S., Hammich, H., Bai, J., Woland, H., Klinkert, K., Rocancourt, M. et al. (2017) Oxidation of F-actin controls the terminal steps of cytokinesis. *Nat. Commun.* **8**, 14528 <https://doi.org/10.1038/ncomms14528>
- 62 Esposito, A., Ventura, V., Petoukhov, M.V., Rai, A., Svergun, D.I. and Vanoni, M.A. (2019) Human MICAL1: activation by the small GTPase Rab8 and small-angle X-ray scattering studies on the oligomerization state of MICAL1 and its complex with Rab8. *Protein Sci.* **28**, 150–166 <https://doi.org/10.1002/pro.3512>
- 63 Bachmann-Gagescu, R., Dona, M., Hetterschijt, L., Tonnaer, E., Peters, T., de Vrieze, E. et al. (2015) The ciliopathy protein CC2D2A associates with NINL and functions in RAB8-MICAL3-regulated vesicle trafficking. *PLoS Genet.* **11**, e1005575 <https://doi.org/10.1371/journal.pgen.1005575>
- 64 Fischer, J., Weide, T. and Barnekow, A. (2005) The MICAL proteins and rab1: a possible link to the cytoskeleton? *Biochem. Biophys. Res. Commun.* **328**, 415–423 <https://doi.org/10.1016/j.bbrc.2004.12.182>
- 65 Grigoriev, I., Yu, K.L., Martinez-Sanchez, E., Serra-Marques, A., Smal, I., Meijering, E. et al. (2011) Rab6, Rab8, and MICAL3 cooperate in controlling docking and fusion of exocytotic carriers. *Curr. Biol.* **21**, 967–974 <https://doi.org/10.1016/j.cub.2011.04.030>
- 66 Ioannou, M.S. and McPherson, P.S. (2016) Regulation of cancer cell behavior by the small GTPase Rab13. *J. Biol. Chem.* **291**, 9929–9937 <https://doi.org/10.1074/jbc.R116.715193>
- 67 Nishimura, N. and Sasaki, T. (2009) Rab family small G proteins in regulation of epithelial apical junctions. *Front. Biosci. (Landmark Ed)* **14**, 2115–2129 <https://doi.org/10.2741/3366>
- 68 Frémont, S., Romet-Lemonne, G., Houdusse, A. and Echard, A. (2017) Emerging roles of MICAL family proteins - from actin oxidation to membrane trafficking during cytokinesis. *J. Cell. Sci.* **130**, 1509–1517 <https://doi.org/10.1242/jcs.202028>
- 69 Giridharan, S.S.P. and Caplan, S. (2014) MICAL-family proteins: complex regulators of the actin cytoskeleton. *Antioxid. Redox Signal.* **20**, 2059–2073 <https://doi.org/10.1089/ars.2013.5487>
- 70 Deng, W., Wang, Y., Zhao, S., Zhang, Y., Chen, Y., Zhao, X. et al. (2018) MICAL1 facilitates breast cancer cell proliferation via ROS-sensitive ERK/cyclin D pathway. *J. Cell. Mol. Med.* **22**, 3108–3118 <https://doi.org/10.1111/jcmm.13588>
- 71 Morinaka, A., Yamada, M., Itofu, R., Funato, Y., Yoshimura, Y., Nakamura, F. et al. (2011) Thioredoxin mediates oxidation-dependent phosphorylation of CRMP2 and growth cone collapse. *Sci. Signal.* **4**, ra26 <https://doi.org/10.1126/scisignal.2001127>
- 72 Zhou, Y., Adolfs, Y., Pijnappel, W.W.M.P., Fuller, S.J., Van der Schors, R.C., Li, K.W. et al. (2011) MICAL-1 is a negative regulator of MST-NDR kinase signaling and apoptosis. *Mol. Cell. Biol.* **31**, 3603–3615 <https://doi.org/10.1128/MCB.01389-10>
- 73 Lu, J., Li, Y., Wu, Y., Zhou, S., Duan, C., Dong, Z. et al. (2018) MICAL2 mediates p53 ubiquitin degradation through oxidating p53 methionine 40 and 160 and promotes colorectal cancer malignance. *Theranostics* **8**, 5289–5306 <https://doi.org/10.7150/thno.28228>
- 74 Wang, Y., Deng, W., Zhang, Y., Sun, S., Zhao, S., Chen, Y. et al. (2018) MICAL2 promotes breast cancer cell migration by maintaining epidermal growth factor receptor (EGFR) stability and EGFR/P38 signalling activation. *Acta Physiol. (Oxf)* **222**, e12920 <https://doi.org/10.1111/apha.12920>
- 75 Bräutigam, L., Schütte, L.D., Godoy, J.R., Prozorovski, T., Gellert, M., Hauptmann, G. et al. (2011) Vertebrate-specific glutaredoxin is essential for brain development. *Proc. Natl. Acad. Sci. U.S.A.* **108**, 20532–20537 <https://doi.org/10.1073/pnas.1110085108>

## Article 2

# Molecular basis for the interactions of human thioredoxins with their respective reductases

Md Faruq Hossain\*, Yana Bodnar\*, Calvin Klein, **Clara Ortegón Salas**, Elias S.J. Arnér, Manuela Gellert and Christopher Horst Lillig

*Oxidative Medicine and Cellular Longevity*

Vol 2021 Article ID 6621292

Published: 02 June 2021

\* These authors contributed equally to this work.

DOI: [10.1155/2021/6621292](https://doi.org/10.1155/2021/6621292)

This research was originally published in the journal of *Oxidative Medicine and Cellular Longevity*, Hossain MD, Bodnar Y, Klein C, Ortegón Salas C, Arnér ESJ, Gellert M, Lillig CH. Molecular basis for the interactions of human thioredoxins with their respective reductases. © 2021 The Author(s). Published by Hindawi as an open access article under the Creative Commons Attribution License.



## Research Article

# Molecular Basis for the Interactions of Human Thioredoxins with Their Respective Reductases

Md Faruq Hossain <sup>1</sup>, Yana Bodnar <sup>1</sup>, Calvin Klein,<sup>1</sup> Clara Ortigón Salas,<sup>1</sup>  
Elias S. J. Arnér <sup>2,3</sup>, Manuela Gellert <sup>1</sup>, and Christopher Horst Lillig <sup>1</sup>

<sup>1</sup>Institute for Medical Biochemistry and Molecular Biology, University Medicine Greifswald, Germany

<sup>2</sup>Department for Biochemistry, Karolinska Institutet, Stockholm, Sweden

<sup>3</sup>Department of Selenoprotein Research, National Institute of Oncology, Budapest, Hungary

Correspondence should be addressed to Christopher Horst Lillig; [horst@lillig.de](mailto:horst@lillig.de)

Received 8 December 2020; Revised 20 April 2021; Accepted 20 May 2021; Published 2 June 2021

Academic Editor: Jesús Tejero

Copyright © 2021 Md Faruq Hossain et al. This is an open access article distributed under the Creative Commons Attribution License, which permits unrestricted use, distribution, and reproduction in any medium, provided the original work is properly cited.

The mammalian cytosolic thioredoxin (Trx) system consists of Trx1 and its reductase, the NADPH-dependent seleno-enzyme TrxR1. These proteins function as electron donor for metabolic enzymes, for instance in DNA synthesis, and the redox regulation of numerous processes. In this work, we analysed the interactions between these two proteins. We proposed electrostatic complementarity as major force controlling the formation of encounter complexes between the proteins and thus the efficiency of the subsequent electron transfer reaction. If our hypothesis is valid, formation of the encounter complex should be independent of the redox reaction. In fact, we were able to confirm that also a redox inactive mutant of Trx1 lacking both active site cysteinyl residues (C32,35S) binds to TrxR1 in a similar manner and with similar kinetics as the wild-type protein. We have generated a number of mutants with alterations in electrostatic properties and characterised their interaction with TrxR1 in kinetic assays. For human Trx1 and TrxR1, complementary electrostatic surfaces within the area covered in the encounter complex appear to control the affinity of the reductase for its substrate Trx. Electrostatic compatibility was even observed in areas that do not form direct molecular interactions in the encounter complex, and our results suggest that the electrostatic complementarity in these areas influences the catalytic efficiency of the reduction. The human genome encodes ten cytosolic Trx-like or Trx domain-containing proteins. In agreement with our hypothesis, the proteins that have been characterised as TrxR1 substrates also show the highest similarity in their electrostatic properties.

## 1. Introduction

The thioredoxin (Trx) family of proteins comprises many key enzymes in redox signalling that catalyse specific reversible redox reactions, e.g., dithiol-disulphide exchange, (de-)glutathionylation, transnitrosylation, or peroxide reduction. The name giving protein, Trx, was first described in 1964 as electron donor for ribonucleotide reductase in *E. coli* [1, 2]; at least one functional thioredoxin system was proposed to have been encoded in the genome of LUCA, the last universal common ancestor of all live forms today [3]. Other family members include the glutaredoxins (Grx) and peroxiredoxins (Prx), often expressed in multiple isoforms in essentially all tissues, cells, and organelles [4–7]. The Trx family of pro-

teins is defined by a common structural motif that, in its most basic form, consists of a central four-stranded  $\beta$ -sheet surrounded by three alpha helices—the thioredoxin fold [8, 9]. Most Trxs are small proteins of approximately 12 kDa size, characterised by their highly conserved CGPC active site motif located on a loop connecting sheet 1 and helix 1 (in the most basic representation of the fold) [10, 11]. Trxs catalyse reversible thiol-disulphide exchange reactions. The reduction of protein disulphides, for instance, is initiated by a nucleophilic attack of the more N-terminal active site cysteinyl residue, characterised by a particularly low  $pK_a$  value, on a sulphur atom of the disulphide in the target protein. This results in an intermediate mixed disulphide that, in the second reaction step, is reduced by the C-terminal

cysteinyll residue, leading to the release of the reduced substrate and the formation of oxidized Trx, and for more details, see for instance [5, 12, 13]. Mammalian genomes encode approx. 20 Trxs or Trx domain-containing proteins [14]. From these, the cytosolic Trx1 (gene: TXN) is the one studied the most. Besides its two active site cysteinyll residues, cytosolic Trx1 possesses three additional structural cysteinyll residues that were implicated in regulatory function and Trx1-dimer formation [15, 16]. Trx1 does not contain a nuclear localization signal nor a signal peptide for secretion, but it was observed to translocate into the nucleus under certain conditions and also to be secreted in a nonclassical way, independent of its redox state [17–21].

Trx-oxidized active sites are reduced at the expense of NADPH by FAD-containing thioredoxin reductases (TrxR) [22]. Evolution has given rise to two classes of NADPH-dependent TrxRs: the low molecular weight (approx. 35 kDa) type and the high molecular weight (approx. 55 kDa) type [23, 24]. Both classes function as homodimers. The low molecular weight type is found in archaea, bacteria, and some eukaryota. The high molecular weight type is encoded in the genomes of higher eukaryotes including humans. Mammalian genomes encode three TrxRs: cytosolic TrxR1 (gene: TXNRD1), mitochondrial TrxR2 (gene: TXNRD2), and the thioredoxin-glutathione reductase TGR or TrxR3 (gene: TXNRD3) [25, 26]. Mammalian TrxRs are selenoproteins that form homodimers in a head-to-tail conformation. They belong to a family of pyridine-nucleotide-disulphide oxidoreductases that also includes, e.g., glutathione reductase and trypanothione reductase [27]. They possess two active sites: one C-terminal GCUG motif and the N-terminal CVNVGC motif adjacent to the FAD domain. In contrast to their small molecular weight counterparts which have a high specificity for their endogenous substrate(s), these TrxRs accept a broad range of substrates [28], for human TrxR1 for instance Trx1, Grx2, and selenite; see overviews in [25, 29]. Electrons are transferred from NADPH to FAD and then to the N-terminal active site. Subsequently, the electrons are transferred to the selenocysteinyll residue containing C-terminal active site of the second protein in the dimeric TrxR and eventually to the target protein disulphides [30–32].

Numerous functions have been described for Trxs; see, e.g., [33]. However, the proteins cannot randomly reduce all possible protein disulphides. Instead, they show a broad but distinct substrate/target specificity, which may also be the reason for the various isoforms and Trx domain-containing proteins encoded in the genomes of higher eukaryotes. Hypotheses for the different activities and substrate specificities of Trx family proteins included differences in redox potential [34, 35], the  $pK_a$  values, i.e., the nucleophilicity, of their more N-terminal active site cysteinyll residue [36], differences in overall dipole moments [37], and an increase in entropy as the major recognition force for Trx family protein target interactions [38].

Based on the analysis of *E. coli* phosphoadenylyl sulfate reductase, we have proposed that the specificity of protein-protein interactions is based mainly on two factors: first is

geometric compatibility, and the second is electrostatic compatibility [39]. Based on electrostatic similarity, we have developed a mathematical approach to categorize Trx family proteins and to predict functions [14].

In this work, we propose that also the interaction of Trxs with their reductases is controlled by electrostatic compatibility. To address this hypothesis, we have analysed the interaction of the mammalian-type Trx1 with its reductase TrxR1. We have generated a number of mutants with alterations in electrostatic properties and characterised their interaction with TrxRs both *in silico* and *in vitro*; the formation and properties of the Trx1-TrxR1 enzyme-substrate complex were analysed with both wild-type proteins as well as mutants that exclude the thiol-disulphide/selenosulphide exchange reaction.

## 2. Material and Methods

**2.1. Materials.** Chemicals and enzymes were purchased at analytical grade or better from Sigma-Aldrich (St. Louis, MO, USA) unless otherwise stated.

**2.2. Structural Analysis.** Structures were acquired from the RSCB PDB Protein Data Bank (<http://www.rcsb.org>), and ligands and water molecules were removed using Pymol. The most representative structure of NMR ensembles was identified using UCSF Chimera [40]. The selected *in silico* mutations were inserted with the Dunbrack rotamer library [41] within the rotamer tool of Chimera; the rotamers with the highest probability were selected. The energy of the structure was minimized using Amberff14SB force field [42] after inserting a mutation in Chimera. The electrostatic calculations were performed as described before [14]. All the structures were preoriented in a way so that N-terminal active site cysteinyll residues face towards the camera perspective. These preoriented protein structures were then used to compute the electrostatic potential and the isosurfaces of the electrostatic potential. The addition of missing atoms and hydrogens, as well as the assignment of atomic charges and radii, was performed using pdb2pqr [43] applying the Amber force-field. VMD (visual molecular dynamics) [44] and APBS (Adaptive Poisson-Boltzmann Solver) [45] were used to compute the electrostatic potential in an aqueous solution containing 150 mM mobile ions, solvent dielectric constant: 78.54 at a temperature of 298.15 K. The electrostatic potential was mapped to the water accessible surface of the proteins from  $-4$  to  $4 k_B \cdot T \cdot e^{-1}$  represented in red and blue colours, respectively. The isosurfaces of the electrostatic potential were computed from  $-1$  to  $1 k_B \cdot T \cdot e^{-1}$  and also depicted in red and blue, respectively.

**2.3. Cloning of Expression Constructs.** Recombinant selenocysteine-containing rat TrxR1 (E. S. [46]) was used for all enzymatic assays, and the human TrxR U498C mutant [47] was used for all spectroscopic interaction studies, i.e., CD and DSF. Human Trx1 was prepared as described in [48]. *E. coli* Trx1 and *E. coli* TrxR cDNAs were amplified by PCR from human cDNA and *E. coli* XL1 blue, respectively, using specific primers which were designed to insert

restriction sites for NdeI and BamHI (see supplementary table 1). The insert was ligated into the expression vector pET15b (Merck, Germany). All constructs and mutations were verified by sequencing (Microsynth Seqlab, Göttingen, Germany).

**2.4. Mutagenesis.** Three different groups of mutants were produced. Group I includes 10 mutants with changes in those particular residues that lead to perturbation at the immediate contact area of hTrx1 and hTrxR. Group II lists the mutants that change the electrostatic properties both in the immediate contact area and outside the contact area of hTrx1 and hTrxR. Group III includes the mutant which changes the electrostatic properties far away from the active site and immediate contact area. Mutations of the amino acid sequence and amplification of the plasmids were performed by rolling circle PCR. We generated the mutants using the indicated primers and the reversible complementary counterparts. Oligonucleotides are listed in supplementary table 1.

**2.5. Recombinant Expression and Purification.** Plasmids for recombinant expression of His-tagged Trx1 variants, *E. coli* TrxR, and human TrxR U498C were transformed into *E. coli* BL21 DE3 pRIL cells (Life Technologies, UK). Transformed cells were grown at 37°C in LB medium (Roth, Germany) with appropriate antibiotics to an optical density of 0.5 to 0.7 at 600 nm. Protein expression was induced by the addition of 0.5 mM isopropyl-1-thio- $\beta$ -D-galactopyranoside (IPTG, Roth, Germany). The proteins were purified via immobilized metal affinity chromatography [49]. Size and purity of recombinantly expressed proteins were confirmed by SDS-PAGE using precasted TGX stain-free gels (4–20%, BioRad, Hercules, CA, USA). Pictures were taken following a five-minute UV-light activation.

**2.6. Reduction of Proteins.** The purified hTrx1 and mutant proteins were reduced with 10 mM TCEP (tris(2-carboxyethyl)phosphine) for 30 minutes and subsequently rebuffed in TE (50 mM Tris-HCl and 2 mM EDTA, pH 7.5) buffer using NAP-5 columns (GE Healthcare, UK). The rebuffed proteins were stored and kept reduced using immobilized TCEP disulphide reducing gel (Thermo Scientific, MA, USA) with a 2:1 ratio of sample volume to TCEP reducing gel volume. The protein and gel suspension was incubated at least 30 minutes rotating and centrifuged at  $1000 \times g$  for 1 minute. Protein concentration in the supernatant was determined based on molar absorptivity at 280 nm ( $\epsilon_{\text{hTrx1}} = 6990 \text{ M}^{-1}\text{cm}^{-1}$  and  $\epsilon_{\text{hTrxR}} = 64290 \text{ M}^{-1}\text{cm}^{-1}$ ).

**2.7. Kinetics of Insulin Reduction by Trx.** The activity of hTrx1 and different mutants was determined by a plate-based NADPH depletion assay adapted from (E. S. J. [50]). The final reaction mixtures of 200  $\mu\text{l}$  contained 50 mM Tris-EDTA buffer (pH 7.5), 150  $\mu\text{M}$  NADPH, 160  $\mu\text{M}$  insulin, 1.25 nM recombinant rat selenocysteine-containing TrxR and variable concentrations of Trx1, and mutant proteins (0–25  $\mu\text{M}$ ). NADPH consumption was measured at 340 nm for 80 minutes using the Clariostar plate reader (BMG Labtech, Offenburg, Germany). The linear range of the decrease in absorption was determined for each reaction individually.

Only reduced proteins were used in this assay. The specific activity of the recombinant selenocysteine-containing enzyme was approx.  $100 \text{ min}^{-1}$ . This was lower than reported before [30] and likely the result of a low degree of selenocysteine incorporation into the enzyme.

**2.8. Differential Scanning Fluorimetry.** Differential scanning fluorimetry (DSF) was performed in the CFX96 real-time PCR detection system from BioRad (Hercules, CA, USA) to obtain the dissociation constant and the thermal stability of the complex as described in [51]. All the proteins were desalted and rebuffed in Tris-EDTA buffer (50 mM Tris and 1 mM EDTA, pH 7.4) after purification using NAP-5 columns (GE Healthcare, UK) prior to this assay. The final reaction mixture of 50  $\mu\text{l}$  contained 10  $\mu\text{M}$  hTrxR protein, hTrx1 with variable concentrations (from 0 to 100  $\mu\text{M}$ ), Sypro Orange (1:500 diluted), and Tris-EDTA buffer. The reaction mixture was then heated with 0.3°C increments from 10.5 to 80°C. The increase in fluorescence due to binding of the dye to hydrophobic regions exposed during denaturation was recorded using the instrument's "FRET"-settings.

The melting temperatures of the thioredoxin reductase were obtained by fitting the first denaturation step (from 25.5°C to 42.6°C) with the Boltzmann fit (Eq. (1)), where FU is the measured fluorescence signal,  $T_m$  is the melting temperature,  $T$  is the temperature, and  $s$  is the slope.

$$\text{FU} = \frac{1}{1 + \exp(T_m - T/s)} \quad (1)$$

The calculated melting temperatures were then plotted against the concentration of thioredoxin to obtain the  $\text{EC}_{50}$  value, which in turn can be used to calculate the dissociation constant  $K_d$  as described in ref. [52]. For more details, see supplementary information.

**2.9. CD Spectroscopy.** CD spectra were recorded in 300 mM NaCl and 50 mM sodium phosphate, pH 8, with the proteins hTrxR and hTrx1 at 10 and 20  $\mu\text{M}$  concentrations, respectively, using a Jasco J-810 spectropolarimeter from 190 nm to 240 nm at 25°C. Buffer-only spectra were subtracted. A standard sensitivity of 100 mdeg was used with a data pitch of 1 nm, 50 nm/min scanning speed, and 0.2 nm band width. In total, 10 spectra were accumulated for each sample. All the purified proteins were desalted and rebuffed in phosphate buffer (50 mM sodium phosphate and 300 mM NaCl, pH 8) using NAP-5 columns (GE Healthcare, UK) prior to CD spectroscopy.

**2.10. Tryptophan Fluorescence.** Fluorescence quenching assays were performed using a Perkin Elmer LS50B fluorimeter. The fluorescence signal was acquired at 25°C at the wavelength range from 310 to 498 nm with excitation at 296 nm. The slit width for excitation and emission was 6 and 4 nm, respectively. All purified proteins were desalted and rebuffed in Tris-EDTA buffer (50 mM Tris and 1 mM EDTA, pH 7.4) using NAP-5 columns (GE Healthcare, UK) prior to fluorescence quenching measurements.



**2.11. All-Atom Molecular Dynamics Simulations.** The crystal structures of TrxR and TrxR-Trx complex were obtained from the RCSB Protein Data Bank (PDB: 2ZZ0 and 3qfa, respectively) and then prepared for the simulations with the DockPrep tool of UCSF Chimera [40]. The MD simulations were performed in Gromacs 2016.3 [53], with AMBER-99ff-ILDN force field. The proteins and complexes were solvated with TIP3P water [54] in a cubic box under periodic boundary conditions and at least 1 nm away from the edge of the box. Na<sup>+</sup> and Cl<sup>-</sup> ions were added to neutralize the charge of the system. An initial energy minimization was performed using the steepest descent algorithm until the system converged to 1000 kJ·mol<sup>-1</sup>·nm<sup>-1</sup>. System equilibration was performed for 100 ps at a constant number of molecules, volume, and temperature 300 K (NVT) and for a duration of 100 ps with constant number of molecules, 1 bar pressure, and temperature 300 K (NPT). The duration of each production simulation was 50–250 ns (2 fs time steps). Simulations were repeated three times. The bonded interactions of hydrogens were constrained with LINCS algorithm [55]. The Parrinello-Rahman [56] method was used for pressure coupling and the modified Berendsen thermostat—velocity rescale [57] for the temperature coupling. The Particle Mesh Ewald [58] method was used for the calculation of the long-range electrostatic interactions; for the short-range interactions, Verlet cut-off scheme with 1.5 nm cut-off distance was applied, for both Coulomb- and van-der-Waals interactions. The parametrisation of FAD was done with Antechamber tool of AmberTools and ACPYPE [59] script with GAFF force field and Gasteiger charge methods. The RMSD and RMSF analyses of simulated data were performed with GROMACS-intern tools.

**2.12. Statistical Analysis.** All the numerical data are reported as mean ± SD unless otherwise stated. Statistical analyses were performed using one-way ANOVA followed by Tukey HSD test (Statistics Kingdom, Melbourne, Australia). A value of  $p < 0.05$  was considered statistically significant.

**2.13. Additional Software.** All numerical calculations (spectra and kinetics) were performed and visualized using Grace (<https://plasma-gate.weizmann.ac.il/Grace/>). Structures were depicted using UCSF Chimera [40]. Picture panels and reaction schemes were generated using Inkscape (<https://inkscape.org/>).

### 3. Results

Based on previously published structures of the complexes between human Trx1 and TrxR1 [60], we have analysed the molecular interactions between the two proteins (Figure 1, supplementary Fig. 1). We have also included, for comparison, *E. coli* Trx1 and TrxR [61]. *E. coli* TrxR has a much narrower substrate specificity compared to the mammalian enzyme and cannot reduce human Trx1, while the mammalian-type TrxR1 can reduce both bacterial and mammalian Trxs (E. S. J. [50]). The first striking observation is the lower amount of molecular interactions (suppl. Fig. 1) and the smaller area of interaction, 448 versus 561 Å<sup>2</sup>, in the

human complex (Figure 1(b)) compared to the bacterial (Figure 1(e)). We have computed the electrostatic properties of the proteins as outlined before [14] (Figures 1(c) and 1(f)). The isosurfaces of the electrostatic potentials at  $\pm 1 k_B \cdot T \cdot e^{-1}$  ( $\pm 25.8$  mV) of the interaction surfaces show an almost perfect complementarity in the immediate contact areas. Moreover, for the human complex, where only the left half of the Trx is in direct contact, as depicted in Figure 1(b), this is even true for the parts of the proteins that do not form direct molecular interactions (other than long-range electrostatic interactions), but only face each other (right side of the marked areas of the proteins in Figure 1(c)).

**3.1. Trx and TrxR Interact Independently of the Redox Reaction and the Redox State of Trx.** We proposed that electrostatic complementarity is the major distinguishing feature that controls the specific interactions of Trx family proteins with their target proteins. The electrostatic landscape of Trx family proteins shows only minor differences between their reduced and oxidized forms (Figures 2(a) and 2(b), respectively). Interactions of the proteins, *i.e.*, the formation of an encounter complex preceding the thiol or thiol-selenol disulphide exchange reactions, should therefore be independent of the subsequent redox reaction. To test this hypothesis, we have generated an inactive mutant of Trx1, in which both active site cysteinyl residues were exchanged for seryl residues (C32,35S). Figures 2(a)–2(c) depict the electrostatic characteristics of the interaction interface of reduced, oxidized, and C32,35S human Trx1 calculated from experimentally determined structures demonstrating their similarity. We have confirmed a previous report that the redox-inactive C32,35S mutant is an inhibitor of the reduction of wild-type Trx1 by TrxR1 [62]. The mutant protein inhibits the reaction by competing with the oxidized wild-type protein for binding to the reduced reductase in the insulin reduction assay (Figure 2(d)). From a secondary Lineweaver-Burk plot (inset of Figure 2(d)), the  $K_i$  was determined as  $5.3 \mu\text{mol}\cdot\text{l}^{-1}$ . Next, we analysed the complex formation by differential scanning fluorimetry (DSF, Figures 2(e)–2(h)). This method allows to determine dissociation constants by monitoring how a binding event influences the thermal stability of a protein. By fitting the data to the Boltzmann equation and plotting the log [Trx] against the  $T_m$  in Hill plots, we have obtained  $K_d$  values of  $13.6 \pm 1.6$  and  $9.8 \pm 0.3 \mu\text{mol}\cdot\text{l}^{-1}$  for the wild-type and mutant proteins, respectively Table 1. For further details of this approach, we refer to the supplementary material. All together, these similarities provide further evidence that both wild-type and C32,35S Trx1 interact with TrxR in the same way. Apparently, the interaction of the two proteins does not require Trx to be oxidized, nor the thiol-disulphide/selenosulphide exchange reaction to occur.

Fritz-Wolf et al. have presented a complex structure of the mixed-disulphide intermediate snapshot between the mutant proteins Trx1 C35S and TrxR1 U498C [60]. Since this complex was enforced by using mutated proteins, which was also possible for various other permutations of point mutants of Trx1 and TrxR1 [63], we have prepared complex structures of reduced wild-type and C32,35S Trx1 with TrxR1 U498C and analysed them as well as the two Trxs

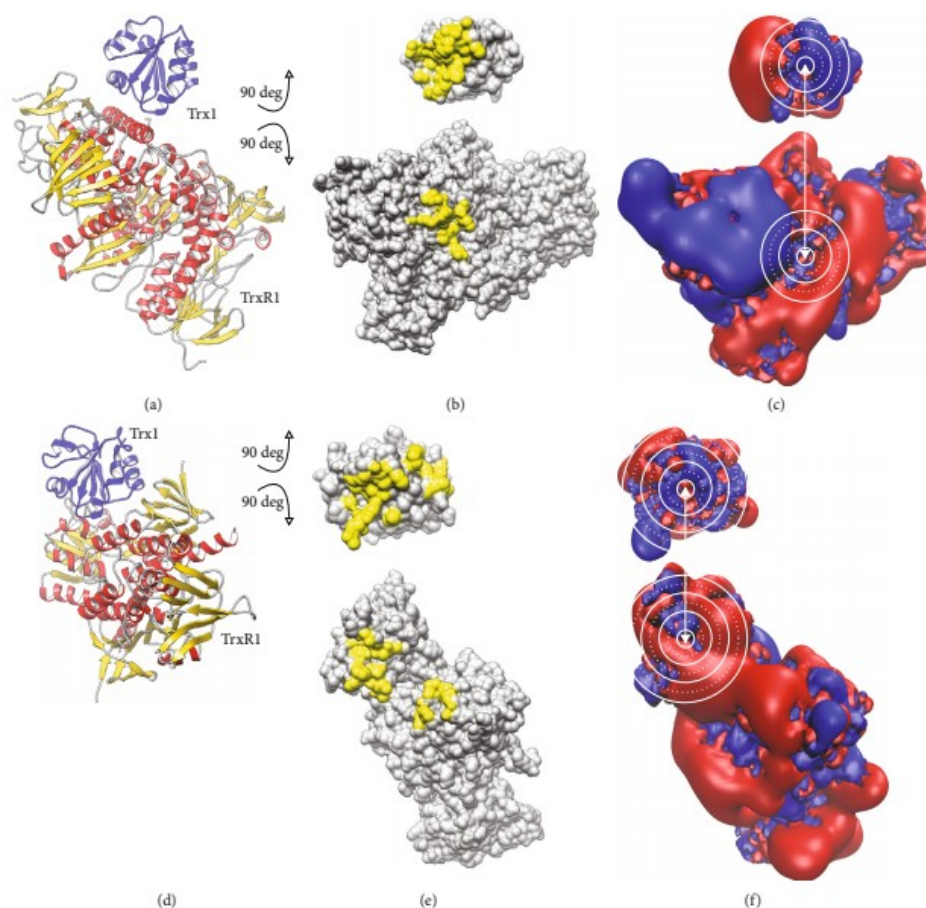


FIGURE 1: Molecular interaction surfaces of the human Trx1-TrxR1 and *E. coli* Trx1-TrxR complexes. Cartoon representation of the secondary structures of (a) human Trx1-TrxR1 complex PDB: 3qfa and (d) *E. coli* Trx1-TrxR complex PDB: 1f6m. The complex structure was opened by rotating both Trx and TrxR structures by  $90^\circ$  forward and backward, respectively. The contact patches with direct molecular contacts were highlighted in yellow using UCSF chimera (b, e). The isosurfaces of the electrostatic potential were depicted at  $\pm 1 k_B \cdot T \cdot e^{-1}$  in blue (positive) and red (negative), respectively. The active site cysteinyl residues and interaction surfaces in the immediate contact area in both proteins were encircled in white lines (c, f).

alone by all-atom molecular dynamics simulations. Over the time course of 250 ns, both Trxs and both complexes behaved in a very similar way (Figures 3(a) and 3(b)). The average RMSD values of the C $\alpha$  atoms during the last 150 ns of the simulations were 1.84 and 1.93 Å for the wild-type and C32,35S complexes, respectively. The RMSD between the two most representative complexes of wild-type and mutant was 2.42 Å (complexes are shown in Figure 3(d)). The fluctuation of the side chains was also very similar, both for the free redoxins as well as for the redoxins bound to TrxR1. In general, the fluctuations of the side chains within the contact area decreased in the complexes, especially in the area of the CxxC active site (Figure 3(c), RMSF).

Essentially all Trxs contain a tryptophanyl residue immediately before the N-terminal active site cysteinyl residue. TrxR1 residue W114 is located close to the active site selenocysteinyl (in our model system cysteinyl) residue. Binding of Trx1 to the reductase should thus decrease the solvent accessibility of these two indole ring systems. Compared to the simulation runs for the redoxins alone, the solvent accessible surface area of Trx1 W31 markedly decreased in the complexes from around 2 to 0.5 Å<sup>2</sup> (Figures 3(e) and 3(f)). Tryptophan indole ring systems exhibit solvatochromatic properties. In general, the fluorescence of tryptophanyl residues buried within a protein core or interaction surface is quenched due to aromatic-aromatic interactions or energy

6

Oxidative Medicine and Cellular Longevity

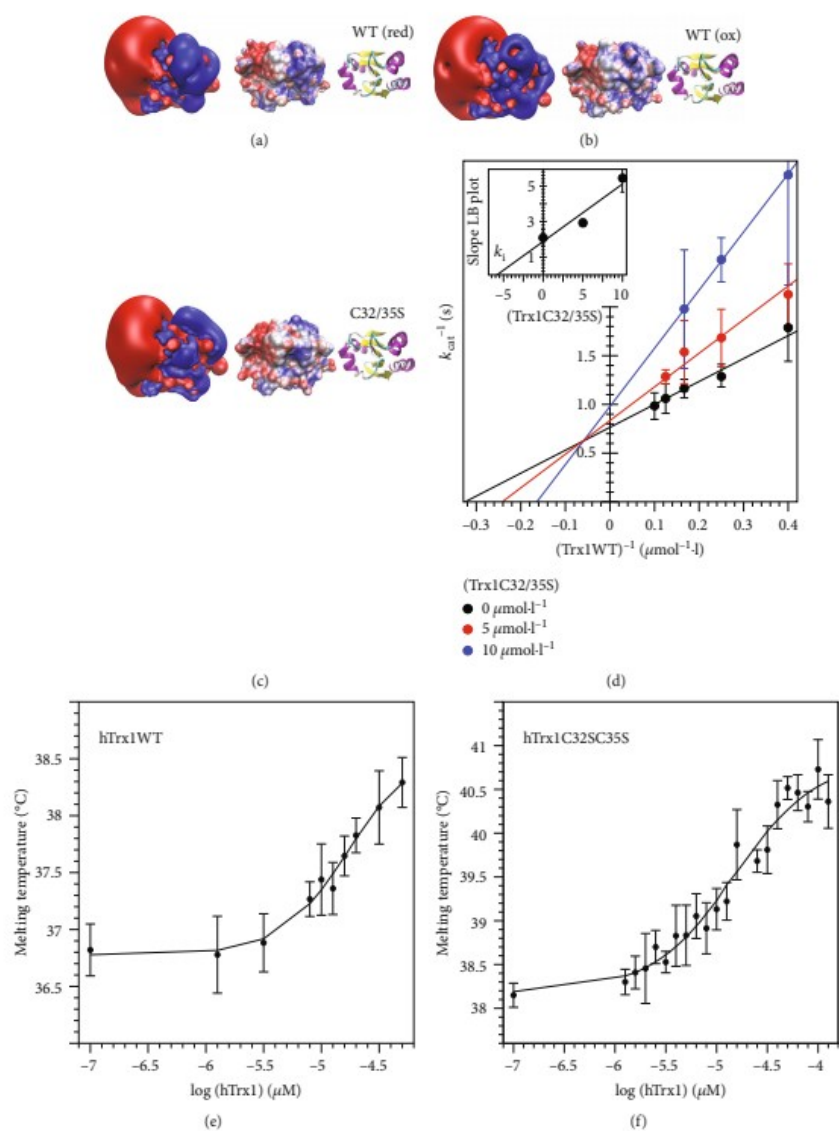


FIGURE 2: Continued.

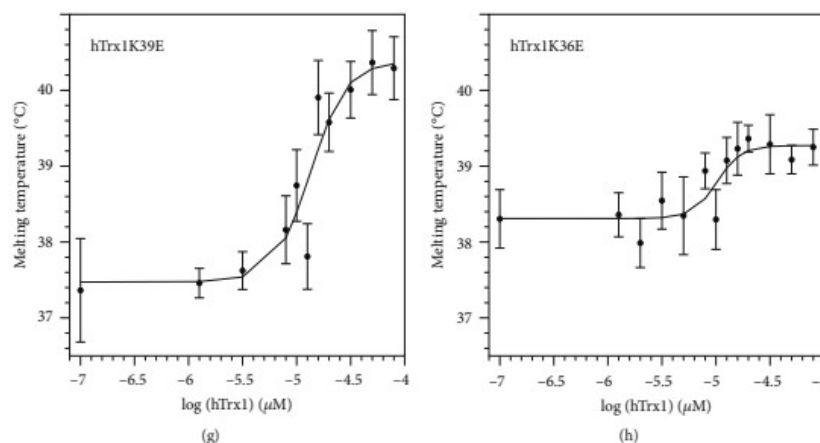


FIGURE 2: Comparison between the wild-type and double cysteinyl mutant of hTrx1 and its respective complex with hTrxR1. (a–c) Reduced and oxidized hTrx1WT compared to double cysteinyl mutant (a–c, respectively) in three different representations: (i) isosurfaces of the electrostatic potential at  $\pm 1 k_B \cdot T \cdot e^{-1}$  in blue (positive) and red (negative), (ii) electrostatic potential mapped on the solvent accessible surface at  $\pm 4 k_B \cdot T \cdot e^{-1}$ , and (iii) secondary structure. (d) Lineweaver-Burk plot of inhibition kinetics measurements in the insulin reduction assay. The inset depicts the plot of the slope of the Lineweaver-Burk plots against the concentration of the redox-inactive mutant for the determination of the  $k_i$ . This assay was performed with the recombinant selenocysteine-containing TrxR. (e–h) Hill plots depicting the  $\log [\text{Trx}]$  against the melting temperature ( $T_m$ ) to determine the  $EC_{50}$  and  $k_d$  values of the complexes. The  $T_m$  values were calculated from the original melting curves fitted to the Boltzmann equation; for further details, see supplementary material. These assays were performed using the U498C mutant of human TrxR1.

TABLE 1: Dissociation constants and binding energy determined for the interactions between Trx1 and TrxR1.

hTrx1 mutants	$n$	$K_d$ $\mu\text{mol}\cdot\text{l}^{-1}$	$\Delta G$ $\text{kJ}\cdot\text{mol}^{-1}$	$\Delta\Delta G$ $\text{kJ}\cdot\text{mol}^{-1}$
WT	12	$13.60 \pm 1.63$	$-27.79 \pm 0.29$	0
C32,35S	12	$9.80 \pm 0.31$	$-28.59 \pm 0.2$	-0.79
K36E	12	$5.28 \pm 0.08$	$-30.12 \pm 0.03$	-2.33
K39E	12	$9.68 \pm 1.25$	$-28.64 \pm 0.31$	-0.85

transfer to neighbouring charged groups; see for instance [64]. The decrease in solvent accessible area should thus quench the tryptophanyl fluorescence upon complex formation. We compared the changes of Trp fluorescence of both wild-type and C32,35S Trx1 upon complex formation with TrxR1 U498C. For both protein complexes, we recorded the expected fluorescence quenching (Figures 3(g) and 3(h)).

Changes in the absorption properties of Trp residues may also induce changes in near and far UV circular dichroism (CD) spectra. We have thus analysed the binding of oxidized wild-type Trx1 and the active site cysteinyl double mutant to the selenocysteinylyl to cysteinyl (U498C) mutant of TrxR by CD spectroscopy (supplementary Fig. 4). We have recorded the individual spectra of both proteins and compared the sum of both spectra to the ellipticity recorded for the proteins together, *i.e.*, in an equilibrium reaction of the formation and dissociation of the enzyme-substrate complex. The insets of supplementary Fig. 4A and B depict the differences in ellipticity between the spectra of the complexes and the sum. Both

difference spectra do not display major differences; however, some smaller changes were found to be highly similar between the wild-type and C32,35S proteins when incubated with TrxR; these are slight increases in ellipticity at 205, 211, 217, and from 220 to 235 nm. While these changes do not prove complex formation *per se*, they provide further evidence that both the wild-type and mutant proteins interact with TrxR in a similar way.

**3.2. Complementary Electrostatic Interaction Surfaces.** To analyse the importance of complementary electrostatic interaction surfaces for the mammalian Trx1-TrxR redox couple, we have generated a number of Trx1 mutants that change the electrostatic potential (Figure 4): first, within the immediate contact area but, with one exception (K72), not involved in direct molecular interactions (for these, please see suppl. Fig. 2A–B); second, outside the immediate contact area but on the surface that faces the reductase; and third, one mutant with profound changes on the opposite side of the interaction surface (Figures 4(a) and 4(b)). Following recombinant expression in *E. coli* and purification applying immobilized metal affinity chromatography, we have confirmed the folding and stability of all mutants using differential scanning fluorimetry (suppl. Fig 3). Using a coupled assay with the reduction of insulin, to keep the Trx in the assay mix oxidized, we have analysed the reaction kinetics of recombinant selenocysteine-containing TrxR1 with these mutants as substrates, as summarized in Table 2 and Figure 5.

The mutations within or partly within the interaction surface (K36E; D60N; D58,60,61N; Q63R; and Q63R,K94E)



8

Oxidative Medicine and Cellular Longevity

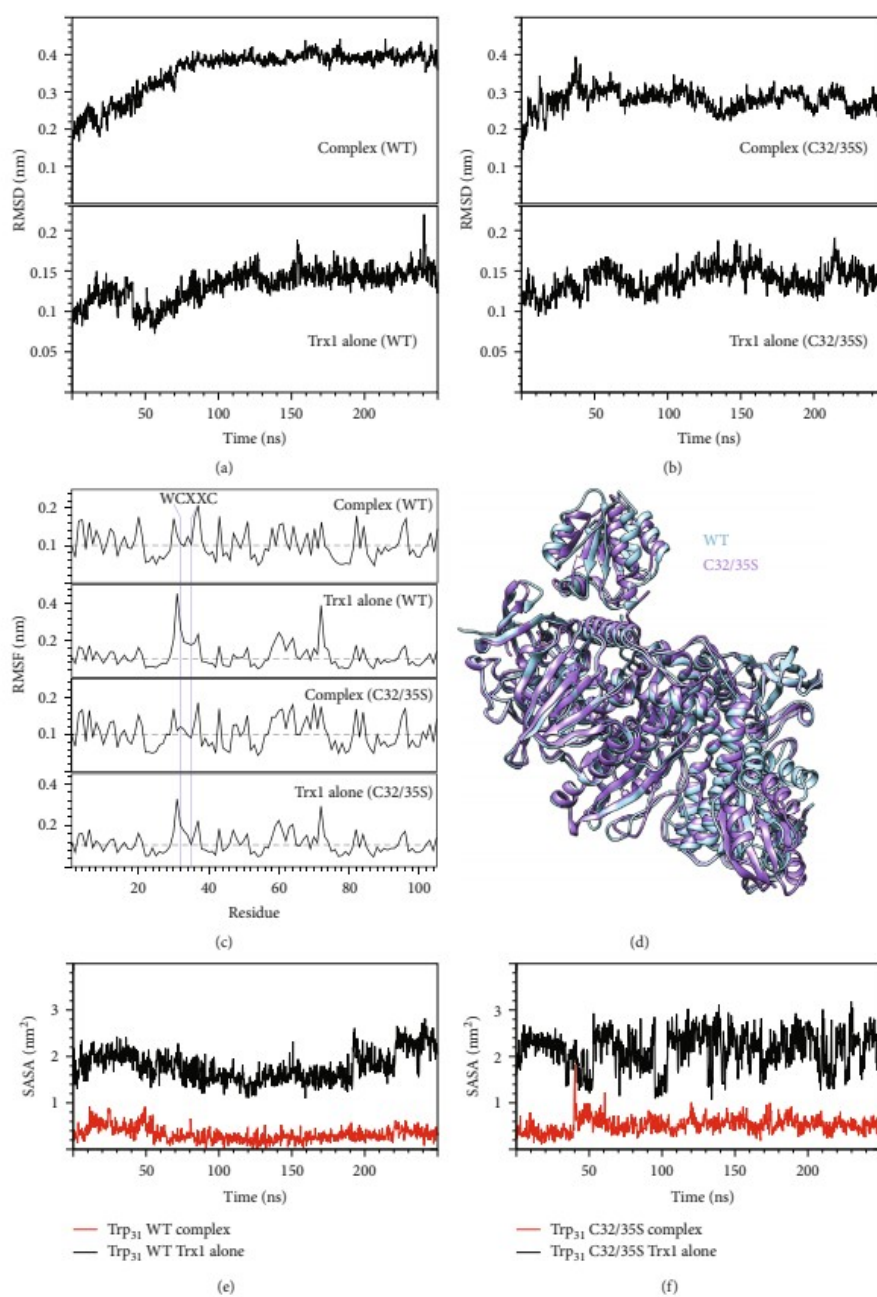


FIGURE 3: Continued.

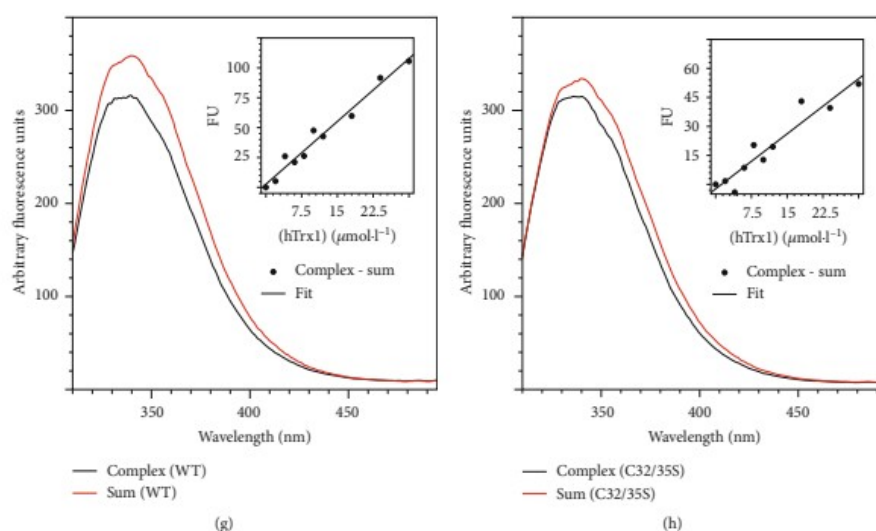


FIGURE 3: Molecular dynamics simulations of the TrxR-Trx complexes. (a, b) RMSD comparison of wild-type and C32,35S Trx alone (lower panels) and in complex with TrxR1 (top panels) over 250 ns. (c) Root-mean-square fluctuations of hTrx1 residues over 250 ns long MD simulation of wild-type and C32,35S Trx and the respective complexes with TrxR1. The active site cysteinyl residues are indicated (blue vertical lines). (d) Comparison of two representative structures from the 250 ns MD simulation of wild-type and cysteinyl double mutant complexes. The calculation of the representative structure was performed by Gromacs' clustering tool with RMSD cut-off of 0.2 nm. Superimposition was performed using UCSF Chimera's MatchMaker tool. (e, f) Solvent accessible surface area of W31 of hTrx1WT and hTrx1C32,35S in both complexes with hTrxR1 (red plot) and free (black plot) over 250 ns of MD simulation. (g, h) Fluorescence spectra of hTrx1-hTrxR1 U498C complexes (black) compared to the sum of the individually recorded spectra of hTrx1 and hTrxR1. The insets include the difference of the fluorescence signal between the complex- and sum spectra at 339.5 nm at different concentrations of thioredoxin.

mostly resulted in a significantly reduced catalytic efficiency of TrxR. This decreased efficiency was the result of an increase in  $K_M$ , *i.e.*, a reduced affinity of TrxR for these proteins as substrates. The exception to this was the S67H mutation with only subtle changes to the electrostatic potential close to the N-terminal active site thiol (Figure 4). For this mutant, the catalytic efficiency did not change significantly. However, this was the result of both a significant decrease in  $K_M$  and  $k_{cat}$ . Two mutants with changes in their electrostatic characteristics outside the immediate contact surface but still facing TrxR (K39E and K94E) were analysed. For K39E, the catalytic efficiency did not change significantly. Again, this was the result of both a significant decrease in  $K_M$  and  $k_{cat}$ . The K94E mutant was the biggest surprise in our analysis. The changes (positive to negative) introduced here (see Figure 4) affected an area approx. 10 Å away from the active site thiol and the immediate contact area. Nevertheless, TrxR displayed the lowest catalytic efficiency with this mutant as a result of both an increase in  $K_M$  and a drop in  $k_{cat}$ . The double mutant Q63R,K94E that combines changes within and outside the area forming molecular interactions with TrxR (other than long-range electrostatic interactions) caused an increase in  $K_M$  and a decrease in  $k_{cat}$ , resulting in a catalytic efficiency comparable to those of the

single mutants (Table 2). Changes in the electrostatic potential on the side opposite to the interaction surface of Trx1 (A17R,I53R) led to a small, but not significant, drop in  $k_{cat}$  and did not change the affinity of TrxR1 for this protein compared to the wild-type.

We have also tested some of our human Trx1 mutants, *i.e.*, those that were more similar to *E. coli* Trx1 (Q63R,K94E; S67H; K72E; and K94E, see Figure 4 and suppl. Fig. 6) as substrate for the *E. coli* reductase. As the wild-type hTrx1, these failed to interact with the bacterial enzyme (suppl. Fig. 5).

**3.3. Human Cytosolic Trxs and Trx Domains.** The human genome encodes at least ten cytosolic Trxs or Trx domain-containing proteins, *i.e.*, Trx1, Txndc2, 3, 6, 8, 9, and 17, Txnl1, and Nrx. To our knowledge, only Trx1, Txndc2, Txndc17 (also known as TRP14), and Txnl1 have been experimentally confirmed as substrates of TrxR1 [65–67]. Grx2, that is expressed in cytosolic and mitochondrial isoforms [68], has also been characterised as substrate for TrxR1 [69]. Nrx (nucleoredoxin) has been suggested as TrxR1 interaction partner [70]. Figure 6 summarizes the electrostatic similarity of these proteins. The highest similarity in the electrostatic properties was observed in the proteins that were

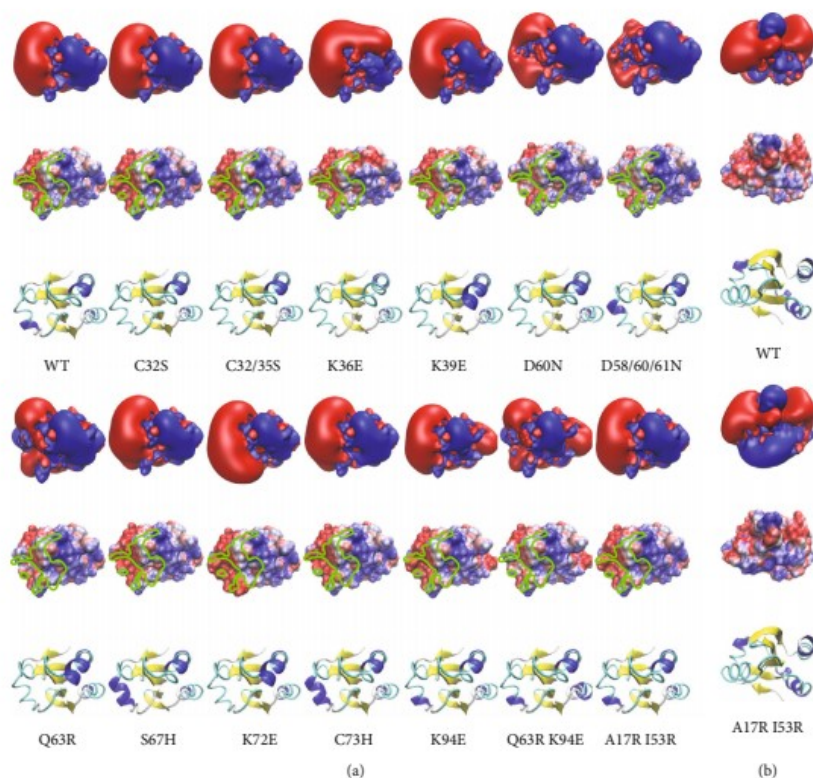


FIGURE 4: Overview of hTrx1 mutants in different representations. The first row shows the isosurfaces of the electrostatic potential at  $\pm 1 k_B \cdot T \cdot e^{-1}$  in blue (positive) and red (negative), respectively. The second row shows the electrostatic potential mapped to the water accessible surface at  $\pm 4 k_B \cdot T \cdot e^{-1}$ . The third row displays the cartoon representation of the secondary structure of wild-type and mutant Trx1s (a, b). The immediate contact areas of interaction surfaces were circled in green in the second row of both panels (a). All the structures are oriented so that the N-terminal active site cysteinyl residues face towards the camera perspective (a) or rotated by  $180^\circ$  (b).

characterised as TrxR1 substrates before. Interestingly, Trxndc17 differs from the other redoxins significantly; however, it does show complementarity when rotated  $180^\circ$ , suggesting that this could reflect a unique mode of interaction with TrxR1 (suppl. Fig. 6).

#### 4. Discussion

The results presented here confirm that the binding of Trx1 to TrxR1 is independent of a subsequent redox reaction between the proteins. Trx1 does not need to be in the oxidized disulphide form to bind to TrxR1. The redox-inactive Trx1 C32,35S, presumably always in a conformation that reflects reduced wild-type protein, binds to both reduced and oxidized TrxR1. The redox reaction-independent binding of Trx to its reductase has been reported before. In 1994, Oblong and coworkers first reported that human Trx1 C32,35S is a competitive inhibitor of the reduction of

wild-type Trx1 by TrxR with a  $K_i$  value of  $6.7 \mu\text{mol}\cdot\text{l}^{-1}$  [62], and the  $K_i$  of  $5.3 \mu\text{mol}\cdot\text{l}^{-1}$  estimated in this study is in good agreement with this. This value is close to the  $K_M$  of the enzyme for wild type Trx1 ( $2.4 \mu\text{mol}\cdot\text{l}^{-1}$ ), demonstrating that TrxR1 has similar affinities for both the wild-type and the redox-inactive mutant. Oblong and coworkers also reported detectable changes in CD spectra when wild-type and C32,C35S were bound to TrxR [62]. Subsequently, the C32,35S mutant has been characterised as a dominant negative mutant of the Trx system when overexpressed *in vivo*. For instance, in 1996, Gallegos et al. analysed the effect of Trx overexpression on the phenotype of breast cancer cells. They reported that wild-type Trx expression increased cell proliferation, but the expression of the C32,35S mutant inhibited cell growth and reversed the transformed phenotype of the cells. Xenografted into immunodeficient mice, wild-type Trx1 expression increased tumour formation, while expression of the redox-inactive mutant inhibited



TABLE 2: Kinetic analysis of the TrxR1 catalysed reduction of Trx1 variants in an insulin reduction-coupled assay.

Categories	hTrx1 mutants	<i>n</i>	$K_M$ $\mu\text{mol}\cdot\text{l}^{-1}$	$k_{\text{cat}}$ $\text{s}^{-1}$	Catalytic efficiency %	$\text{mol}\cdot\text{l}^{-1}\cdot\text{s}^{-1}$
Wild-type	WT	43	$2.43 \pm 0.54$	$1.55 \pm 0.42$	100.00%	$6.38 \cdot 10^{-7}$
	K36E	13	$9.82 \pm 1.83^*$	$1.33 \pm 0.28$	21.23%	$1.35 \cdot 10^{-7}$
	D60N	16	$3.26 \pm 1.76$	$1.19 \pm 0.42$	57.23%	$3.65 \cdot 10^{-7}$
	D58,60,61N	17	$5.83 \pm 2.05^*$	$0.93 \pm 0.16$	25.01%	$1.6 \cdot 10^{-7}$
Inside or partly within the contact surface	Q63R	15	$6.37 \pm 1.57^*$	$1.25 \pm 0.57$	30.76%	$1.96 \cdot 10^{-7}$
	S67H	18	$1.36 \pm 0.75^*$	$1.03 \pm 0.31^*$	118.73%	$7.57 \cdot 10^{-7}$
	K72E	18	$2.22 \pm 0.86$	$1.99 \pm 0.39^*$	140.53%	$8.96 \cdot 10^{-7}$
	C73H	16	$1.24 \pm 0.36^*$	$1.22 \pm 0.17$	154.25%	$9.84 \cdot 10^{-7}$
Mixed type	Q63R,K94E	15	$7.09 \pm 1.88^*$	$0.88 \pm 0.3^*$	19.46%	$1.24 \cdot 10^{-7}$
	K39E	18	$1.45 \pm 0.43^*$	$0.86 \pm 0.14^*$	92.98%	$5.93 \cdot 10^{-7}$
Outside the contact surface but facing TrxR	Q63R,K94E	15	$7.09 \pm 1.88^*$	$0.88 \pm 0.3^*$	19.46%	$1.24 \cdot 10^{-7}$
	K94E	6	$3.78 \pm 1.56^*$	$0.45 \pm 0.16^*$	18.66%	$1.19 \cdot 10^{-7}$
Opposite side	A17R,I53R	18	$2.73 \pm 0.49$	$1.24 \pm 0.32$	71.21%	$4.54 \cdot 10^{-7}$

tumour formation [71]. Yamamoto *et al.* reported in 2003 that transgenic cardiac-specific overexpression of the C32,35S mutant of Trx1 diminished the endogenous activity of Trx [72]. Oh *et al.* reported in 2004 the up- and downregulation of matrix metalloproteinase 2 activities upon expression of wild-type and C32,35S Trx1, respectively, in human dermal fibroblasts [73]. More recently, Das reported on the effects of transgenic overexpression of both wild-type and C32,35S Trx1 in lung tissue. Wild-type Trx1 increased the resistance to hyperoxia-induced lung injury and increased the levels of reduced Trx in the lung. Overexpression of the redox-inactive mutant, however, decreased Trx activity and even increased the degree of oxidation of endogenous wild-type Trx in the tissue [74]. Taken together, these results demonstrate that the binding of Trx1 to TrxR is independent of the subsequent thiol-disulphide/selenosulphide exchange reaction and does not require Trx to be in the oxidized disulphide form.

Based on the analysis of the interaction of *E. coli* Trx and phosphoadenylyl sulfate (PAPS) reductase, Palde and Carroll suggested that Trxs recognize the oxidized form of its target proteins with higher selectivity compared to their reduced counterparts and that an increase in entropy may be a major recognition force for their interaction [38]. Based on this observation, the authors proposed a universal entropy-driven mechanism for thioredoxin-target recognition. It should, however, be mentioned that the Trx/PAPS redox couple may not be the most representative redox couple to study the importance of the individual redox states, because reduction and oxidation of PAPS reductase require extensive conformational changes of the protein [75–78]. For the Trx-TrxR redox couple discussed here, our results—as well as all the before mentioned evidence—imply that the redox state does not seem to have a major influence on the recognition and formation of a complex between the two proteins.

Peng *et al.* studied the reactivity of TrxA, TrxP, and TrxQ from *Staphylococcus aureus* with persulphidated pyruvate kinase as a model substrate. The three redoxins displayed small differences in substrate specificity that were also discussed to be the result of electrostatic differences in the area surrounding the N-terminal active site thiol [79]. We have previously proposed and provided evidence that the binding of Trx family proteins to their interaction partners and likely all protein-protein interactions in aqueous solution require geometrically compatible surfaces and, that given, are controlled by complementary electrostatic surfaces [14, 39, 80]. Here, we have engineered mutants of Trx1 with changes in their electrostatic potential landscape within and outside the contact patch with TrxR. In summary, the inversion of positive or negative potentials in areas that fell within the immediate contact area with TrxR1 decreased the affinity of the enzyme for its substrate without affecting  $k_{\text{cat}}$ . The subtle changes introduced with the S67H mutation close to the cysteinyl residue attacked by the selenol of TrxR in the reaction cycle decreased both  $K_M$  and  $k_{\text{cat}}$ . The effects of the reversals in the electrostatic potential outside the immediate contact surface but still facing TrxR depend on the positions. While the more negative potential “north” of the N-terminal active site cysteinyl residue (see Figures 1(c) and 2) did not change the catalytic efficiency of TrxR, and the positive to negative inversion 10 Å “east” of the active side (K94E) caused the largest decrease in catalytic efficiency. The positive potential of K94 faces complementary negative potentials on TrxR; however, the oxygen atoms of the hydroxyl and carboxy groups responsible for this negative potential are in 18–22 Å distance of the  $\epsilon$ -amino group of K94. These distances exclude direct long-range electrostatic interactions as a potential explanation. Under the given conditions, these should only be significant until a distance of around 6 Å.



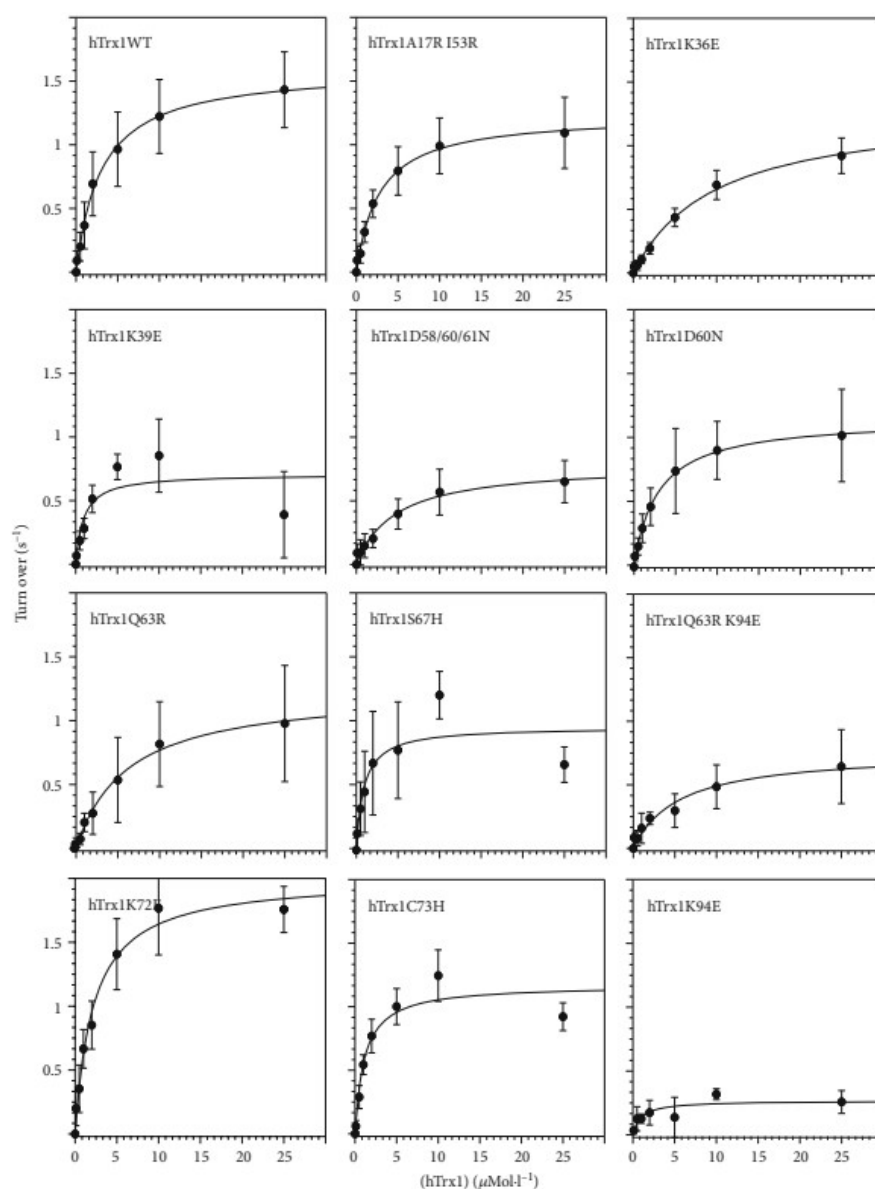


FIGURE 5: Kinetics of the reduction of the Trx1 mutants by TrxR. Michaelis-Menten plots for the proteins analysed. For details, e.g., on statistics and number of independent experiments, see Table 1 of the main text. All data are shown as mean  $\pm$  SD. The curves are the nonlinear curve fittings to the Michaelis-Menten equation from which the kinetic constants were obtained. These assays were performed with the recombinant selenocysteine-containing TrxR.

For our study, the tryptophanyl residues W31 and W114 of Trx1 and TrxR1, respectively, proved to be valuable for the analysis of the interaction between these two proteins. W114

of TrxR1 is an unusually reactive residue. If not part of the interaction surface with Trx, W114 is a solvent accessible residue susceptible to oxidation. It was suggested that this may

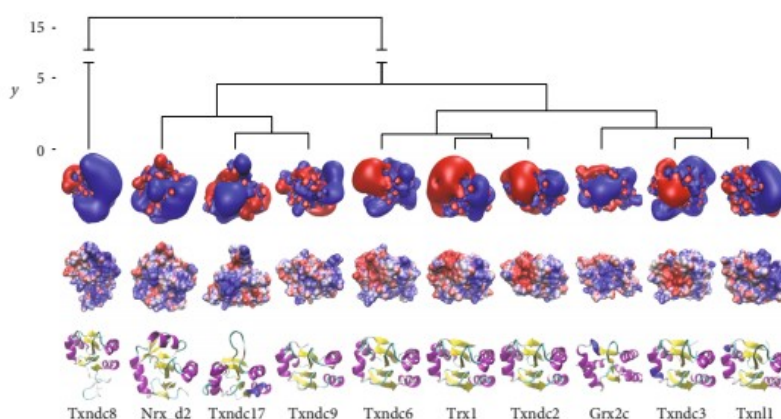


FIGURE 6: Electrostatic similarity of human cytosolic thioredoxins and thioredoxin domain-containing proteins. The tree of electrostatic similarity (on top) was prepared as described in [14]. The first row shows the isosurfaces of the electrostatic potential at  $\pm 1 k_B \cdot T \cdot e^{-1}$  in blue (positive) and red (negative), respectively. The second row shows the electrostatic potential mapped to the water accessible surface at  $\pm 4 k_B \cdot T \cdot e^{-1}$ . The third row displays the cartoon representation of the secondary structure of wild-type and mutant Trxs. The orientation of the structures is the same as in Figures 1 and 4(a).

serve regulatory functions; it may also serve as an electron relay communicating with the FAD moiety. When oxidized, it facilitates oligomerisation of TrxR1 into tetramers that were also found in a crystal structure of TrxR1 [63]. Moreover, oxidatively modified W114 was suggested to contribute to covalently bonded, but not disulphide-linked, dimers between TRP14 and TrxR1 in cells [81].

Human and *E. coli* TrxR exhibit significant differences in their substrate specificities. While the human reductase accepts Trxs from different species and various low molecular weight compounds, *E. coli* TrxR is basically restricted to its endogenous Trx substrates, and for an overview, see (E. S. J. [50]). To some degree, especially for the reduction of low molecular weight compounds, this may be due to the higher reactivity of the selenolate active site in the human enzyme compared to the thiolate in its bacterial counterpart. Our study here provides a hypothesis for the distant specificities of the bacterial and mammalian reductases for Trxs. The *E. coli* enzyme requires significant more molecular interactions (see Figure 1 and suppl. Figs. 2C and D). The contact area is larger and concave. This requires a considerably higher degree of geometrical complementarity. Moreover, its electrostatic properties are more delicate and less binary compared to the human. The human genome encodes at least ten cytosolic Trxs or Trx domain-containing proteins, *i.e.*, Trx1, Txndc2, 3, 6, 8, 9, and 17, Txn11, and Nrxd. Trx1, Txndc2, and Txn11 have been confirmed as substrates of TrxR1 [66, 67]. Txndc17 (also known as TRP14) was reported to be reduced efficiently by TrxR1 but not by TrxR2 ([65, 82], 14). This is in contrast to Trx1 that can be reduced by both reductases. Grx2, that is expressed in cytosolic and mitochondrial isoforms [68], has also been characterised as substrate for TrxR1 [69]. Nrxd (nuclerothiolate) has been suggested as TrxR1 interaction partner [70]. Figure 6 summarizes the electrostatic similarity of these proteins. In

agreement with our hypothesis, the proteins that have been characterised as TrxR1 substrates also show the highest similarity in their electrostatic properties. The only exception to this is Txndc17 that is clearly more distant. In fact, the electrostatic properties of its interaction surface are basically the opposite to the other functional redoxins (see Figure 6 and suppl. Fig. 6). Since this ought to block any fruitful interaction with TrxRs, we propose that Txndc17 must interact in a different way with TrxR1 compared to the other proteins. If the orientation of the interaction surface of Txndc17 is rotated by  $180^\circ$ , a fruitful interaction may become possible (see suppl. Fig. 6). The lack of activity with TrxR2 may then be the result of geometric constraints that inhibit these alternative interactions, since the attack of the selenolate on the redoxin disulphide has to occur in an  $180^\circ$  angle in line with the disulphide. A high geometric and electrostatic complementarity is required for the binding of a Trx to *E. coli* TrxR. For the human TrxR1, the lower number of direct molecular interactions and its more protruding active site (see Figure 1(a)) may contribute to its ability to bind and reduce a greater variety of Trxs. With this decreased importance of geometric complementarity, the electrostatic compatibility may be the primary factor controlling the enzyme affinity for different redoxins as well as the efficiency of catalysis (see Figure 4 and Table 2). That is why the human enzyme also reduces *E. coli* Trx1 that only displays limited complementarity (see Figure 1 and suppl. Fig. 6), albeit with 14-fold lower affinity and 15.4-fold lower catalytic efficiency (E. S. J. [50]).

#### Conclusions

Our study provides new insights into the molecular interactions between human Trx1 and its reductase TrxR1. We confirmed that the transient protein-protein interactions, *i.e.*, the formation of an encounter complex between the proteins, are independent of the subsequent redox reaction. The

proteins must have an inherent affinity for each other in the area of the thiol-disulphide/selenosulphide exchange reaction controlling fruitful collisions in solution. The velocity of the reaction is too fast to be the result of random collisions between the proteins only. The only molecular forces that act in considerable distance in solution are electrostatic attraction and repulsion. For human Trx1 and TrxR1 electrostatic complementarity within the area covered in the encounter complex, it appears to control the affinity of the reductase for Trx, whereas electrostatic complementarity in areas outside this contact area can have a large influence on the catalytic efficiency.

### Data Availability

All data not already contained with the manuscript will be made available by the corresponding author upon reasonable request.

### Conflicts of Interest

The authors declare that they have no conflicts of interest.

### Authors' Contributions

Md Faruq Hossain and Yana Bodnar contributed equally to this work.

### Acknowledgments

The authors wish to express their gratitude to Katja Becker (Gießen, Germany) for the expression construct encoding human TrxR1 U498C. The financial support of the Deutsche Forschungsgemeinschaft (grants Li 984/3-2 and GRK1947-A1 to CHL), Karolinska Institutet, the Knut and Alice Wallenberg Foundations, the Swedish Cancer Society, the Swedish Research Council, and the Hungarian Thematic Excellence Programme (TKP2020-NKA-26, all to ESJA) is gratefully acknowledged.

### Supplementary Materials

The following supplementary material is available separately: Supp. Table 1: oligonucleotides used in this study; further details on the  $K_d$  determination from the differential scanning fluorimetry data; Suppl. Fig. 1: examples for the determination of  $T_m$  values; Suppl. Fig. 2: molecular interactions between Trxs and their reductase; Suppl. Fig. 3: thermal stability of the Trx mutants analysed in this study; Suppl. Fig. 4: circular dichroism spectra of hTrx1-hTrxR1 complexes; Suppl. Fig. 5: human Trx mutants as potential substrates of E. coli TrxR; Suppl. Fig. 6: comparison of the electrostatic features of human TrxR1, TrxR2, E. coli TrxR, human Trx1, and Trp14, as well as E. coli Trx1; additional references. (*Supplementary Materials*)

### References

- [1] T. C. Laurent, E. C. Moore, and P. Reichard, "Enzymatic synthesis of deoxyribonucleotides. Iv. Isolation and characterization of thioredoxin, the hydrogen donor from *Escherichia coli* B," *The Journal of Biological Chemistry*, vol. 239, pp. 3436–3444, 1964.
- [2] E. C. Moore, P. Reichard, and L. Thelander, "Enzymatic synthesis of deoxyribonucleotides. V. Purification and properties of thioredoxin reductase from *Escherichia coli* B," *The Journal of Biological Chemistry*, vol. 239, pp. 3445–3452, 1964.
- [3] M. C. Weiss, F. L. Sousa, N. Mrnjavac et al., "The physiology and habitat of the last universal common ancestor," *Nature Microbiology*, vol. 1, no. 9, pp. 1–8, 2016.
- [4] C. H. Lillig, C. Berndt, and A. Holmgren, "Glutaredoxin systems," *Biochimica et Biophysica Acta (BBA) - General Subjects*, vol. 1780, no. 11, pp. 1304–1317, 2008.
- [5] C. H. Lillig and A. Holmgren, "Thioredoxin and related molecules from biology to health and disease," *Antioxidants & Redox Signaling*, vol. 9, no. 1, pp. 25–47, 2007.
- [6] S. G. Rhee and H. A. Woo, "Multiple functions of peroxiredoxins: peroxidases, sensors and regulators of the intracellular messenger  $H_2O_2$ , and protein chaperones," *Antioxidants & Redox Signaling*, vol. 15, no. 3, pp. 781–794, 2011.
- [7] M. D. Shelton, P. Boon Chock, and J. J. Mieyal, "Glutaredoxin: role in reversible protein S-glutathionylation and regulation of redox signal transduction and protein translocation," *Antioxidants & Redox Signaling*, vol. 7, no. 3–4, pp. 348–366, 2005.
- [8] A. Holmgren, B. O. Söderberg, H. Eklund, and C. I. Brändén, "Three-dimensional structure of *Escherichia coli* thioredoxin-S2 to 2.8 Å resolution," *Proceedings of the National Academy of Sciences of the United States of America*, vol. 72, no. 6, pp. 2305–2309, 1975.
- [9] J. L. Martin, "Thioredoxin—a fold for all reasons," *Structure*, vol. 3, no. 3, pp. 245–250, 1995.
- [10] A. Holmgren, "Thioredoxin. 6. The amino acid sequence of the protein from *Escherichia coli* B," *European Journal of Biochemistry/FEBS*, vol. 6, no. 4, pp. 475–484, 1968.
- [11] A. Holmgren, "Thioredoxin," *Annual Review of Biochemistry*, vol. 54, no. 1, pp. 237–271, 1985.
- [12] G. B. Kallis and A. Holmgren, "Differential reactivity of the functional sulfhydryl groups of cysteine-32 and cysteine-35 present in the reduced form of thioredoxin from *Escherichia coli*," *The Journal of Biological Chemistry*, vol. 255, no. 21, pp. 10261–10265, 1980.
- [13] G. Roos, N. Foloppe, and J. Messens, "Understanding the pK(a) of redox cysteines: the key role of hydrogen bonding," *Antioxidants & Redox Signaling*, vol. 18, no. 1, pp. 94–127, 2013.
- [14] M. Gellert, M. F. Hossain, F. J. F. Berens et al., "Substrate specificity of thioredoxins and glutaredoxins - towards a functional classification," *Heliyon*, vol. 5, no. 12, article e02943, 2019.
- [15] S. I. Hashemy and A. Holmgren, "Regulation of the catalytic activity and structure of human thioredoxin 1 via oxidation and S-nitrosylation of cysteine residues," *The Journal of Biological Chemistry*, vol. 283, no. 32, pp. 21890–21898, 2008.
- [16] A. Weichsel, J. R. Gasdaska, G. Powis, and W. R. Montfort, "Crystal structures of reduced, oxidized, and mutated human thioredoxins: evidence for a regulatory homodimer," *Structure*, vol. 4, no. 6, pp. 735–751, 1996.
- [17] R. Bertini, O. M. Z. Howard, H.-F. Dong et al., "Thioredoxin, a redox enzyme released in infection and inflammation, is a unique chemoattractant for neutrophils, monocytes, and T cells," *The Journal of Experimental Medicine*, vol. 189, no. 11, pp. 1783–1789, 1999.

- [18] K. Hirota, M. Murata, Y. Sachi et al., "Distinct roles of thioredoxin in the cytoplasm and in the nucleus. A two-step mechanism of redox regulation of transcription factor NF-KappaB," *The Journal of Biological Chemistry*, vol. 274, no. 39, pp. 27891–27897, 1999.
- [19] A. Rubartelli, A. Bajetto, G. Allavena, E. Wollman, and R. Sitia, "Secretion of thioredoxin by normal and neoplastic cells through a leaderless secretory pathway," *The Journal of Biological Chemistry*, vol. 267, no. 34, pp. 24161–24164, 1992.
- [20] M. Tanudji, S. Hevi, and S. L. Chuck, "The nonclassic secretion of thioredoxin is not sensitive to redox state," *American Journal of Physiology-Cell Physiology*, vol. 284, no. 5, pp. C1272–C1279, 2003.
- [21] Y. Zhang, F. Chen, G. Tai et al., "TIGAR knockdown radiosensitizes TrxR1-overexpressing glioma in vitro and in vivo via inhibiting Trx1 nuclear transport," *Scientific Reports*, vol. 7, no. 1, article 42928, 2017.
- [22] A. Holmgren and M. Björnstedt, "Thioredoxin and thioredoxin reductase," *Methods in Enzymology*, vol. 252, pp. 199–208, 1995.
- [23] A. Holmgren, "Thioredoxin and glutaredoxin systems," *The Journal of Biological Chemistry*, vol. 264, no. 24, pp. 13963–13966, 1989.
- [24] T. Sandalova, L. Zhong, Y. Lindqvist, A. Holmgren, and G. Schneider, "Three-dimensional structure of a mammalian thioredoxin reductase: implications for mechanism and evolution of a selenocysteine-dependent enzyme," *Proceedings of the National Academy of Sciences of the United States of America*, vol. 98, no. 17, pp. 9533–9538, 2001.
- [25] E. S. J. Arnér, "Focus on mammalian thioredoxin reductases - important selenoproteins with versatile functions," *Biochimica et Biophysica Acta*, vol. 1790, no. 6, pp. 495–526, 2009.
- [26] J. Lu and A. Holmgren, "Selenoproteins," *Journal of Biological Chemistry*, vol. 284, no. 2, pp. 723–727, 2009.
- [27] A. Argyrou and J. S. Blanchard, "Flavoprotein disulfide reductases: advances in chemistry and function," in *Progress in Nucleic Acid Research and Molecular Biology*, pp. 89–142, Academic Press, 2004.
- [28] M. L. Tsang and J. A. Weatherbee, "Thioredoxin, glutaredoxin, and thioredoxin reductase from cultured HeLa cells," *Proceedings of the National Academy of Sciences of the United States of America*, vol. 78, no. 12, pp. 7478–7482, 1981.
- [29] J. Lu, C. Berndt, and A. Holmgren, "Metabolism of selenium compounds catalyzed by the mammalian selenoprotein thioredoxin reductase," *Biochimica et Biophysica Acta (BBA) - General Subjects*, vol. 1790, no. 11, pp. 1513–1519, 2009.
- [30] Q. Cheng, T. Sandalova, Y. Lindqvist, and E. S. J. Arnér, "Crystal structure and catalysis of the selenoprotein thioredoxin reductase 1," *Journal of Biological Chemistry*, vol. 284, no. 6, pp. 3998–4008, 2009.
- [31] L. Zhong, E. S. J. Arnér, and A. Holmgren, "Structure and mechanism of mammalian thioredoxin reductase: the active site is a redox-active selenolthiol/selenenylsulfide formed from the conserved cysteine-selenocysteine sequence," *Proceedings of the National Academy of Sciences of the United States of America*, vol. 97, no. 11, pp. 5854–5859, 2000.
- [32] L. Zhong and A. Holmgren, "Essential role of selenium in the catalytic activities of mammalian thioredoxin reductase revealed by characterization of recombinant enzymes with selenocysteine mutations," *Journal of Biological Chemistry*, vol. 275, no. 24, pp. 18121–18128, 2000.
- [33] E.-M. Hanschmann, J. R. Godoy, C. Berndt, C. Hudemann, and C. H. Lillig, "Thioredoxins, glutaredoxins, and peroxiredoxins—molecular mechanisms and health significance: from cofactors to antioxidants to redox signaling," *Antioxidants & Redox Signaling*, vol. 19, no. 13, pp. 1539–1605, 2013.
- [34] M. Hirasawa, P. Schürmann, J. P. Jacquot et al., "Oxidation-reduction properties of chloroplast thioredoxins, ferredoxin:thioredoxin reductase, and thioredoxin f-regulated enzymes," *Biochemistry*, vol. 38, no. 16, pp. 5200–5205, 1999.
- [35] M. Huber-Wunderlich and R. Glockshuber, "A single dipeptide sequence modulates the redox properties of a whole enzyme family," *Folding & Design*, vol. 3, no. 3, pp. 161–171, 1998.
- [36] K. S. Jensen, J. T. Pedersen, J. R. Winther, and K. Teilum, "The pKa value and accessibility of cysteine residues are key determinants for protein substrate discrimination by glutaredoxin," *Biochemistry*, vol. 53, no. 15, pp. 2533–2540, 2014.
- [37] V. Bunik, G. Raddatz, S. Lemaire, Y. Meyer, J. P. Jacquot, and H. Bisswanger, "Interaction of thioredoxins with target proteins: role of particular structural elements and electrostatic properties of thioredoxins in their interplay with 2-oxoacid dehydrogenase complexes," *Protein Science: A Publication of the Protein Society*, vol. 8, no. 1, pp. 65–74, 1999.
- [38] P. B. Palde and K. S. Carroll, "A universal entropy-driven mechanism for thioredoxin-target recognition," *Proceedings of the National Academy of Sciences of the United States of America*, vol. 112, no. 26, pp. 7960–7965, 2015.
- [39] C. Berndt, J.-D. Schwenn, and C. H. Lillig, "The specificity of thioredoxins and glutaredoxins is determined by electrostatic and geometric complementarity," *Chemical Science*, vol. 6, no. 12, pp. 7049–7058, 2015.
- [40] E. F. Pettersen, T. D. Goddard, C. C. Huang et al., "UCSF chimera—a visualization system for exploratory research and analysis," *Journal of Computational Chemistry*, vol. 25, no. 13, pp. 1605–1612, 2004.
- [41] M. V. Shapovalov and R. L. Dunbrack Jr., "A smoothed backbone-dependent rotamer library for proteins derived from adaptive kernel density estimates and regressions," *Structure*, vol. 19, no. 6, pp. 844–858, 2011.
- [42] J. A. Maier, C. Martinez, K. Kasavajhala, L. Wickstrom, K. E. Hauser, and C. Simmerling, "FF14SB: improving the accuracy of protein side chain and backbone parameters from Ff99SB," *Journal of Chemical Theory and Computation*, vol. 11, no. 8, pp. 3696–3713, 2015.
- [43] T. J. Dolinsky, P. Czodrowski, H. Li et al., "PDB2PQR: expanding and upgrading automated preparation of biomolecular structures for molecular simulations," *Nucleic Acids Research*, vol. 35, pp. W522–W525, 2007.
- [44] W. Humphrey, A. Dalke, and K. Schulten, "VMD: visual molecular dynamics," *Journal of Molecular Graphics*, vol. 14, no. 1, pp. 33–38, 1996, 27–28.
- [45] N. A. Baker, D. Sept, S. Joseph, M. J. Holst, and J. A. McCammon, "Electrostatics of nanosystems: application to microtubules and the ribosome," *Proceedings of the National Academy of Sciences of the United States of America*, vol. 98, no. 18, pp. 10037–10041, 2001.
- [46] E. S. Arnér, H. Sarioglu, F. Lottspeich, A. Holmgren, and A. Böck, "High-level expression in *Escherichia coli* of selenocysteine-containing rat thioredoxin reductase utilizing gene fusions with engineered bacterial-type SECIS elements and co-expression with the selA, selB and selC genes," *Journal of Molecular Biology*, vol. 292, no. 5, pp. 1003–1016, 1999.

- [47] S. Urig, J. Lieske, K. Fritz-Wolf, A. Irmeler, and K. Becker, "Truncated mutants of human thioredoxin reductase 1 do not exhibit glutathione reductase activity," *FEBS Letters*, vol. 580, no. 15, pp. 3595–3600, 2006.
- [48] D. Su, C. Berndt, D. E. Fomenko, A. Holmgren, and V. N. Gladyshev, "A conserved cis-proline precludes metal binding by the active site thiolates in members of the thioredoxin family of proteins," *Biochemistry*, vol. 46, no. 23, pp. 6903–6910, 2007.
- [49] D. L. Wilkinson, N. T. Ma, C. Haught, and R. G. Harrison, "Purification by immobilized metal affinity chromatography of human atrial natriuretic peptide expressed in a novel thioredoxin fusion protein," *Biotechnology Progress*, vol. 11, no. 3, pp. 265–269, 1995.
- [50] E. S. J. Arnér and A. Holmgren, "Measurement of thioredoxin and thioredoxin reductase," *Current Protocols in Toxicology*, vol. 24, no. 1, pp. 7.4.1–7.4.14, 2005.
- [51] U. B. Ericsson, B. Martin Hallberg, G. T. Detitta, N. Dekker, and P. Nordlund, "Thermofluor-based high-throughput stability optimization of proteins for structural studies," *Analytical Biochemistry*, vol. 357, no. 2, pp. 289–298, 2006.
- [52] N. Bai, H. Roder, A. Dickson, and J. Karanicolas, "Isothermal analysis of ThermoFluor data can readily provide quantitative binding affinities," *Scientific Reports*, vol. 9, no. 1, 2019.
- [53] D. SpoelVan Der, E. Lindahl, B. Hess, G. Groenhof, A. E. Mark, and H. J. C. Berendsen, "GROMACS: fast, flexible, and free," *Journal of Computational Chemistry*, vol. 26, no. 16, pp. 1701–1718, 2005.
- [54] K. Lindorff-Larsen, S. Piana, K. Palmo et al., "Improved side-chain torsion potentials for the Amber Ff99SB protein force field," *Proteins*, vol. 78, no. 8, pp. 1950–1958, 2010.
- [55] B. Hess, H. Bekker, H. J. C. Berendsen, and J. G. E. M. Fraaije, "LINCS: a linear constraint solver for molecular simulations," *Journal of Computational Chemistry*, vol. 18, no. 12, pp. 1463–1472, 1997.
- [56] M. Parrinello and A. Rahman, "Polymorphic transitions in single crystals: a new molecular dynamics method," *Journal of Applied Physics*, vol. 52, no. 12, pp. 7182–7190, 1981.
- [57] G. Bussi, D. Donadio, and M. Parrinello, "Canonical sampling through velocity rescaling," *Journal of Chemical Physics*, vol. 126, no. 1, p. 014101, 2007.
- [58] T. Darden, D. York, and P. Lee, "Particle mesh Ewald: an N-log(N) method for Ewald sums in large systems," *The Journal of Chemical Physics*, vol. 98, no. 12, pp. 10089–10092, 1993.
- [59] S. da Silva, W. Alan, and W. F. Vranken, "ACPYPE - ante-chamber python parser interface," *BMC Research Notes*, vol. 5, no. 1, p. 367, 2012.
- [60] K. Fritz-Wolf, S. Kehr, M. Stumpf, S. Rahlfs, and K. Becker, "Crystal structure of the human thioredoxin reductase-thioredoxin complex," *Nature Communications*, vol. 2, no. 1, p. 383, 2011.
- [61] B. W. Lennon, C. H. Williams, and M. L. Ludwig, "Twists in catalysis: alternating conformations of *Escherichia coli* thioredoxin reductase," *Science*, vol. 289, no. 5482, pp. 1190–1194, 2000.
- [62] J. E. Oblong, M. Berggren, P. Y. Gasdaska, and G. Powis, "Site-directed mutagenesis of active site cysteines in human thioredoxin produces competitive inhibitors of human thioredoxin reductase and elimination of mitogenic properties of thioredoxin," *The Journal of Biological Chemistry*, vol. 269, no. 16, pp. 11714–11720, 1994.
- [63] J. Xu, S. E. Eriksson, M. Cebula et al., "The conserved Trp114 residue of thioredoxin reductase 1 has a redox sensor-like function triggering oligomerization and crosslinking upon oxidative stress related to cell death," *Cell Death & Disease*, vol. 6, no. 1, article e1616, 2015.
- [64] G. Hernández-Alcántara, A. Rodríguez-Romero, H. Reyes-Vivas et al., "Unraveling the mechanisms of tryptophan fluorescence quenching in the triosephosphate isomerase from *Giardia lamblia*," *Biochimica et Biophysica Acta*, vol. 1784, no. 11, pp. 1493–1500, 2008.
- [65] W. Jeong, H. W. Yoon, S.-R. Lee, and S. G. Rhee, "Identification and characterization of TRP14, a thioredoxin-related protein of 14 kDa. New insights into the specificity of thioredoxin function," *The Journal of Biological Chemistry*, vol. 279, no. 5, pp. 3142–3150, 2004.
- [66] A. Miranda-Vizuete, J. A. Gustafsson, and G. Spyrou, "Molecular cloning and expression of a cDNA encoding a human thioredoxin-like protein," *Biochemical and Biophysical Research Communications*, vol. 243, no. 1, pp. 284–288, 1998.
- [67] A. Miranda-Vizuete, J. Ljung, A. E. Damdimopoulos et al., "Characterization of Sptrx, a novel member of the thioredoxin family specifically expressed in human spermatozoa," *The Journal of Biological Chemistry*, vol. 276, no. 34, pp. 31567–31574, 2001.
- [68] M. E. Lönn, C. Hudemann, C. Berndt et al., "Expression pattern of human glutaredoxin 2 isoforms: identification and characterization of two testis/cancer cell-specific isoforms," *Antioxidants & Redox Signaling*, vol. 10, no. 3, pp. 547–558, 2008.
- [69] C. Johansson, C. H. Lillig, and A. Holmgren, "Human mitochondrial glutaredoxin reduces S-glutathionylated proteins with high affinity accepting electrons from either glutathione or thioredoxin reductase," *The Journal of Biological Chemistry*, vol. 279, no. 9, pp. 7537–7543, 2004.
- [70] C. Urbainsky, R. Nölker, M. Imber et al., "Nucleoredoxin-dependent targets and processes in neuronal cells," *Oxidative Medicine and Cellular Longevity*, vol. 2018, Article ID 4829872, 11 pages, 2018.
- [71] A. Gallegos, J. R. Gasdaska, C. W. Taylor et al., "Transfection with human thioredoxin increases cell proliferation and a dominant-negative mutant thioredoxin reverses the transformed phenotype of human breast cancer cells," *Cancer Research*, vol. 56, no. 24, pp. 5765–5770, 1996.
- [72] M. Yamamoto, G. Yang, C. Hong et al., "Inhibition of endogenous thioredoxin in the heart increases oxidative stress and cardiac hypertrophy," *The Journal of Clinical Investigation*, vol. 112, no. 9, pp. 1395–1406, 2003.
- [73] J.-H. Oh, A.-S. Chung, H. Steinbrenner, H. Sies, and P. Brenneisen, "Thioredoxin secreted upon ultraviolet A irradiation modulates activities of matrix metalloproteinase-2 and tissue inhibitor of metalloproteinase-2 in human dermal fibroblasts," *Archives of Biochemistry and Biophysics*, vol. 423, no. 1, pp. 218–226, 2004.
- [74] K. C. Das, "Thioredoxin-deficient mice, a novel phenotype sensitive to ambient air and hypersensitive to hyperoxia-induced lung injury," *American Journal of Physiology-Lung Cellular and Molecular Physiology*, vol. 308, no. 5, pp. L429–L442, 2015.
- [75] C. H. Lillig, A. Potamitou, J.-D. Schwenn, A. Vlamis-Gardikas, and A. Holmgren, "Redox regulation of 3'-phosphoadenylylsulfate reductase from *Escherichia coli* by



- glutathione and glutaredoxins," *The Journal of Biological Chemistry*, vol. 278, no. 25, pp. 22325–22330, 2003.
- [76] C. H. Lillig, A. Prior, J. D. Schwenn et al., "New thioredoxins and glutaredoxins as electron donors of 3'-phosphoadenylylsulfate reductase," *The Journal of Biological Chemistry*, vol. 274, no. 12, pp. 7695–7698, 1999.
- [77] G. Montoya, C. Svensson, H. Savage, J. D. Schwenn, and I. Sinning, "Crystallization and preliminary X-ray diffraction studies of phospho-adenylylsulfate (PAPS) reductase from *E. coli*," *Acta Crystallographica Section D Biological Crystallography*, vol. 54, no. 2, pp. 281–283, 1998.
- [78] J. D. Schwenn and U. Schriek, "PAPS-reductase from *Escherichia coli*: characterization of the enzyme as probe for thioredoxins," *Zeitschrift für Naturforschung C*, vol. 42, no. 1–2, pp. 93–102, 1987.
- [79] H. Peng, Y. Zhang, J. C. Trinidad, and D. P. Giedroc, "Thioredoxin profiling of multiple thioredoxin-like proteins in *Staphylococcus aureus*," *Frontiers in Microbiology*, vol. 9, p. 2385, 2018.
- [80] M. Deponte and C. H. Lillig, "Enzymatic control of cysteinyl thiol switches in proteins," *Biological Chemistry*, vol. 396, no. 5, pp. 401–413, 2015.
- [81] S. Prast-Nielsen, M. Cebula, I. Pader, and E. S. J. Arnér, "Noble metal targeting of thioredoxin reductase-covalent complexes with thioredoxin and thioredoxin-related protein of 14 kDa triggered by cisplatin," *Free Radical Biology & Medicine*, vol. 49, no. 11, pp. 1765–1778, 2010.
- [82] I. Pader, R. Sengupta, M. Cebula et al., "Thioredoxin-related protein of 14 kDa is an efficient L-cystine reductase and S-nitrosylase," *Proceedings of the National Academy of Sciences of the United States of America*, vol. 111, no. 19, pp. 6964–6969, 2014.

**Manuscript 3****NADPH-dependent oxidation of CRMP2 through a  
MICAL1-Prx1 redox relay controls neurite  
outgrowth**

**Clara Ortegón Salas**, Yana Bodnar, Dennis Uhlenkamp, Katharina Schneider, Lara Knaup,  
Marcel Deponte, Carsten Berndt, Christopher Horst Lillig and Manuela Gellert

Submitted to *Science*

Manuscript number: abj9997

Submitted on 15.06.2021

This manuscript was submitted and may be published in the journal of Science, Ortegón Salas C, Bodnar Y, Uhlenkamp D, Schneider K, Knaup L, Deponte M, Berndt C, Lillig CH, Gellert M. NADPH-dependent oxidation of CRMP2 through a MICAL1-Prx1 redox relay controls neurite outgrowth. According to this journal's policy, the authors retain copyright as well as rights to make uses of the work prior to manuscript acceptance.

## NADPH-dependent oxidation of CRMP2 through a MICAL1-Prx1 redox relay controls neurite outgrowth

Clara Ortegón Salas<sup>1</sup>, Yana Bodnar<sup>1</sup>, Dennis Uhlenkamp<sup>1</sup>, Katharina Schneider<sup>1</sup>, Lara Knaup<sup>1</sup>, Marcel Deponte<sup>2</sup>, Carsten Berndt<sup>3</sup>, Christopher Horst Lillig<sup>1\*</sup>, and Manuela Gellert<sup>1\*</sup>

From the Institute for Medical Biochemistry and Molecular Biology, University Medicine Greifswald, Germany (1), the Department of Chemistry, Technical University, Kaiserslautern, Germany (2), and the Department of Neurology, Medical Faculty, Heinrich Heine University Düsseldorf, Germany, (3).

\* Corresponding authors: Manuela Gellert and Christopher Horst Lillig, Institute for Medical Biochemistry and Molecular Biology, University Medicine Greifswald, Ferdinand-Sauerbruch-Straße, DE-17475 Greifswald, Germany, Tel: +49 3834 865407, Fax: +49 3834 865402, E-mails: [manuela@gellert.org](mailto:manuela@gellert.org), [horst@lillig.de](mailto:horst@lillig.de)

Running title: The MICAL1-Prx1-CRMP2 redox relay

Keywords: MICAL, CRMP2, DPYL2, redox relay, redox regulation, thiol switch, neurite outgrowth

### Abstract

CRMP2/DPYL2 is an effector protein in the semaphorin signaling pathway that controls cytoskeletal dynamics, linking extracellular signals to the formation of axonal networks. CRMP2 is regulated by post-translational modifications including a dithiol-disulfide redox switch. The mechanisms of reduction of this switch were established, the signal-induced oxidation, however, remained unclear. Here, we show that CRMP2 is oxidized through a redox relay involving the flavin-moxygenase MICAL1 and the peroxidase Prx1 as specific signal transducers. Using molecular oxygen and electrons provided by NADPH, MICAL produces hydrogen peroxide and specifically oxidizes Prx1 through direct interactions between the proteins. Subsequently, Prx1 oxidizes CRMP2. The lack of any components of this redox relay dysregulates neurite outgrowth. Consequently, both oxidation and reduction of CRMP2 require reducing equivalents in the form of NADPH.

### One-sentence-summary

The neurite outgrowth controlling protein CRMP2 is regulated by a redox switch that is oxidized through a MICAL1-Prx1 relay.

### Introduction

The semaphorin (Sem) signaling pathway contributes to the regulation of axonal outgrowth and neuronal connectivity. Activation of the Sem3A pathway induces growth cone collapse and retraction of the outgrowths by controlling the de-polymerization of the cytoskeleton that subsequently allows the axons to change their direction. Sem3A acts via a hetero-dimeric trans-membrane receptor composed of neuropilin 1 (NP1) and a plexin A (PlexA) family member (1, 2). Effector proteins include the kinases CDK5 and GSK3 $\beta$  that sequentially phosphorylate collapsin response mediator protein 2 (CRMP2, gene: DPYSL2) (3). CRMP2 was reported to regulate microtubuli dynamics by binding to  $\alpha$ - $\beta$ -tubulin dimers. MICAL (molecule interacting with CasL) proteins bind to the cytoplasmic domain of PlexAs (4). The human genome encodes three MICAL proteins. All contain an N-terminal FAD-dependent monooxygenase (MO) domain, followed by a calponin homology (CH) and a LIM domain. Human MICAL 1 and 3 contain an additional C-terminal Rab-binding domain (RBD) (5). MICALs can produce H<sub>2</sub>O<sub>2</sub> upon activation of the Sem3A pathway (6). Furthermore, MICALs were characterized as specific oxidases of actin methionyl residues (7, 8), thus regulating microfilament dynamics.

In general, redox-mediated signal transduction occurs by both reversible oxidation and reduction of



key molecules. The side chains most vulnerable to redox modifications are cysteinyl and methionyl residues. Redox modifications occur – often rapidly – under physiological conditions and they are highly specific with respect to both, the molecules involved and the nature of the redox modification; reversible oxidation and reduction are key mechanisms in cell signaling (9, 10). While the specificity of the reduction of cysteinyl and methionyl residues has always been attributed to catalysis by enzymes of the thioredoxin (Trx) family (11), the oxidation reactions were often attributed to rather unspecific reactions of the proteins with ‘reactive’ species, most of all  $H_2O_2$ . This model has been increasingly challenged, in particular by the low reaction rates of the modified side chains with  $H_2O_2$ . Cellular peroxidases, *i.e.* the glutathione peroxidases and peroxiredoxins (Prxs) display  $\approx 10^6$ -fold higher rate constants and are generally high abundant proteins in mammalian cells. It was thus suggested that these peroxidases may function as receptors and transducers of redox signaling, *e.g.* (12). CRMP2 has been reported to be regulated by a dithiol-disulfide redox switch of two cysteinyl 504 residues in the homo-tetrameric quaternary complex, that is essential for neurite outgrowth and axonal connectivity (6, 13). *In vivo*, the reduction of this disulfide appears to be specifically regulated by the cytosolic isoform of glutaredoxin 2 (Grx2c), a process linked to both formation of a neuronal network and the progression of cancer cells (13–15). MICAL-produced  $H_2O_2$  was suggested as potential source of CRMP2 oxidation (14), however, the rate constant of the direct reaction of CRMP2 with  $H_2O_2$  is also too low to be of significance *in vivo* (16). In fact, two studies provided evidence for the involvement of Prx1 in the oxidation of CRMP2 (17, 18). We thus hypothesized a signal-induced redox relay in the semaphorin signaling pathway that involves both MICAL1 and Prx1 as signal transducers and CRMP2 as effector protein.

## Results

We hypothesized that Sem3A signaling induces a redox relay involving a FAD-dependent monooxygenase of the MICAL family, one of the cytosolic Prxs, and CRMP2. The latter should then

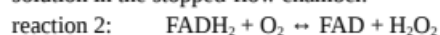
affect axonal outgrowth by binding to tubulin and actin, thus controlling cytoskeletal dynamics. We have used purified recombinant human CRMP2 to perform affinity capture assays in cell extracts. Using Western blotting, we confirmed the interaction between CRMP2 and both actin and tubulin (Fig. 1A). Moreover, also MICAL1 and Prx1 were captured in this assay; their release from the complex required reducing equivalents, indicating redox-dependent associations.

We proposed the production of hydrogen peroxide by a MICAL protein that leads to the oxidation of a Prx. Subsequently, this Prx may oxidize the Cys504 redox switch in tetrameric CRMP2. We cloned, recombinantly expressed, and purified the two cytosolic Prxs (Prx1-2) and the monooxygenase domains of MICAL1-3, henceforth named MICAL(1-3)-MO. All three recombinant MICAL-MO domains contained oxidized FAD, indicated by additional absorption bands at approx. 370 and 450 nm (Fig. 1B). For the comparison of spectra of both liberated and MICAL bound FAD, see Fig. S1. These proteins oxidized NADPH in the presence of  $O_2$ , a reaction that yields  $H_2O_2$ , proving their activity as monooxygenases (Fig. 1C). Next, we incubated both Prx1 and Prx2 with the three MICAL-MO domains in a one-to-one stoichiometry (one Prx dimer to one MICAL-MO) in the presence of NADPH. In this setting, all MICAL-MOs led to the oxidation of the two Prxs, *i.e.* the formation of the catalytic inter-molecular disulfide between the peroxidatic and resolving cysteinyl residues of two Prx monomers (Fig. 1D). When a mutant of the resolving cysteinyl residue of the Prxs was used, dimer formation could not be observed. As a control, we have also confirmed that MICALs (in a 1:1 stoichiometry in the presence of oxygen and NADPH) do not directly oxidize CRMP2 (Fig. S2).

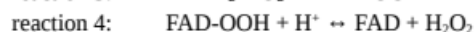
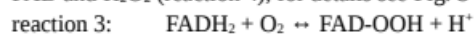
To analyze the mechanisms of the MICAL reaction and the oxidation of the Prxs, we have turned to stopped-flow kinetics. As seen before, MICAL1-MO oxidized NADPH in a concentration-dependent manner in the presence of  $O_2$  at pH 7.4 and 298 K (Fig. 2A-B, reaction 1).

reaction 1:  $NADPH/H^+ + O_2 \leftrightarrow NADP^+ + H_2O_2$   
Using linearized integrated second order kinetics, we determined the rate constant of this reaction to be  $137 \pm 14 \text{ M}^{-1} \cdot \text{s}^{-1}$  (Fig. 2C, Suppl. Material). The

exemplary difference spectra shown in Fig. 2D demonstrate a decrease in absorbance between 340-350 nm (NADPH oxidation), but not at 450 nm (FAD reduction), indicating that FAD is oxidized during all phases of this reaction. Noteworthy, decrease in pH (to 6.0) and temperature (to 277 K) did not significantly affect the rate constant of reaction 1:  $126 \pm 7 \text{ M}^{-1} \cdot \text{s}^{-1}$  (Fig. 2E-F). To analyze the oxidation of the MICAL1-MO (reaction 2), we incubated the protein with exactly the amount of NADPH required to fully reduce the FAD to FADH<sub>2</sub>, *i.e.* the concentration that equaled the sum of the MICAL-MO and O<sub>2</sub> concentrations in the reaction mix (Fig. S3). The reaction was started by mixing this protein solution with an oxygen-containing solution in the stopped-flow chamber.



The concentration of O<sub>2</sub> was determined from the amount of (excess) NADPH oxidized by the enzyme in a separate control experiment, see Fig. S3. The oxidation of MICAL1-MO occurred fast, equilibrium was reached in less than a second (Fig. 2G-H). When we analyzed this reaction applying linearized integrated second order kinetics, we found the reaction to be bi-phasic (Fig. 2I, Suppl. Material). We determined the rate constant of the first reaction to be  $\geq 1.9 \pm 0.2 \cdot 10^5 \text{ M}^{-1} \cdot \text{s}^{-1}$ , the rate constant of the second phase to be  $2.4 \pm 0.3 \cdot 10^4 \text{ M}^{-1} \cdot \text{s}^{-1}$ . The spectra recorded during these reactions did not provide any evidence for the formation of any form of stable intermediate. The difference spectra (Fig. 2J) display a decrease at 462 nm and, to a lesser degree at 378 nm, typical for the oxidation of FADH<sub>2</sub> to FAD. We thus concluded that the reaction of the FADH<sub>2</sub> with O<sub>2</sub> occurs via an unstable peroxy-flavin intermediate (reaction 3), that immediately decays to oxidized FAD and H<sub>2</sub>O<sub>2</sub> (reaction 4), for details see Fig. S4.



We have also performed the oxidation of MICAL-MO in the presence of Prxs. The remaining spectra, however, did not suggest any other intermediates, *e.g.* a charge transfer complex between the FAD and the Prx. The reaction remained bi-phasic and the rate constants were in the range of those determined for the reaction in the absence of a Prx (Fig. 2K-L, Table 1). We thus conclude that the Prx is oxidized by H<sub>2</sub>O<sub>2</sub> produced by the MICAL-MO domain and not

by direct transfer from the FAD to the peroxidatic cysteinyl residue.

Next, we have analyzed the oxidation of Prx1-2 by catalytic amounts of the MICAL(1-3)-MOs. As shown in Fig. 3A and Fig. S5,  $60 \text{ nmol} \cdot \text{l}^{-1}$  of the MICAL-MOs efficiently oxidize  $10 \text{ } \mu\text{mol} \cdot \text{l}^{-1}$  of either Prx when NADPH was present. This reaction was in no way inhibited by the presence of excess catalase ( $> 1000 \text{ U}$ ), suggesting that the H<sub>2</sub>O<sub>2</sub> produced by the MICAL-MOs is not released into the solution to be turned over by the Prxs. Although all MICAL-MOs were able to oxidize the Prxs, the time course of these reactions (Fig. 3B) evinced a clear preference of MICAL1-MO for the oxidation of either Prx. We have thus focused, from here on, on MICAL1. Michaelis-Menten kinetics of the Prxs' oxidation by the MICAL1-MO suggested that the Prxs are in fact substrates of the monooxygenase. Both Prxs were oxidized at similar rates (Fig. 3C, Table 1, Fig. S6). We also analyzed this reaction using a MICAL1-MO variant elongated by the calponin homology domain of the native protein (MICAL1-MO-CH, Fig. S6). As reported for the oxidation of actin by MICAL, this enhanced the catalytic efficiency, here approx. 3-fold (Fig. 3D, Table 1). Together, these results support the formation of an enzyme-substrate complex between the two proteins in which the H<sub>2</sub>O<sub>2</sub> produced by MICAL is directly shuttled to the peroxidatic cysteinyl residue of the Prx. We have performed all atomistic molecular dynamics simulation of this proposed complex between MICAL1 and dimeric Prx1. Using a start structure obtained by molecular docking, we have analyzed the dynamics of the complex over the time course of 250 ns (Fig. 4). Within 50 ns, the simulation reached an equilibrium (Fig. 4D-E). In this complex, one of the peroxidatic cysteinyl residues of the Prx-dimer is placed at the exit of a channel in MICAL1 that connects to the FAD/FADH<sub>2</sub> active site of the enzyme (Fig. 4F-G), the side chains of both the peroxidatic and resolving cysteinyl were at the low end of the spectrum (Fig. 4H), suggesting a rather stable conformation.

Next, we aimed to confirm the proposed redox relay in an established human cellular model of neuronal differentiation. SH-SY5Y neuroblastoma cells can be differentiated into mature neurons through a variety of different mechanisms including

treatment with retinoic acid (RA) (19). At first, we have treated the cells in the neuroblast state with  $1\mu\text{g}\cdot\text{ml}^{-1}$  Sem3A and analyzed the oxidation of Prx1 and CRMP2. Both proteins form a homodimeric inter-molecular disulfide that can be identified after non-reducing Western blotting. We found an increase in both oxidized Prx1 and CRMP2 between 5 to 10 minutes after addition of the ligand (Fig. 5A). Since we proposed a Sem3A-induced redox-relay from MICAL1 to Prx1 to CRMP2, we repeated the experiment with cells silenced for the expression of MICAL1 (Fig. 5B-C). In the presence of MICAL1, we confirmed the oxidation of CRMP2 within minutes following Sem3A treatment (Fig. 5C). With silenced MICAL1 expression, however, Prx1 oxidation (Fig. 5B, analyzed by diagonal electrophoresis, non-reducing vs. reducing dimension, see Fig. S7), as well as CRMP2 oxidation (Fig. 5C) were prevented. In the following, we have induced the differentiation from the neuroblast state to the neuron-like cells by treatment with RA over the time course of 7 days. Oxidized CRMP2 started to appear 48 hours after induction and reached a maximum at day 5 (Fig. 5D-E), confirming earlier results (13). With silenced expression of MICAL1 in this model, Prx1 (Fig. 5F-H), but not Prx2 (Fig. 5J-L), was significantly less oxidized 5 days after induction of differentiation. The lack of increase in the oxidized dimeric form of the Prx was not the result of an over-oxidation of the monomeric form (Fig. 5I). With silenced expression of Prx1, oxidation of CRMP2 did not occur (Fig. 5M-N). Next, we investigated neurite outgrowth as physiological function of the characterized redox relay. Compared to controls, SH-SY5Y cells with silenced expression of either MICAL1, Prx1, or CRMP2 featured significantly longer neurites (Fig. 5O-U). The average neurite length of cells lacking MICAL1 and Prx1 increased 1.6-fold at day 5, the lack of CRMP2 led to a 1.4-fold increase at day 3 following the beginning of RA treatment.

## Discussion

The semaphorin signaling pathways are part of the regulatory networks controlling the processes that shape the developing nervous system, *i.e.* axon guidance, synaptic plasticity, and neuronal migration

(2, 20, 21). Both MICAL and CRMP2 are required for the Sem signaling pathway and interact with the cytosolic domain of the Sem receptor plexin A (4, 22). The activity of the MICAL monooxygenases is required for their function in the pathway, for instance MICALs directly oxidize actin and promote growth cone collapse and cellular repulsion (4, 7, 8, 23, 24). CRMP2 contains a dithiol-disulfide redox switch that is operated in the SH-SY5Y model of neuronal differentiation. Previous studies suggested MICAL-produced  $\text{H}_2\text{O}_2$  as source of the oxidation equivalents (6, 13, 14), however, this was put into question by the low rate constant of the reaction, *i.e.*  $0.82\text{ M}^{-1}\text{ s}^{-1}$  (16). In fact, more recent studies pointed to 2-Cys Prxs as mediators of CRMP2 oxidation (18, 25, 26).

Here, we propose the following pathway and mechanism of CRMP2 oxidation: MICAL1 is activated in response to Sem3A signaling, presumably by direct interaction with the Sem3A receptor. Next, reduced MICAL1 ( $\text{FADH}_2$ ) reacts fast with molecular oxygen yielding a peroxy-flavin intermediate ( $\text{FAD}\cdot\text{OO}\cdot$ ). This immediately decays to  $\text{H}_2\text{O}_2$  and oxidized MICAL (FAD). The efficient oxidation of the Prxs in the presence of excess catalase (Fig. 1D) suggests that the  $\text{H}_2\text{O}_2$  is not released but rather directly channeled to the peroxidatic cysteinyl residue of Prx1, oxidizing it to the sulfenic acid intermediate. This induces the attack of the resolving cysteinyl residue of the second Prx monomer, resulting in partial unfolding, conformational changes and disulfide formation, characteristic for the 2-Cys Prx reaction mechanism, see *e.g.* (27). This ought to induce to the dissociation of the MICAL-Prx complex. MICAL is re-reduced by NADPH and Prx1 can transfer the disulfide to CRMP2 in dithiol-disulfide exchange reaction.

Various stages of development in the central nervous system appear to be associated with changes in the intra-cellular redox milieu. This has been demonstrated for the production of  $\text{H}_2\text{O}_2$  (28, 29) that participates, for instance, in axonal path finding (30). MICAL proteins can produce  $\text{H}_2\text{O}_2$ , which made them prime candidates as oxidases in redox signaling pathways.

MICAL family proteins are conserved from insects to vertebrates. The proteins are  $\text{O}_2$ - and NADPH-dependent monooxygenases. The domain

structure of the three human isoforms, however, differs. All three MICALs contain the monooxygenase domain (MO) with FAD as prosthetic group at the N-terminus followed by calponin homology and LIM domains. MICAL1 and 3 contain an additional C-terminal Rab-binding domain (31). The C-terminal region of MICAL is involved in the modulation of its activity and mediates the interaction between MICAL and plexin (32). This interaction was reported to release the auto-inhibition of MICALs by their C-terminal domain upon the binding of SemA to its receptor. This release of MICALs is required for their redox activity (33). Unlike Rab1, CasL, or Vimentin, CRMP2 doesn't seem to bind to the C-terminal region but closer to the N-terminus including the LIM domain (32, 34, 35). It remains unclear how the interaction of MICALs with the Sem receptor protein plexinA affects the binding of CRMP2 (32). MICALs catalyze the stereo-specific oxidation of two methionyl residues (M44 and M47) in actin filaments to methionyl-R-sulfoxides by the production of  $H_2O_2$ , thereby facilitating actin depolymerization (8, 36–39). These modifications are reversible through the action of methionine sulfoxide reductases (40). These redox modifications of actin were implied in axonal outgrowth, neuronal plasticity, cell division, and cancer progression (31, 41, 42). The oxidation of actin by MICAL-MO was enhanced when the following CH domain was included in the recombinant protein (43, 44). We confirm the higher catalytic efficiency of this construct for the oxidation of the Prxs as well (Fig. 3C-D, Table 1).

The crystal structures available for MICAL-MO domains imply a conformational change of the FAD from an 'out' conformation in the oxidized state to an 'in' conformation in the reduced state (38, 45). This may be the explanation why the reduction of the FAD by NADPH is the rate limiting step in the MICAL monooxygenase reaction mechanism (Fig. S4). It may also explain why the rate constant of this fully reversible reaction step appeared to be independent of temperature or pH (Fig. 2A-F). The rate was likely not limited by the electron transfer reaction itself, but rather by the following conformational changes. Reduced FAD immediately reacted with molecular oxygen. The apparently bi-

phasic reaction likely resulted from the formation of an unstable peroxy-flavin, which decays to  $H_2O_2$  and the oxidized flavin (Fig. S4) (37). The rate constant of the first step was too high for us to spectroscopically verify the peroxy-flavin intermediate (Fig. 2G-L). No spectroscopic evidence, *e.g.* charge transfer complex, was detected that could point to a direct reaction of Prx's peroxidatic Cys<sub>p</sub> with a peroxy-flavin. Despite the high homology between the three human MICALs (4), their catalytic efficiency towards the oxidation of Prx1 and Prx2 differ distinctly (Fig. 3C-D, Table 1) with MICAL1 being the most efficient. Our structural models suggest large differences in the electrostatic properties that may be key to their diverse enzymatic activities (Fig. S8) (46). Our molecular dynamic simulations suggest an area of contact between dimeric Prx1 and the MICAL1-MO domain that complies with both the geometric restraints and complementary electrostatic surfaces (Fig. 4A-C, Fig. S8). Such a binding event brings the peroxidatic cysteinyl residue of one monomer of the dimeric Prx in close proximity to the active site opening in the MICAL1-MO domain where the FAD is bound (Fig. 4F-G), the  $H_2O_2$  produced may then be directly channeled to the Prx, which is supported by the finding that catalase does not inhibit Prx oxidation (Fig. 3). The oxidation of CRMP2 by Prx1 was demonstrated before. However, it seems that this reaction requires at least one additional factor that may act as scaffold bringing Prx1 and CRMP2 into close enough proximity for the reaction to take place (18, 32).

Different studies suggested an involvement of the oxidized form of CRMP2 in the semaphorin signaling pathway before although without clarifying the mechanism of oxidation nor a sufficient explanation for the specific reduction. The use of a mutant thioredoxin in this enzymatic reaction leads to the formation of an artificial disulfide (6, 37).

CRMP2 is subject to a variety of post-translational modifications. Five phosphorylation sites are located at the C-terminus (3, 47–50), following the redox-sensitive cysteinyl residue 504 (13). The accessibility of the phosphorylation sites may depend on the redox state of Cys504, implying a cross talk between redox- and phosphorylation signaling (16). Oxidation of the CRMP2 redox

switch appears to be required for growth cone retraction of outgrowing neurites. We have analyzed the proposed redox relay in an established model of neuronal differentiation (Fig. 5). Treatment of the cells with Sem3A led to a fast increase in oxidation of both Prx1 and CRMP2. Induction of differentiation with retinoic acid triggers the transcriptional induction of class 3 semaphorins (13, 51–53), as well as CRMP2 oxidation (13). Using gene silencing in the differentiation model, we have shown that the oxidation of Prx1 depends on the presence of MICAL1 and the oxidation of CRMP2 on the presence of MICAL1 and Prx1. In contrast, we did not find evidence for the involvement of Prx2. As demonstrated here, the silencing of any of the components of the oxidation redox relay results in a 1.6-fold increase in average neurite length in the differentiation model (Fig. 5O-U). CRMP2's redox switch is reduced by the cytosolic isoform of glutaredoxin 2 and its operation was implied in neuronal development and the control of cell migration and invasion (14, 15). Collaboratively, over-expression of Grx2c leads to an increase in average neurite length (14). Silencing of the expression of Grx2c in zebrafish embryos results in an increase in oxidized CRMP2 in the developing brain. In consequence, outgrowing axons are 4-fold shorter, fail to establish an axonal scaffold, and virtually all neurons perish apoptotically (14).

We propose receptor-induced redox relays for both the oxidation and reduction of CRMP2 (Fig. 6) that control these proteins functions, *e.g.* the regulation of neurite outgrowth and neuronal connectivity. Activation of the NP1/PlexA receptor activates MICAL1. Using molecular oxygen and electrons provided by NADPH, MICAL specifically oxidizes Prx1, that in turn oxidizes the regulatory CRMP2 disulfide, thereby affecting its biological

activity. This is reverted by reduction of the switch catalyzed by Grx2c (13) or Trx1 (6). These oxidoreductases are reduced by GSH and glutathione reductase and thioredoxin reductase, respectively, both at the expense of NADPH. One of the most surprising conclusions of this study may thus be that both the oxidation and the reduction of the CRMP2 thiol switch require reducing equivalents provided in the form of NADPH (Fig. 6).

## Acknowledgements

The financial support of the Deutsche Forschungsgemeinschaft (grants Li 984/3-1, Li 984/3-2 and GRK1947-A1 to CHL, BE3259/5-1 and 5-2 to CB), and the start-up fund through the research associations GANI\_MED, Community Medicine and Molecular Medicine of the University Medicine Greifswald (FOVB-2019-09, FOVB-2020-11 to MG) is gratefully acknowledged.

## Author contributions

CB, CHL, MD, and MG conceived the study and designed the experiments. COS, DU, KS, LG, and MG performed the experiments, YB the molecular dynamics analysis. All authors analyzed the data. CB, CHL, COS, and MG wrote the paper.

## Competing interests

Authors declare that they have no competing interests.

## Supplementary Materials

Materials and Methods

Table S1 – S2

Fig. S1 – S8

References (54-67)

## References

1. G. Neufeld, O. Kessler, The semaphorins: versatile regulators of tumour progression and tumour angiogenesis. *Nat. Rev. Cancer.* **8**, 632–645 (2008).
2. B. C. Jongbloets, R. J. Pasterkamp, Semaphorin signalling during development. *Development.* **141**, 3292–3297 (2014).
3. Y. Uchida, T. Ohshima, Y. Sasaki, H. Suzuki, S. Yanai, N. Yamashita, F. Nakamura, K. Takei, Y. Ihara, K. Mikoshiba, P. Kolattukudy, J. Honnorat, Y. Goshima, Semaphorin3A signalling is mediated via sequential Cdk5 and GSK3beta phosphorylation of CRMP2: implication of common phosphorylating

- mechanism underlying axon guidance and Alzheimer's disease. *Genes Cells*. **10**, 165–179 (2005).
4. J. R. Terman, T. Mao, R. J. Pasterkamp, H.-H. Yu, A. L. Kolodkin, MICALs, a family of conserved flavoprotein oxidoreductases, function in Plexin-mediated axonal repulsion. *Cell*. **109**, 887–900 (2002).
  5. S. M. Kolk, R. J. Pasterkamp, MICAL flavoprotein monooxygenases: structure, function and role in semaphorin signaling. *Adv. Exp. Med. Biol.* **600**, 38–51 (2007).
  6. A. Morinaka, M. Yamada, R. Itofusa, Y. Funato, Y. Yoshimura, F. Nakamura, T. Yoshimura, K. Kaibuchi, Y. Goshima, M. Hoshino, H. Kamiguchi, H. Miki, Thioredoxin mediates oxidation-dependent phosphorylation of CRMP2 and growth cone collapse. *Sci Signal*. **4**, ra26 (2011).
  7. R.-J. Hung, U. Yazdani, J. Yoon, H. Wu, T. Yang, N. Gupta, Z. Huang, W. J. H. van Berkel, J. R. Terman, Mical links semaphorins to F-actin disassembly. *Nature*. **463**, 823–827 (2010).
  8. R.-J. Hung, C. W. Pak, J. R. Terman, Direct redox regulation of F-actin assembly and disassembly by Mical. *Science*. **334**, 1710–1713 (2011).
  9. D. P. Jones, Redefining oxidative stress. *Antioxid. Redox Signal*. **8**, 1865–1879 (2006).
  10. P. Ghezzi, V. Bonetto, M. Fratelli, Thiol-disulfide balance: from the concept of oxidative stress to that of redox regulation. *Antioxid Redox Signal*. **7**, 964–972 (2005).
  11. E.-M. Hanschmann, J. R. Godoy, C. Berndt, C. Hudemann, C. H. Lillig, Thioredoxins, glutaredoxins, and peroxiredoxins—molecular mechanisms and health significance: from cofactors to antioxidants to redox signaling. *Antioxid. Redox Signal*. **19**, 1539–1605 (2013).
  12. L. Flohé, The impact of thiol peroxidases on redox regulation. *Free Radic. Res*. **50**, 126–142 (2016).
  13. M. Gellert, S. Venz, J. Mitlöhner, C. Cott, E.-M. Hanschmann, C. H. Lillig, Identification of a dithiol-disulfide switch in collapsin response mediator protein 2 (CRMP2) that is toggled in a model of neuronal differentiation. *J. Biol. Chem*. **288**, 35117–35125 (2013).
  14. L. Bräutigam, L. D. Schütte, J. R. Godoy, T. Prozorovski, M. Gellert, G. Hauptmann, A. Holmgren, C. H. Lillig, C. Berndt, Vertebrate-specific glutaredoxin is essential for brain development. *Proc. Natl. Acad. Sci. U.S.A.* **108**, 20532–20537 (2011).
  15. M. Gellert, E. Richter, J. Mostertz, L. Kantz, K. Masur, E.-M. Hanschmann, S. Ribback, N. Kroeger, E. Schaeffeler, S. Winter, F. Hochgräfe, M. Schwab, C. H. Lillig, The cytosolic isoform of glutaredoxin 2 promotes cell migration and invasion. *Biochimica et Biophysica Acta - General Subjects*. **1864**, 129599 (2020).
  16. D. Möller, M. Gellert, W. Langel, C. H. Lillig, Molecular dynamics simulations and in vitro analysis of the CRMP2 thiol switch. *Mol Biosyst*. **13**, 1744–1753 (2017).
  17. S. Stöcker, M. Maurer, T. Ruppert, T. P. Dick, A role for 2-Cys peroxiredoxins in facilitating cytosolic protein thiol oxidation. *Nat. Chem. Biol*. **14**, 148–155 (2018).
  18. P. E. Pace, A. V. Peskin, A. Königstorfer, C. J. Jasoni, C. C. Winterbourn, M. B. Hampton, Peroxiredoxin interaction with the cytoskeletal-regulatory protein CRMP2: Investigation of a putative redox relay. *Free Radic. Biol. Med*. **129**, 383–393 (2018).
  19. M. M. Shipley, C. A. Mangold, M. L. Szpara, Differentiation of the SH-SY5Y Human Neuroblastoma Cell Line. *J Vis Exp* (2016), doi:10.3791/53193.
  20. O. Behar, J. A. Golden, H. Mashimo, F. J. Schoen, M. C. Fishman, Semaphorin III is needed for normal patterning and growth of nerves, bones and heart. *Nature*. **383**, 525–528 (1996).
  21. N. Uesaka, M. Uchigashima, T. Mikuni, T. Nakazawa, H. Nakao, H. Hirai, A. Aiba, M. Watanabe, M. Kano, Retrograde semaphorin signaling regulates synapse elimination in the developing mouse brain. *Science*. **344**, 1020–1023 (2014).
  22. T. Jiang, G. Zhang, Y. Liang, Z. Cai, Z. Liang, H. Lin, M. Tan, PlexinA3 interacts with CRMP2 to mediate Sema3A signalling during dendritic growth in cultured cerebellar granule neurons. *Neuroscience*. **434**, 83–92 (2020).
  23. E. F. Schmidt, S. M. Strittmatter, The CRMP family of proteins and their role in Sema3A signaling. *Adv. Exp. Med. Biol*. **600**, 1–11 (2007).
  24. N. Arimura, C. Menager, Y. Fukata, K. Kaibuchi, Role of CRMP-2 in neuronal polarity. *J. Neurobiol*. **58**, 34–47 (2004).
  25. S. Stöcker, M. Maurer, T. Ruppert, T. P. Dick, A role for 2-Cys peroxiredoxins in facilitating cytosolic protein thiol oxidation. *Nat. Chem. Biol*. **14**, 148–155 (2018).

26. L. van Dam, M. Pagès-Gallego, P. E. Polderman, R. M. van Es, B. M. T. Burgering, H. R. Vos, T. B. Dansen, The Human 2-Cys Peroxiredoxins form Widespread, Cysteine-Dependent- and Isoform-Specific Protein-Protein Interactions. *Antioxidants (Basel)*. **10** (2021), doi:10.3390/antiox10040627.
27. L. B. Poole, in *Peroxiredoxin Systems: Structures and Functions*, L. Flohé, J. R. Harris, Eds. (Springer Netherlands, Dordrecht, 2007; [https://doi.org/10.1007/978-1-4020-6051-9\\_4](https://doi.org/10.1007/978-1-4020-6051-9_4)), *Subcellular Biochemistry*, pp. 61–81.
28. H. Guo, G. Chen, M. Gao, R. Wang, Y. Liu, F. Yu, Imaging of Endogenous Hydrogen Peroxide during the Process of Cell Mitosis and Mouse Brain Development with a Near-Infrared Ratiometric Fluorescent Probe. *Anal. Chem.* **91**, 1203–1210 (2019).
29. C. Wilson, E. Muñoz-Palma, C. González-Billault, From birth to death: A role for reactive oxygen species in neuronal development. *Semin. Cell Dev. Biol.* **80**, 43–49 (2018).
30. C. Gauron, F. Meda, E. Dupont, S. Albadri, N. Quenech'Du, E. Ipendey, M. Volovitch, F. Del Bene, A. Joliot, C. Rampon, S. Vríz, Hydrogen peroxide (H<sub>2</sub>O<sub>2</sub>) controls axon pathfinding during zebrafish development. *Dev Biol.* **414**, 133–141 (2016).
31. C. Ortegón Salas, K. Schneider, C. H. Lillig, M. Gellert, Signal-regulated oxidation of proteins via MICAL. *Biochemical Society Transactions*. **48**, 613–620 (2020).
32. E. F. Schmidt, S.-O. Shim, S. M. Strittmatter, Release of MICAL autoinhibition by semaphorin-plexin signaling promotes interaction with collapsin response mediator protein. *J. Neurosci.* **28**, 2287–2297 (2008).
33. T. Vitali, E. Maffioli, G. Tedeschi, M. A. Vanoni, Properties and catalytic activities of MICAL1, the flavoenzyme involved in cytoskeleton dynamics, and modulation by its CH, LIM and C-terminal domains. *Archives of Biochemistry and Biophysics*. **593**, 24–37 (2016).
34. T. Suzuki, T. Nakamoto, S. Ogawa, S. Seo, T. Matsumura, K. Tachibana, C. Morimoto, H. Hirai, MICAL, a novel CasL interacting molecule, associates with Vimentin\*. *Journal of Biological Chemistry*. **277**, 14933–14941 (2002).
35. T. Weide, J. Teuber, M. Bayer, A. Bamekow, MICAL-1 isoforms, novel Rab1 interacting proteins. *Biochemical and Biophysical Research Communications*. **306**, 79–86 (2003).
36. E. E. Grintsevich, P. Ge, M. R. Sawaya, H. G. Yesilyurt, J. R. Terman, Z. H. Zhou, E. Reisler, Catastrophic disassembly of actin filaments via Mical-mediated oxidation. *Nat Commun.* **8**, 2183 (2017).
37. M. A. Vanoni, T. Vitali, D. Zucchini, MICAL, the Flavoenzyme Participating in Cytoskeleton Dynamics. *Int J Mol Sci.* **14**, 6920–6959 (2013).
38. M. Nadella, M. A. Bianchet, S. B. Gabelli, J. Barrila, L. M. Amzel, Structure and activity of the axon guidance protein MICAL. *Proc. Natl. Acad. Sci. U.S.A.* **102**, 16830–16835 (2005).
39. R.-J. Hung, J. R. Terman, Extracellular Inhibitors, Repellents, and Semaphorin/Plexin/MICAL-mediated Actin Filament Disassembly. *Cytoskeleton (Hoboken)*. **68**, 415–433 (2011).
40. S. Boschi-Muller, A. Gand, G. Branlant, The methionine sulfoxide reductases: Catalysis and substrate specificities. *Arch. Biochem. Biophys.* **474**, 266–273 (2008).
41. H. Wu, H. G. Yesilyurt, J. Yoon, J. R. Terman, The MICALs are a family of F-actin dismantling oxidoreductases conserved from Drosophila to humans. *Scientific Reports*. **8**, 937 (2018).
42. S. Frémont, H. Hammich, J. Bai, H. Wioland, K. Klinkert, M. Rocancourt, C. Kikuti, D. Stroebel, G. Romet-Lemonne, O. Pylypenko, A. Houdusse, A. Echard, Oxidation of F-actin controls the terminal steps of cytokinesis. *Nat Commun.* **8**, 14528 (2017).
43. J. Kim, H. Lee, Y. J. Roh, H.-U. Kim, D. Shin, S. Kim, J. Son, A. Lee, M. Kim, J. Park, S. Y. Hwang, K. Kim, Y. K. Lee, H. S. Jung, K. Y. Hwang, B. C. Lee, Structural and kinetic insights into flavin-containing monooxygenase and calponin-homology domains in human MICAL3. *IUCrJ.* **7**, 90–99 (2020).
44. S. S. Alqassim, M. Urquiza, E. Borgia, M. Nagib, L. M. Amzel, M. A. Bianchet, Modulation of MICAL Monooxygenase Activity by its Calponin Homology Domain: Structural and Mechanistic Insights. *Sci Rep.* **6**, 22176 (2016).
45. C. Siebold, N. Berrow, T. S. Walter, K. Harlos, R. J. Owens, D. I. Stuart, J. R. Terman, A. L. Kolodkin, R. J. Pasterkamp, E. Y. Jones, High-resolution structure of the catalytic region of MICAL (molecule interacting with CasL), a multidomain



- flavoenzyme-signaling molecule. *Proc. Natl. Acad. Sci. U.S.A.* **102**, 16836–16841 (2005).
46. M. Gellert, M. F. Hossain, F. J. F. Berens, L. W. Bruhn, C. Urbainsky, V. Liebscher, C. H. Lillig, Substrate specificity of thioredoxins and glutaredoxins - towards a functional classification. *Heliyon*. **5**, e02943 (2019).
47. N. Yamashita, Y. Goshima, Collapsin response mediator proteins regulate neuronal development and plasticity by switching their phosphorylation status. *Mol Neurobiol.* **45**, 234–246 (2012).
48. T. Yoshimura, Y. Kawano, N. Arimura, S. Kawabata, A. Kikuchi, K. Kaibuchi, GSK-3 $\beta$  Regulates Phosphorylation of CRMP-2 and Neuronal Polarity. *Cell.* **120**, 137–149 (2005).
49. M. Brown, T. Jacobs, B. Eickholt, G. Ferrari, M. Teo, C. Monfries, R. Z. Qi, T. Leung, L. Lim, C. Hall, Alpha2-chimaerin, cyclin-dependent Kinase 5/p35, and its target collapsin response mediator protein-2 are essential components in semaphorin 3A-induced growth-cone collapse. *J Neurosci.* **24**, 8994–9004 (2004).
50. T. Sumi, T. Imasaki, M. Aoki, N. Sakai, E. Nitta, M. Shirouzu, R. Nitta, Structural Insights into the Altering Function of CRMP2 by Phosphorylation. *Cell Struct Funct.* **43**, 15–23 (2018).
51. K. Brenig, L. Grube, M. Schwarzländer, K. Köhrer, K. Stühler, G. Poschmann, The Proteomic Landscape of Cysteine Oxidation That Underpins Retinoic Acid-Induced Neuronal Differentiation. *J. Proteome Res.* **19**, 1923–1940 (2020).
52. F. Pezzini, L. Bettinetti, F. Di Leva, M. Bianchi, E. Zoratti, R. Carozzo, F. M. Santorelli, M. Delledonne, M. Lalowski, A. Simonati, Transcriptomic Profiling Discloses Molecular and Cellular Events Related to Neuronal Differentiation in SH-SY5Y Neuroblastoma Cells. *Cell Mol Neurobiol.* **37**, 665–682 (2017).
53. J. Ryyänen, C. Kriebitzsch, M. B. Meyer, I. Janssens, J. W. Pike, L. Verlinden, A. Verstuyf, Class 3 semaphorins are transcriptionally regulated by 1,25(OH)2D3 in osteoblasts. *The Journal of Steroid Biochemistry and Molecular Biology.* **173**, 185–193 (2017).
54. J. R. Godoy, M. Funke, W. Ackermann, P. Haunhorst, Sabrina Oesteritz, F. Capani, H.-P. Elsässer, C. H. Lillig, Redox atlas of the mouse. Immunohistochemical detection of glutaredoxin-, peroxiredoxin-, and thioredoxin-family proteins in various tissues of the laboratory mouse. *Biochim. Biophys. Acta.* **1810**, 2–92 (2011).
55. L. Mullen, E.-M. Hanschmann, C. H. Lillig, L. A. Herzenberg, P. Ghezzi, Cysteine Oxidation Targets Peroxiredoxins 1 and 2 for Exosomal Release through a Novel Mechanism of Redox-Dependent Secretion. *Mol Med.* **21**, 98–108 (2015).
56. G. Weng, E. Wang, Z. Wang, H. Liu, F. Zhu, D. Li, T. Hou, HawkDock: a web server to predict and analyze the protein-protein complex based on computational docking and MM/GBSA. *Nucleic Acids Res.* **47**, W322–W330 (2019).
57. D. Van Der Spoel, E. Lindahl, B. Hess, G. Groenhof, A. E. Mark, H. J. C. Berendsen, GROMACS: Fast, flexible, and free. *Journal of Computational Chemistry.* **26**, 1701–1718 (2005).
58. K. Lindorff-Larsen, S. Piana, K. Palmo, P. Maragakis, J. L. Klepeis, R. O. Dror, D. E. Shaw, Improved side-chain torsion potentials for the Amber ff99SB protein force field. *Proteins.* **78**, 1950–1958 (2010).
59. A. W. Sousa da Silva, W. F. Vranken, ACPYPE - AnteChamber PYthon Parser interfacE. *BMC research notes.* **5**, 367 (2012).
60. B. Hess, H. Bekker, H. J. C. Berendsen, J. G. E. M. Fraaije, LINCS: A linear constraint solver for molecular simulations. *Journal of Computational Chemistry.* **18**, 1463–1472 (1997).
61. M. Parrinello, A. Rahman, Polymorphic transitions in single crystals: A new molecular dynamics method. *Journal of Applied Physics.* **52**, 7182–7190 (1981).
62. G. Bussi, D. Donadio, M. Parrinello, Canonical sampling through velocity rescaling. *Journal of Chemical Physics.* **126** (2007), doi:10.1063/1.2408420.
63. T. Darden, D. York, L. Pedersen, Particle mesh Ewald: An N $\cdot$ log(N) method for Ewald sums in large systems. *The Journal of Chemical Physics.* **98**, 10089–10092 (1993).
64. E. F. Pettersen, T. D. Goddard, C. C. Huang, G. S. Couch, D. M. Greenblatt, E. C. Meng, T. E. Ferrin, UCSF Chimera--a visualization system for exploratory research and analysis. *J Comput Chem.* **25**, 1605–1612 (2004).
65. C. Urbainsky, R. Nölker, M. Imber, A. Lübken, J. Mostertz, F. Hochgräfe, J. R. Godoy, E.-M. Hanschmann, C. H. Lillig, Nucleoredoxin-Dependent Targets and Processes in Neuronal Cells. *Oxidative*



- Medicine and Cellular Longevity*. **2018**, e4829872 (2018).
66. J. I. Romero, E.-M. Hanschmann, M. Gellert, S. Eitner, M. I. Holubiec, E. Blanco-Calvo, C. H. Lillig, F. Capani, Thioredoxin 1 and glutaredoxin 2 contribute to maintain the phenotype and integrity of neurons following perinatal asphyxia. *Biochimica et Biophysica Acta (BBA) - General Subjects*. **1850**, 1274–1285 (2015).
67. T. Smafield, V. Pasupuleti, K. Sharma, R. L. Haganir, B. Ye, J. Zhou, Automatic Dendritic Length Quantification for High Throughput Screening of Mature Neurons. *Neuroinformatics*. **13**, 443–458 (2015).

## Tables

**Table 1 – Kinetic analysis of the reaction of MICAL1 with NADPH, molecular oxygen, and Prxs.** The apparent rate constants of MICAL1-MO with NADPH and molecular oxygen were determined by stopped-flow kinetics (see Fig. 2). The  $K_m$  and  $V_{max}$  of MICAL1-MO and MICAL1-MO-CH with Prx1 and 2 as substrates were determined in end-point assays (see Fig. 3).

Enzyme	Substrate	2 <sup>nd</sup> order rate constant ( $k_{app}$ )	n	pH	Temperature
		$\text{mol}^{-1}\cdot\text{l}\cdot\text{s}^{-1}$			K
MICAL1-MO	NADPH	$163.8 \pm 13.9$	14	7.4	298
MICAL1-MO	NADPH	$140.5 \pm 19.2$	8	7.4	277
MICAL1-MO	NADPH	$126 \pm 6.7$	10	6.0	277
MICAL1-MO	O <sub>2</sub>	(1) $1.9 \pm 0.2 \cdot 10^5$ (2) $2.4 \pm 0.3 \cdot 10^4$	5	7.4	298
MICAL1-MO	O <sub>2</sub> (Prx1 present)	(1) $2.3 \pm 0.1 \cdot 10^5$ (2) $3.2 \pm 0.5 \cdot 10^4$	7	7.4	298

Enzyme	Substrate	$K_m$	$V_{max}$	n	pH	Temperature
		$\mu\text{mol}\cdot\text{l}^{-1}$	$\text{s}^{-1}$			K
MICAL1-MO	Prx1	$30.4 \pm 0.8$	$0.28 \pm 0.03$	3	7.4	298
MICAL1-MO	Prx2	$22.7 \pm 3.1$	$0.31 \pm 0.05$	3	7.4	298
MICAL1-MO-CH	Prx1	$23.5 \pm 1.7$	$0.72 \pm 0.03$	3	7.4	298
MICAL1-MO-CH	Prx2	$14.2 \pm 0.8$	$0.57 \pm 0.01$	3	7.4	298

## Figure legends

### Figure 1 – Prxs as potential targets of MICALs

(A) Affinity capture assay using immobilized recombinant pre-oxidized and pre-reduced CRMP2 as bait. Lysates of HeLa cells (left) and HeLa-Grx2c<sup>+</sup> (right) cells (15) were incubated with the protein, and eluted first under denaturing and second under reducing conditions. The input, flow through, and eluates were analyzed by Western blotting for proteins implied in the semaphorin (Sem3A) signaling pathway before. (B) UV-Vis spectra of the recombinantly expressed monooxygenase domains of MICAL1, 2, and 3 demonstrate the presence of (oxidized) FAD in the proteins. (C) Consumption of NADPH measured as decrease in A340 by MICAL1 in the presence of oxygen confirms the monooxygenase activity of the purified protein. (D) Oxidation of 7  $\mu\text{mol}\cdot\text{l}^{-1}$  Prx1 and 2 by 3.5  $\mu\text{mol}\cdot\text{l}^{-1}$  MICAL1, 2, and 3 in the absence and presence of 1150 units catalase per 100  $\mu\text{l}$  assay. MICALs, in the presence of molecular oxygen and 200  $\mu\text{mol}\cdot\text{l}^{-1}$  NADPH were incubated with two-fold molecular excess of wildtype Prx1 and 2 or mutants lacking the resolving cysteinyl residue (C<sub>R</sub> → S). The activity of all MICALs led to the oxidation of wildtype Prxs both in the presence and absence of 1150 units ( $\mu\text{mol H}_2\text{O}_2$  per minute) of catalase.

### Figure 2 – Reaction of the MICAL1 flavin monooxygenase domain with NADPH and oxygen

The reaction of the FAD in the MICAL1 monooxygenase domain was analyzed by stopped flow kinetics. (A) Consumption of 150  $\mu\text{mol}\cdot\text{l}^{-1}$  NADPH by 10  $\mu\text{mol}\cdot\text{l}^{-1}$  MICAL1 at pH 7.4 and 298 K over the time course of 6 minutes analyzed by UV-Vis spectroscopy. (B) NADPH-dependence of the reactivity of 10  $\mu\text{mol}\cdot\text{l}^{-1}$  MICAL1 at pH 7.4 and 298 K followed by UV-Vis spectroscopy at 340 nm. (C) Linearized integrated second order kinetics of the data displayed in (B) for the determination of the apparent second order rate constant (see Suppl. Material). (D) Differences of the spectra shown in (A) at 311 and 35 s minus the first spectrum taken at 1.78 ms. (E) NADPH-dependence of the reactivity of 10  $\mu\text{mol}\cdot\text{l}^{-1}$  MICAL1 at pH 6.0 and 277 K followed by UV-Vis spectroscopy at 340 nm. (F) Linearized integrated second order kinetics of the data displayed in (E) for the determination of the apparent second order rate constant (see Suppl. Material). (G) Oxidation of the FAD in 10  $\mu\text{mol}\cdot\text{l}^{-1}$  MICAL1 at pH 7.4 and 298 K over the time course of 1 second analyzed by UV-Vis spectroscopy. (H) Time course of the FAD oxidation followed by UV-Vis spectroscopy at 360, 370, and 450 nm. (I) Linearized integrated second order kinetics of the data displayed in (h, 450 nm) for the determination of the apparent second order rate constants suggest a two-phasic reaction (see Suppl. Material). (J) Differences of the spectra shown in (a) at 1780, 100, and 35.2 ms minus the first spectrum taken at 1.78 ms. (K) Time course of the FAD oxidation in 10  $\mu\text{mol}\cdot\text{l}^{-1}$  MICAL1 in the presence of 20  $\mu\text{mol}\cdot\text{l}^{-1}$  Prx followed by UV-Vis spectroscopy at 360, 370, and 450 nm. (L) Linearized integrated second order kinetics of the data displayed in (K, 450 nm) for the determination of the apparent second order rate constants suggest a two-phasic reaction (see Suppl. Material)

### Figure 3 – Recombinant Prxs are oxidized by catalytical amounts of MICALs

Michaelis-Menten kinetics of the Prxs' oxidation by the MICAL1 monooxygenase domain (MO) and the MICAL1 monooxygenase-calponin homology domains (MO-CH). (A) Analysis of the oxidation of 10  $\mu\text{mol}\cdot\text{l}^{-1}$   $\mu\text{M}$  Prx1 and 2 by 60  $\text{nmol}\cdot\text{l}^{-1}$  MICAL1, 2, and 3-MO by SDS-PAGE. The reaction requires NADPH and is not inhibited by the addition of 1150 units ( $\mu\text{mol H}_2\text{O}_2$  per minute) of catalase. (B) The time-course of 50  $\mu\text{mol}\cdot\text{l}^{-1}$  Prxs' oxidation by 60  $\text{nmol}\cdot\text{l}^{-1}$  MICALs suggests a preference of MICAL1 for the reaction. (C-D) Michaelis-Menten kinetics of the oxidation of Prx1 and 2 (as indicated) by 60  $\text{nmol}\cdot\text{l}^{-1}$  MICAL-MO (C) or 20

nmol $\cdot$ l $^{-1}$  MICAL-MO-CH (D). All measurements were performed in the presence of 1150 units of catalase per 100  $\mu$ l assay and 200  $\mu$ mol $\cdot$ l $^{-1}$  NADPH.

### Figure 4 – Docking and all atomistic molecular dynamics simulation of a MICAL1-Prx1 complex

(A) Water accessible surface of the complex in side view (dimeric Prx1 in green, MICAL1-MO in gray, interaction surfaces in yellow). (B-C) Interaction surfaces (in yellow) on Prx1 (B) and MICAL1 (C); the complex was opened by 90° left (Prx1) and 90° right (MICAL1). (D) Root mean square deviation (rmsd) of the peptide backbones in the complex over the course of the simulation (250 ns). (E) Solvent accessible surface area (sasa) of the complex over the course of the simulation. (F-G) One of the peroxidatic cysteinyl residues of the dimeric Prx1 faces the active site cavity of MICAL1; (G) is a magnification of (F, square). (H) Average side chain fluctuations of the residues in the Prx1 dimer-MICAL1 complex, the peroxidatic (Cys<sub>P</sub>) and the resolving (Cys<sub>R</sub>) are highlighted.

### Figure 5 – The MICAL1-Prx1-CRMP2 redox relay in a model of neuronal differentiation

(A) Time course of the redox states of CRMP2 and Prx1 in SH-SY5Y cells treated with 1 $\mu$ g $\cdot$ ml $^{-1}$  Sem3A. (B-C) Redox states of Prx1 (B, 2-D diagonal SDS-PAGE) and CRMP2 (C) in SH-SY5Y cells with silenced expression of MICAL1 and treated with 1 $\mu$ g $\cdot$ ml $^{-1}$  Sem3A for 150 s; the siRNA control was included in (C). (D-E) Levels of oxidized (D) and reduced (E) CRMP2 in SH-SY5Y cells during their differentiation into neuron-like cells induced by 10  $\mu$ mol $\cdot$ l $^{-1}$  retinoic acid (RA) added to the medium; n=3. (F-L) Redox states of Prx1 and Prx2 in RA-treated SH-SY5Y cells depend on MICAL1; n=6. (F, J) Quantification of the redox states analyzed by 2-D diagonal (G) and 1-D gel electrophoresis (H), n=7 and 6 for Prx1, n=9 and 8 for Prx2, respectively. siRNA controls were included in (H) and (L). Silencing of MICAL1 in cells did not induce over-oxidation of Prxs as demonstrated with a Prx-SO<sub>2/3</sub> specific antibody, control cell lysate treated with 1 mmol $\cdot$ l $^{-1}$  H<sub>2</sub>O<sub>2</sub> was used as positive control (I). (M-N) Redox state of CRMP2 in the SH-SY5Y differentiation model depends on Prx1. (M) Quantification of the redox state; n=4. (N) siRNA control and exemplary Western blots. (O-U) Neurite outgrowth during SH-SY5Y differentiation depends on MICAL1, Prx1, and CRMP2. (O) Neurite length in control, MICAL1 and Prx1-depleted cells after 120 hours of differentiation. Each point represents the automated analysis of one picture of n=3 biological replicates. (P) Neurite length in control and CRMP2-depleted cells after 72 hours of differentiation. Each point represents the automated analysis of one picture of n=3 biological replicates. Sample pictures of the cells treated with siControl (Q), siMICAL1 (R), siPrx1 (S), siCRMP2 (T, the associated siControl at the 72 hour time point is not shown), and exemplary siRNA controls (U) are shown in the lower row. All box-plots depict the median (line), the 75% quartiles (box) and the minimum and maximum values (whiskers). All densitometric analyses were normalized to the total amount of protein on the respective lane of the blot. The p-values were calculated applying an unpaired T-test analysis.

### Figure 6 - NADPH-dependent redox relays in both the oxidation and reduction of the CRMP2 thiol switch control axonal outgrowth

Figure 1

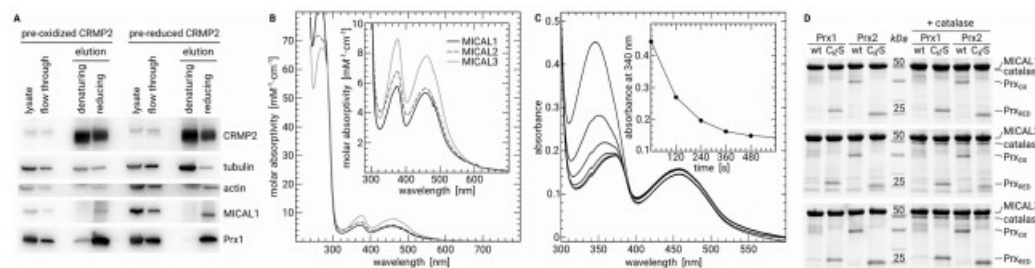


Figure 2

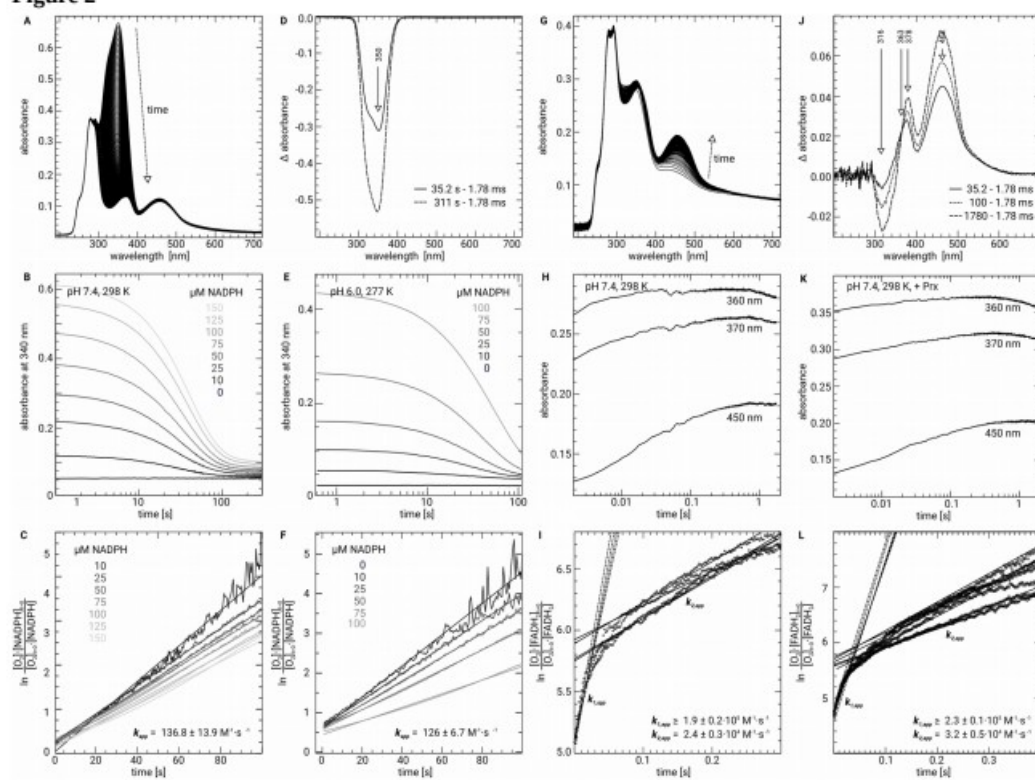


Figure 3

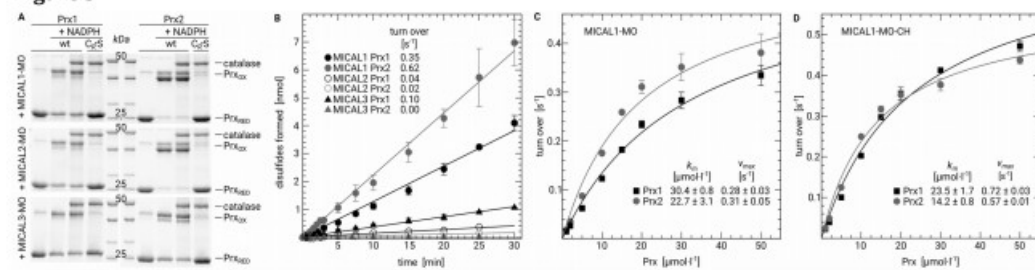


Figure 4

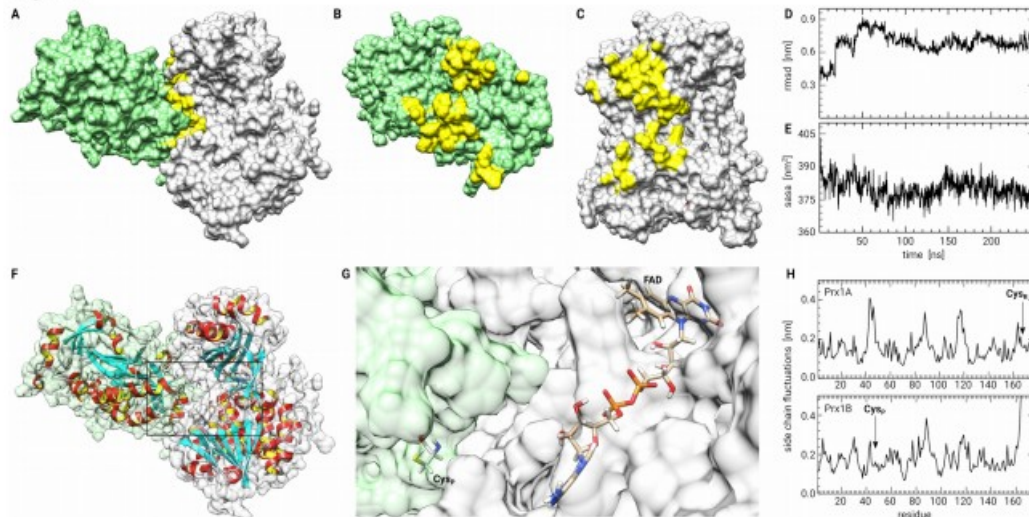
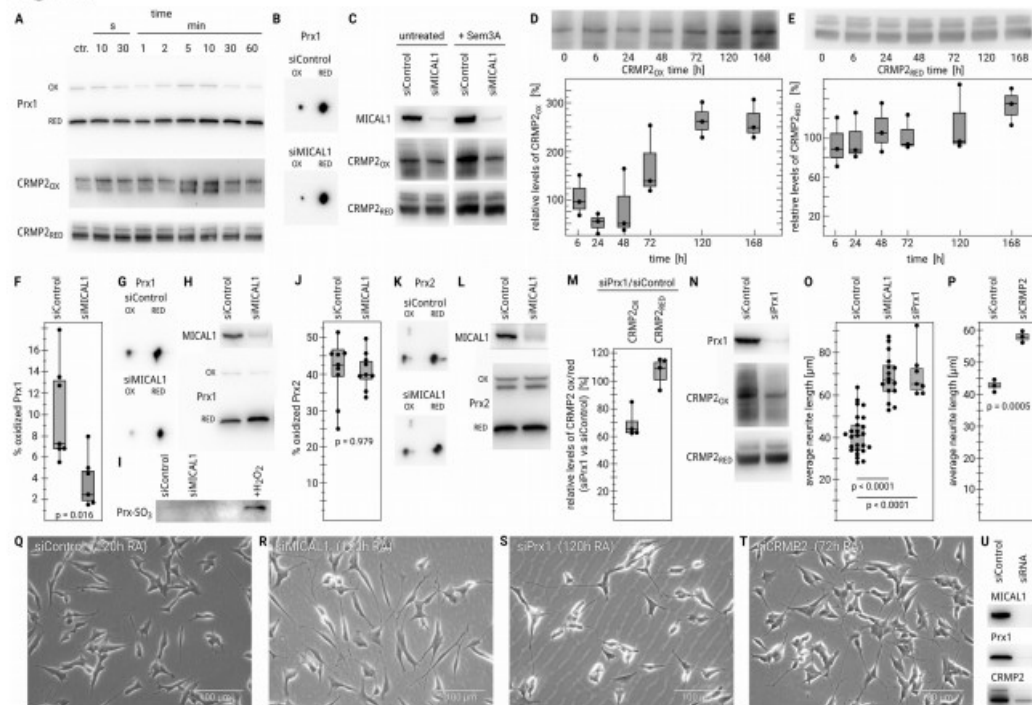
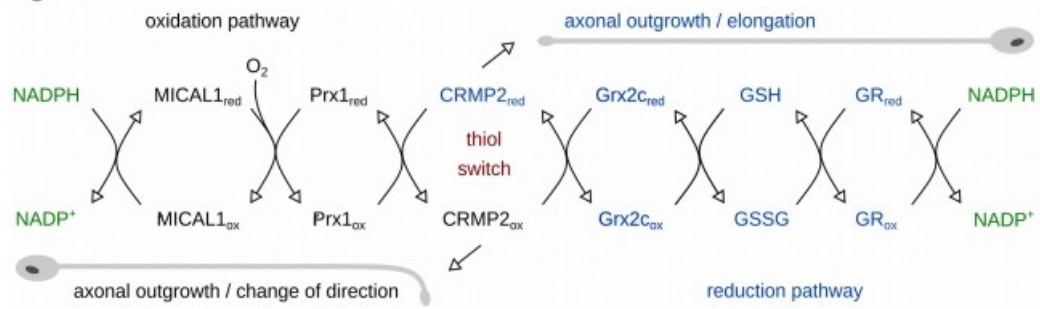


Figure 5



**Figure 6**





Supplementary material to:

## **NADPH-dependent oxidation of CRMP2 through a MICAL1-Prx1 redox relay controls neurite outgrowth**

Clara Ortegón Salas<sup>1</sup>, Yana Bodnar<sup>1</sup>, Dennis Uhlenkamp<sup>1</sup>, Katharina Schneider<sup>1</sup>, Lara Knaup<sup>1</sup>, Marcel Deponte<sup>2</sup>, Carsten Berndt<sup>3</sup>, Christopher Horst Lillig<sup>1\*</sup>, and Manuela Gellert<sup>1\*</sup>

From the Institute for Medical Biochemistry and Molecular Biology, University Medicine Greifswald, Germany (1), the Department of Chemistry, Technical University, Kaiserslautern, Germany (2), and the Department of Neurology, Medical Faculty, Heinrich Heine University Düsseldorf, Germany, (3).

\* Corresponding authors: Manuela Gellert and Christopher Horst Lillig, Institute for Medical Biochemistry and Molecular Biology, University Medicine Greifswald, Ferdinand-Sauerbruch-Straße, DE-17475 Greifswald, Germany, Tel: +49 3834 865407, Fax: +49 3834 865402, E-mails: [manuela@gellert.org](mailto:manuela@gellert.org), [horst@lillig.de](mailto:horst@lillig.de)

### **Table of Contents**

Material and Methods.....	1
Table S1 – Oligonucleotides used for the cloning of expression vectors.....	6
Table S2 – siRNA sequences.....	6
Figure S1 – Quantification of MICAL-bound and liberated FAD.....	7
Figure S2 – MICALs do not directly oxidize CRMP2 in vitro.....	7
Figure S3 – Reduction of the FAD in MICAL1-MO by NADPH; O <sub>2</sub> quantification in the assay solution.....	8
Figure S4 – Proposed reaction mechanism of the MICAL1-catalyzed Prx1 oxidation.....	9
Figure S5 – Time course of the oxidation of the Prxs by catalytic amounts of MICAL(1-3)-MO....	10
Figure S6 – Oxidation of Prxs by catalytic amounts of MICAL1-MO and MICAL1-MO-CH.....	10
Figure S7 – Principle of the diagonal electrophoresis.....	11
Figure S8 – Further structural insights into the MICAL-Prx interactions.....	11

### **Material and Methods**

**Materials** – Chemicals and enzymes were purchased from Sigma-Aldrich (St. Louis MO, USA), unless otherwise stated, and were of analytical grade or better. The antibodies used in this work were as follows: MICAL1 (14818-1-AP, Proteintech, Manchester, UK), Prx1 (LF-MA0214, Abfrontier, Liestal, Switzerland), Prx2 (54), PrxSO<sub>2/3</sub> (ab16830, abcam, Cambridge, UK), CRMP2 (ab129082, abcam), actin (sc-47778, Santa Cruz, Heidelberg, Germany), tubulin (T9026, Sigma-Aldrich), horseradish peroxidase conjugated anti-rabbit and anti-mouse IgGs (Bio-Rad, Hercules, CA, USA).

**Electrophoresis, Western blotting, and densitometric analysis** – Protein concentrations were determined using Bradford reagent (Bio-Rad, Hercules, CA, USA). All one-dimensional SDS-PAGE were run using precasted mini-Protean TGX Stain-free gels (4-20%, Bio-Rad, Hercules, CA, USA). In two-dimensional diagonal SDS-PAGE, proteins from cell lysates were denatured in sample buffer (1% SDS, 50% glycerol, 60 mM Tris/HCl pH 6.8, 2 mM EDTA, Bromphenol blue) and separated in the first dimension under non-reducing conditions. Gel slices were incubated in 250 mM DTT (AppliChem, Darmstadt, Germany) and 100 mM pH neutral TCEP in sample buffer for 30 minutes at 65°C. After washing with sample buffer, the gel slices were incubated for 20 minutes at room temperature and mild agitation with 100 mM NEM (Thermo

Scientific, Weltham, MA, USA) in sample buffer. After a washing step with sample buffer, every single gel lane was placed horizontally onto a pre-casted mini-Protean TGX Stain-free gels (4-20%, 7 cm IPG, Bio-Rad, Hercules, CA, USA). Western blots were carried out using Trans-Blot Turbo system and the RTA Mini PVDF Transfer Kit according to manufacturer's instructions (Bio-Rad, Hercules, CA, USA). Blots were developed by enhanced chemiluminescence staining and documented using a ChemiDoc XRS+ documentation system (Bio-Rad, Hercules, CA, USA). Densitometric analyses of Western blots were performed with the ImageJ software (version 1.53e). All values were normalized to the total amount of protein on the blot, determined using the stain-free technology and the ImageLab software (version 6.0) according to the manufacturer's instructions (Bio-Rad, Hercules, CA, USA).

**Cloning of expression constructs** – MICALs monoxygenase (MO) domains and MICAL1-monoxygenase and calponin homology (MO-CH) domains were amplified by PCR from human cDNA using described oligonucleotides, ligated into pGEM-T vector (Promega, Madison, WI, USA), excised with restriction endonucleases NdeI and BglII (New England Biolabs, Ipswich, MA, USA), and ligated into the NdeI and BamHI restricted pET15b vector (Merck, Darmstadt, Germany). Correct sequences were confirmed by sequencing (SeqLab, Göttingen, Germany). The oligonucleotides are listed in Table S1 (13, 55).

**Recombinant expression and purification** – For recombinant protein expression, 400 ml medium containing the selective antibiotics were inoculated with 2% of an overnight culture of cells harboring the dedicated expression construct, and incubated at 37°C under agitation. At  $OD_{600} = 0.6$ , expression was induced by addition of 0.5 mM IPTG (isopropyl- $\beta$ -D-thiogalactopyranoside, Carl Roth, Kaiserslautern, Germany) and the temperature was lowered (to 20°C for Prxs, to 15°C for MICALs, or to 10°C for CRMP2). Cells were harvested after 18-24 hours by centrifugation at 1500 x g for 30 minutes at 4°C. Bacteria were lysed by incubation with lysis buffer for 20 minutes at room temperature and mild agitation, and subsequent ultrasonic treatment with 2 cycles of 2.5 minutes, 70% intensity, 0.5 s cycle time (50% cycling) using a Sonoplus HD2070 ultrasonic homogenizer (Bandelin, Berlin, Germany). Extracted lysate was clarified by centrifugation at 17000 x g for 30 minutes at 4°C. Recombinant His-tagged proteins were purified by immobilized metal affinity chromatography at 4°C using an Äkta FPLC system according to manufacturer's protocol (GE Healthcare, Buckinghamshire, UK).

Cells used for the expression: *E. coli* BL21 (DE3) pRIL (Life Technologies, Paisley, UK) strain was used for Prxs and CRMP2, *E. coli* Rosetta 2 (DE3) pLysS (Merck, Darmstadt, Germany) strain was used for MICALs. The following media were used: LB-Medium (Carl Roth, Kaiserslautern, Germany) for Prxs and CRMP2, SOC medium (2% (w/v) Bacto tryptone, 0.5% (w/v) Bacto yeast extract, 8.5 mM NaCl, 2.5 mM KCl, 10 mM MgCl<sub>2</sub>, 20 mM glucose, pH 7) for MICALs. Lysis buffers: 1 mg/ml lysozyme and 0.05 mg/ml DNase I in a 50 mM NaP buffer containing 140 mM NaCl, 20 mM Imidazole, pH 8 for Prxs and CRMP2, 1 mg/ml lysozyme, 0.05 mg/ml DNase I, 1 mM DTT, and 0.2% Tween 20 in a 50 mM Tris buffer containing 140 mM NaCl, 20 mM Imidazole, pH 8 for MICALs. The following buffers were used for the purification: 50 mM NaP, 300 mM NaCl, 20 mM Imidazole, pH 8, as washing buffer, and 50 mM NaP, 300 mM NaCl, 250 mM Imidazole, pH 8, as elution buffer for recombinant Prxs and CRMP2; for recombinant MICALs, a 50 mM Tris washing buffer containing 140 mM NaCl, 20 mM Imidazole, pH 8, and a 50 mM Tris elution buffer containing 140 mM NaCl, 300 mM Imidazole, pH 8, were used.

**Electrophoretic mobility shift assays** – Protein concentrations were determined using NanoDrop 2000c Spectrophotometer (VWR, Radnor, PA, USA), and calculated extinction coefficients (Prx1  $\epsilon_{280} = 18450 \text{ M}^{-1}\cdot\text{cm}^{-1}$ , Prx2  $\epsilon_{280} = 21430 \text{ M}^{-1}\cdot\text{cm}^{-1}$ , and MICALs-FAD  $\epsilon_{450} = 11300 \text{ M}^{-1}\cdot\text{cm}^{-1}$ ). Purified Prxs were incubated with 20 mM DTT (AppliChem, Darmstadt, Germany) and 10 mM TCEP pH 7 for 30 minutes at room temperature and mild agitation. Excess of reductants were removed by gel filtration using NAP5 columns according to manufacturer's instructions (GE Healthcare, Buckinghamshire, UK) in 50 mM Tris buffer, 100 mM NaCl, pH 8. The reaction was started by the addition of indicated FAD containing MICALs to the



reduced Prxs in presence of NADPH, and absence or presence of catalase, and stopped by denaturation with sample buffer. The reaction was performed at room temperature for 15 minutes, unless otherwise stated.

**Stopped-flow kinetics** – Purified MICAL1-MO and reduced Prxs were rebuffered in 50 mM Tris, 140 mM NaCl, pH 7.4 buffer using PD-10 or NAP5 columns, respectively, according to manufacturer's instructions (GE Healthcare, Buckinghamshire, UK). Flavin-containing MICAL concentration was determined at 450 nm in a Jasco instrument. The kinetics of flavin NADPH consumption, flavin reduction, as well as flavin oxidation, were measured in a stopped-flow spectrophotometer (SX20; Applied Photophysics, Leatherhead, UK) with a mixing time of less than 2 milliseconds. The NADPH consumption was analyzed following its absorbance at 340 nm, while the reduction of 10  $\mu$ M flavin was followed by the absorbance decrease at 450 nm in the presence of different NADPH concentrations at indicated temperature; upon flavin reduction with excess of NADPH for 20 minutes, flavin oxidation was analyzed following the absorbance increase at 450 nm after mixing with oxygenated buffer, in presence or absence of 40  $\mu$ M reduced Prx2. All data were collected and analyzed using the Pro-Data SX and Pro-Data Viewer software, respectively. Deviations of the second order rate constants for the MICAL-catalyzed reduction of  $O_2$  by NADPH and the oxidation of MICAL-FADH<sub>2</sub> by  $O_2$  were calculated as follows:

1.) For the MICAL-catalyzed reduction of  $O_2$  by NADPH with the following reaction:  $NADPH/H^+ + O_2 \leftrightarrow NADP^+ + H_2O_2$ , the reaction rate of can be expressed as:

$$(1) \quad \frac{\delta[NADPH]}{\delta t} = -k \cdot [NADPH] \cdot [O_2]$$

With the following substitutions,

$$(2) \quad x = [NADPH]_0 - [NADPH]_t = [O_2]_0 - [O_2]_t$$

the expression rate law becomes:

$$(3) \quad \Rightarrow -\frac{\delta x}{\delta t} = -k \cdot ([NADPH]_0 - x) \cdot ([O_2]_0 - x)$$

$$(4) \quad \Leftrightarrow \frac{\delta x}{([NADPH]_0 - x) \cdot ([O_2]_0 - x)} = k \cdot \delta t$$

Integration:

$$(5) \quad \Leftrightarrow \int_0^x \frac{\delta x}{([NADPH]_0 - x) \cdot ([O_2]_0 - x)} = k \cdot \int_0^t \delta t$$

Integration using the method of partial fractions:

$$(6) \quad \Rightarrow \frac{1}{[O_2]_0 - [NADPH]_0} \cdot \ln \frac{[NADPH]_0}{[NADPH]_0 - x} - \ln \frac{[O_2]_0}{[O_2]_0 - x} = k \cdot t$$

Rearrangement and re-substitution yields:

$$(7) \quad \Leftrightarrow \frac{1}{[O_2]_0 - [NADPH]_0} \cdot \ln \frac{[O_2]_t \cdot [NADPH]_0}{[NADPH]_t \cdot [O_2]_0} = k \cdot t$$

Upon re-arrangement, we obtain the linearized equation of the integrated second order kinetics:

$$(8) \quad \Leftrightarrow \ln \frac{[O_2]_t \cdot [NADPH]_0}{[NADPH]_t \cdot [O_2]_0} = k \cdot [O_2]_0 - [NADPH]_0 \cdot t$$

In practice,  $[NADPH]_0$  was given and controlled based on its molar absorptivity at 340 nm;  $[NADPH]$  was calculated based on its molar absorptivity at 340 nm;  $[O_2]_0$  was determined experimentally based on the

maximal NADPH consumption in the assay mixture; and  $[O_2]$  was calculated as  $[O_2]_0 - [NADPH]_0 + [NADPH]$ .

2.) For the oxidation of MICAL-FADH<sub>2</sub> by O<sub>2</sub> with the following reaction: M-FADH<sub>2</sub> + O<sub>2</sub> ↔ M-FAD + H<sub>2</sub>O<sub>2</sub>, the reaction rate can be expressed as:

$$(1) \quad \frac{\delta[FADH_2]}{\delta t} = -k \cdot [FADH_2] \cdot [O_2]$$

With the following substitutions,

$$(2) \quad x = [FADH_2]_0 - [FADH_2]_t = [O_2]_0 - [O_2]_t$$

the expression rate law becomes:

$$(3) \quad \Rightarrow -\frac{\delta x}{\delta t} = -k \cdot ([FADH_2]_0 - x) \cdot ([O_2]_0 - x)$$

$$(4) \quad \Leftrightarrow \frac{\delta x}{([FADH_2]_0 - x) \cdot ([O_2]_0 - x)} = k \cdot \delta t$$

Integration:

$$(5) \quad \Leftrightarrow \int_0^x \frac{\delta x}{([FADH_2]_0 - x) \cdot ([O_2]_0 - x)} = k \cdot \int_0^t \delta t$$

Integration using the method of partial fractions:

$$(6) \quad \Rightarrow \frac{1}{[O_2]_0 - [FADH_2]_0} \cdot \ln \frac{[FADH_2]_0}{[FADH_2]_0 - x} - \ln \frac{[O_2]_0}{[O_2]_0 - x} = k \cdot t$$

Rearrangement and re-substitution yields:

$$(7) \quad \Leftrightarrow \frac{1}{[O_2]_0 - [FADH_2]_0} \cdot \ln \frac{[O_2]_t \cdot [FADH_2]_0}{[FADH_2]_t \cdot [O_2]_0} = k \cdot t$$

Upon re-arrangement, we obtain the linearized equation of the integrated second order kinetics:

$$(8) \quad \Leftrightarrow \ln \frac{[O_2]_t \cdot [FADH_2]_0}{[FADH_2]_t \cdot [O_2]_0} = k \cdot [O_2]_0 - [FADH_2]_0 \cdot t$$

In practice,  $[FADH_2]_0$  was given and controlled based on the maximal conversion to FAD in the assay mixture;  $[FADH_2]$  was calculated based on its molar absorptivity at 450 nm;  $[O_2]_0$  was determined experimentally based on the maximal NADPH consumption in the assay mixture in control experiments; and  $[O_2]$  was calculated as  $[O_2]_0 - [FADH_2]_0 + [FADH_2]$ .

**Molecular Dynamics Simulations** – The starting structure for the molecular dynamics simulation of the MICAL1-Prx1 complex was prepared using HawkDock (56). The human MICAL1 and Prx1 models were prepared by homology modeling using pdb entries 6ici and 5hqp, respectively. The simulations were performed in GROMACS 2016.3 (57), with AMBER-99ff-ILDN force field (58). The parametrization of FAD was done with ACPYPE (59) script. The protein structure was solvated with TIP3P water in a cubic box under periodic boundary conditions and at least 1 nm away from the edge of the box. Na<sup>+</sup> and Cl<sup>-</sup> ions were added to neutralize the charge of the system. An initial energy minimization was performed using steepest descent algorithm until the system converged to 1000 kJ·mol<sup>-1</sup>·nm<sup>-1</sup>. System equilibration was performed for 100 ps at a constant number of molecules, volume, and temperature 300 K (NVT) and for duration of 100 ps with constant number of molecules, 1 bar pressure, and temperature 300 K (NPT). The duration of the production simulation was 250 ns (125,000,000 time steps, 2 fs each). The bonded interactions of hydrogens were constrained with LINCS algorithm (60). The Parrinello-Rahman (61) method was used for pressure

coupling and the modified Berendsen thermostat – velocity rescale (62) for the temperature coupling. The Particle Mesh Ewald (63) method was used for the calculation of the long-range electrostatic interactions; for the short-range interactions, Verlet cut-off scheme with 1.5 nm cut-off distance was applied, for both Coulomb- and van-der-Waals interactions. The RMSD and RMSF analysis and calculation of solvent accessible surface area were performed with GROMACS. The representative structure of the simulation was calculated with the linkage algorithm of cluster tool in GROMACS with the distance cut-off of 0.2 nm. The further evaluation including the calculation of the surface of the representative structure was performed in UCSF Chimera (64).

**Cell culturing** – DMEM, serum (FCS), antibiotics (penicillin, streptomycin), trypsin, and PBS were purchased from PAN-Biotech (Aidenbach, Germany), disposable plastics from Sarstedt (Nümbrecht, Germany), and culture flasks from Greiner (Merck, Darmstadt, Germany). HeLa cells were propagated in Dulbecco modified Eagle Medium (DMEM) with 1 g/l glucose, SH-SY5Y cells in HyClone MEM medium with Earle's Balanced Salt Solution (EBSS) and 2 mM L-Glutamine (GE Healthcare, Buckinghamshire, UK) each supplemented with 10% (v/v) FCS, 100 units/ml penicillin, and 0.1 mg/ml streptomycin at 37°C.

**Affinity capture assay** – Purified recombinant CRMP2 was coupled to a cyano-bromid (CNBr)-activated sepharose 4B matrix using coupling buffer (0.1 M NaHCO<sub>3</sub>, 0.5 M NaCl, pH 8.3) according to manufacturer's instructions (GE Healthcare, Buckinghamshire, UK). Immobilized CRMP2 was either oxidized (1 mM H<sub>2</sub>O<sub>2</sub>) or reduced (5 mM pH-neutralized TCEP) for 30 minutes at room temperature and agitation prior to the incubation with lysates of HeLa WT or HeLa Grx2c<sup>+</sup> (15) cells, respectively (cells were harvested, washed once with PBS and lysed for 20 minutes at room temperature. Lysis buffer: 50 mM Tris, 150 mM NaCl, 1% (w/v) CHAPS, pH 7.5, 1-fold protease and phosphatase inhibitor mixture (Roche Applied Science, Mannheim, Germany)). After 12-16 hours incubation, unbound proteins were removed by washing followed by elution of bound proteins first under denaturing (100 mM acetic acid, pH 2.1) and second under reducing (10 mM pH-neutralized TCEP) conditions. The input, flow-through and eluates were subjected to SDS-PAGE and Western blot analysis.

**Transient transfection** – Cells were transiently transfected with 15 µg specific, custom-made siRNA (Eurogentech, Seraing, Belgium) against MICAL1, Prx1, CRMP2 and an unspecific control (see Table S2). 5·10<sup>6</sup> SH-SY5Y cells were resuspended with the required siRNA in electroporation buffer (21 mM HEPES, 137 mM NaCl, 5 mM KCl, 0.7 mM Na<sub>2</sub>HPO<sub>4</sub>, 6 mM D-glucose, pH 7.15) (65, 66). Transfections were performed using the BTX ECM 630 electroporator at 230 V, 1050 µF, 500 Ω. SH-SY5Y cells were transfected three times, 72 hours apart each. 72 hours after the last transfection, cells were harvested, washed with PBS containing 100 mM N-ethyl maleimide (NEM, Thermo Scientific, Weltham, MA, USA), and lysed (40 mM HEPES, 50 mM NaCl, 1 mM EDTA, 1 mM EGTA, 100 mM NEM, 2% (w/v) CHAPS, 1-fold protease inhibitor mixture (Roche Applied Science, Mannheim, Germany)) for 20 minutes at room temperature.

**Semaphorin treatment** – SH-SY5Y cells were treated with 1 µg/ml recombinant human Semaphorin 3A Fc Chimera Protein (Bio-Techne, Minneapolis, MN, USA) for indicated times. Treatment was stopped by harvesting, washing and lysis of the cells as indicated above.

**Retinoic acid treatment** – To initiate the differentiation into a neuron-like phenotype, SH-SY5Y cells were treated with 10 µM retinoic acid (AppliChem, Darmstadt, Germany) solved in dimethyl sulfoxide (AppliChem, Darmstadt, Germany) for 120 hours, unless otherwise stated. Culturing medium containing retinoic acid was replaced every 48 hours.

**Neurite outgrowth analysis** – Bright field microscopy (EVOS XL core microscope, AMG, Mill Creek, WA, USA) pictures were taken 72 hours after the last transfection of specific siRNA and indicated time of retinoic acid treatment. Analysis of the neurites length was performed using the dendrite length quantifier plug in of ImageJ (67) and plotted with xmGrace.

**Table S1 – Oligonucleotides used for the cloning of expression vectors**

Target mRNA	Oligonucleotides (forward and reverse)
MICAL1-MO 1-485	5'-CACACACATATGGCTTCACCTACCTCCACCAAC 5'-GTGTGTAGATCTCTACACATCATAACAGGTCTCGTACCTGATTGG
MICAL2-MO 1-505	5'-CACACACATATGGGGGAAAACGAGGATGAG 5'-GTGTGTAGATCTCTACACATCATAACAGGTCTCGTACCTGATTGG
MICAL3-MO 1-490	5'-CACACATATGATGGAGGAGAGGAAGCATGAGACCATGAACCC 5'-GTGTAGATCTCTAAGTATCATATAAATGGCGCACCTGGCTTGGCC
MICAL1-MO-CH 1-616	5'-CACACACATATGGCTTCACCTACCTCCACCAAC 5'-GTGTAGATCTCTAGTGGGCCATGCTCTTGAAGGC

**Table S2 – siRNA sequences**

siRNA target	siRNA (sense/antisense)
siMICAL1	5'-CCAUCCAACGGCGACUAAA 5'-UUUAGUCGCCGUUGGAUGG
siPrx1	5'-GGCUGAUGAAGGCAUCUCG 5'-CGAGAUGCCUUCAUCAGCC
siCRMP2	5'-GAACCACUAUGAUCAUUGA 5'-UCAAUGAUCAUAGUGGUUC
siControl	5'-CAUUCACUCAGGUCAUCAG 5'-CUGAUGACCUGAGUGAAUG

### Figure S1 – Quantification of MICAL-bound and liberated FAD

The absorbance spectra of the freshly purified  $28.3 \mu\text{mol}\cdot\text{l}^{-1}$  MICAL1-MO domain (black) and FAD after denaturation of the protein with 0.2% SDS (red). The inset displays the linear dependence of the absorbance at 450 nm of the concentration for both non-treated and 0.2% SDS treated free FAD.

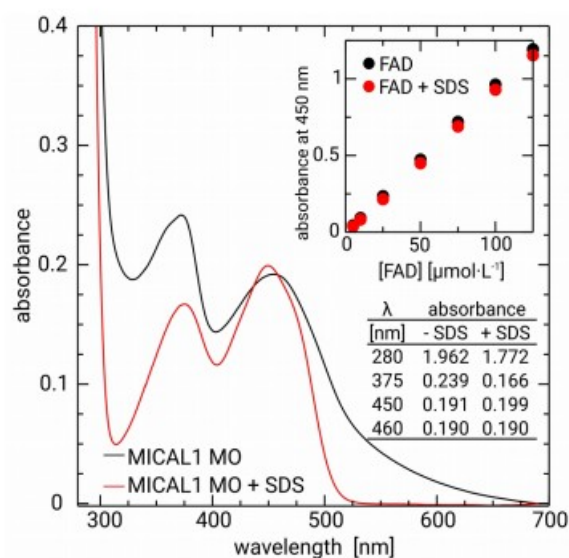


### Figure S2 – MICALs do not directly oxidize CRMP2 in vitro

Oxidation of CRMP2 by MICAL-MO was followed by the formation of the inter-molecular disulfide between two CRMP2 monomers, see refs. (6, 13). As for the Prxs, the reaction was measured in the absence and presence of catalase. The first lane contained pre-reduced CRMP2, the second pre-oxidized CRMP2. The reaction was performed in the presence of  $150 \mu\text{mol}\cdot\text{l}^{-1}$  NADPH. As depicted, the MICAL-MO could not oxidize the regulatory CRMP2 disulfide.

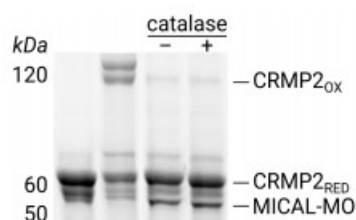


**Figure S3 – Reduction of the FAD in MICAL1-MO by NADPH; O<sub>2</sub> quantification in the assay solution**

10  $\mu\text{M}$  MICAL1-MO were incubated with excess NADPH over a time frame of 6 minutes. The reduction of the FAD was followed by the decrease in absorbance at 450 nm. **(A)** Reduction of 10  $\mu\text{mol}\cdot\text{l}^{-1}$  FAD in the MICAL1-MO domain by 400  $\mu\text{mol}\cdot\text{l}^{-1}$  NADPH at pH 7.4 and 298 K over a time course of 6 minutes analyzed by UV-Vis spectroscopy. **(B)** NADPH-dependent reduction of 10  $\mu\text{mol}\cdot\text{l}^{-1}$  MICAL bound FAD at pH 7.4 and 298 K followed by UV-Vis spectroscopy at 450 nm. **(C)** Linearized integrated second order kinetics of the data displayed in (B) for the determination of the apparent second order rate constant (detailed information for the calculations, see material and methods). This analysis was also used to quantify the amount of molecular oxygen dissolved in the reaction solutions from the amount of NADPH consumed for the full reduction of MICAL-MO in the nitrogen atmosphere of the stopped-flow instrument. The lag phase in (B) and (C) was the time before all oxygen in the assay solution was consumed.

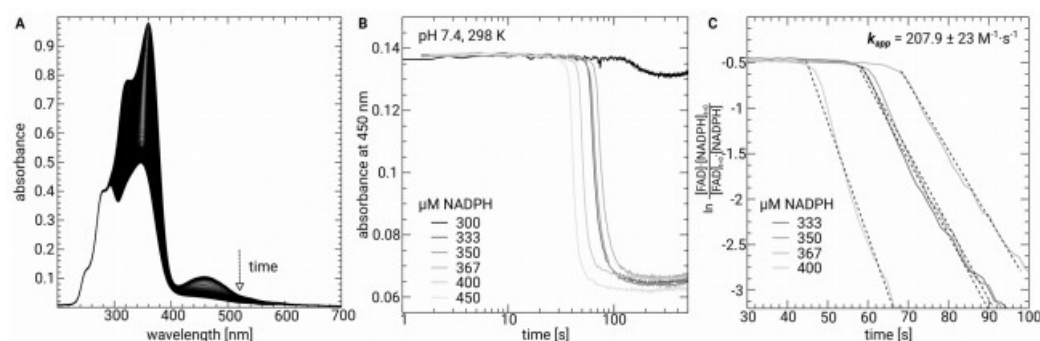


### Figure S4 – Proposed reaction mechanism of the MICAL1-catalyzed Prx1 oxidation

After reduction of the FAD by NADPH at  $2.1 \cdot 10^2 \text{ M}^{-1} \cdot \text{s}^{-1}$ , an unstable peroxy-flavin intermediate is formed at  $\geq 1.9 \cdot 10^5 \text{ M}^{-1} \cdot \text{s}^{-1}$ , that immediately decays to oxidized FAD and  $\text{H}_2\text{O}_2$ . This  $\text{H}_2\text{O}_2$ , however, is not released but directly channelled to one of the peroxidatic cysteinyl residue ( $\text{C}_\text{P}$ ) of a bound Prx dimer. The resulting sulfenic acid is attacked by the resolving cysteinyl residue ( $\text{C}_\text{R}$ ) leading to the inter-molecular disulfide between two Prx monomers.

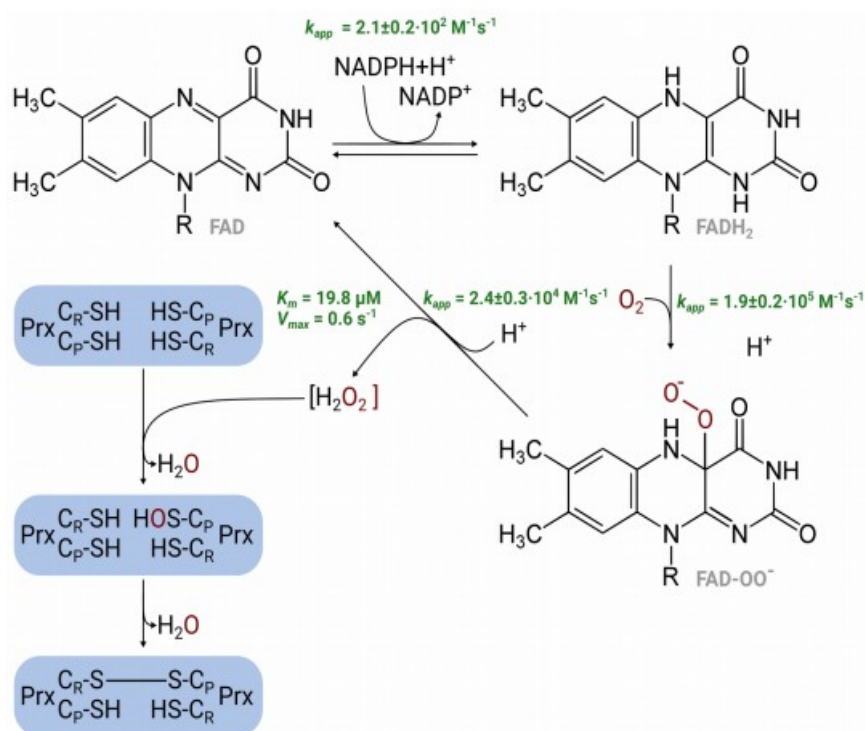




### Figure S5 – Time course of the oxidation of the Prxs by catalytic amounts of MICAL(1-3)-MO

Purified Prxs were pre-reduced with DTT and TCEP; excess of reductants were removed by gel filtration chromatography. The reaction was started by the addition of MICALs in presence of NADPH and catalase, and stopped by denaturation of all proteins with sample buffer. The reaction mixtures were analyzed by SDS-PAGE. Oxidation of Prxs was quantified from the densitometric analyses of the monomeric (reduced) and dimeric (oxidized) bands at 45 kDa with one (upper band) or two (lower band) disulfides. Oxidation of Prx1 and Prx2 by MICALs-MO over 15 minutes, n1 (left panel) and n2 (right panel).

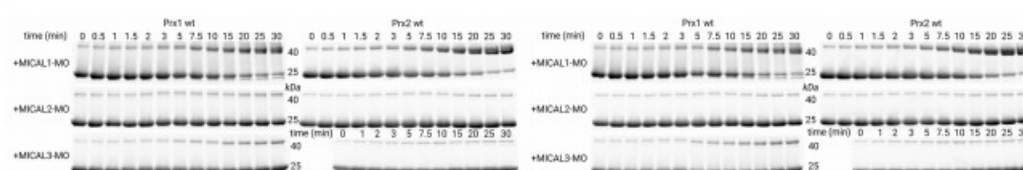


### Figure S6 – Oxidation of Prxs by catalytic amounts of MICAL1-MO and MICAL1-MO-CH.

Purified Prxs were pre-reduced with DTT and TCEP; excess of reductants were removed by gel filtration chromatography. The reaction was started by the addition of MICAL1-MO (A) or MICAL1-MO-CH (B) to the reduced Prxs in presence of NADPH and catalase, and stopped by denaturation of all proteins with sample buffer. The reaction mixtures were analyzed by SDS-PAGE. Oxidation of Prxs was quantified from the densitometric analyses of the monomeric (reduced) and dimeric (oxidized) bands at 45 kDa with one (upper band) or two (lower band) disulfides. For more details on the MICAL domain structures, see ref. (31).

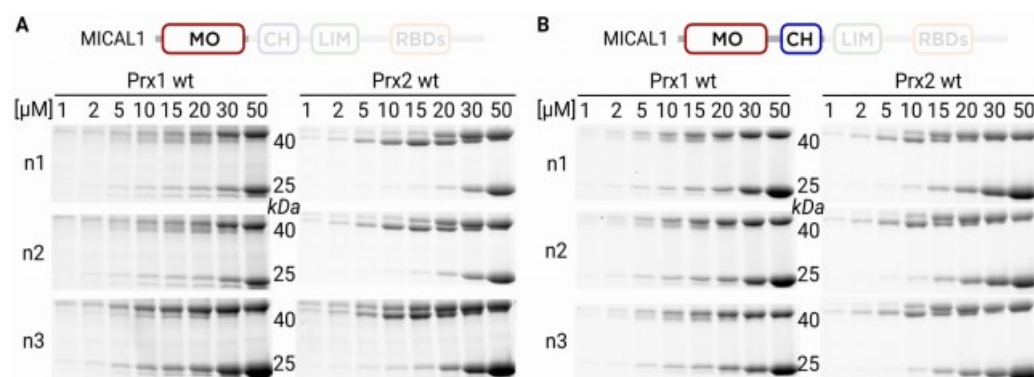


### Figure S7 – Principle of the diagonal electrophoresis

Principle (left) and example (right) for the 2D-diagonal electrophoresis. The first dimension SDS PAGE is performed under non-reducing conditions, the second under reducing conditions. Oxidized proteins may be shifted from the diagonal in two ways. Inter-molecular disulfides, such as in the reaction mechanism of the Prxs, drop from the diagonal down to their normal molecular weight. Proteins harboring intra-molecular disulfides may remain on the diagonal or slightly shift to the side.

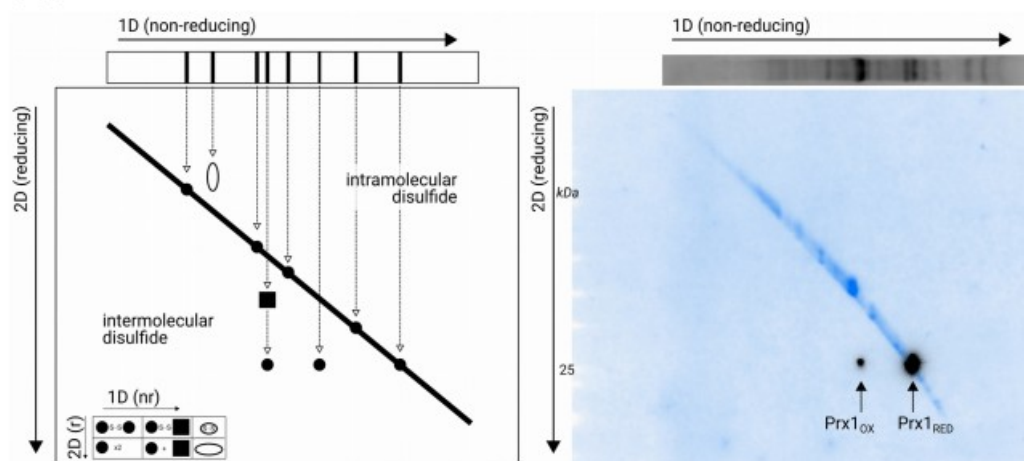
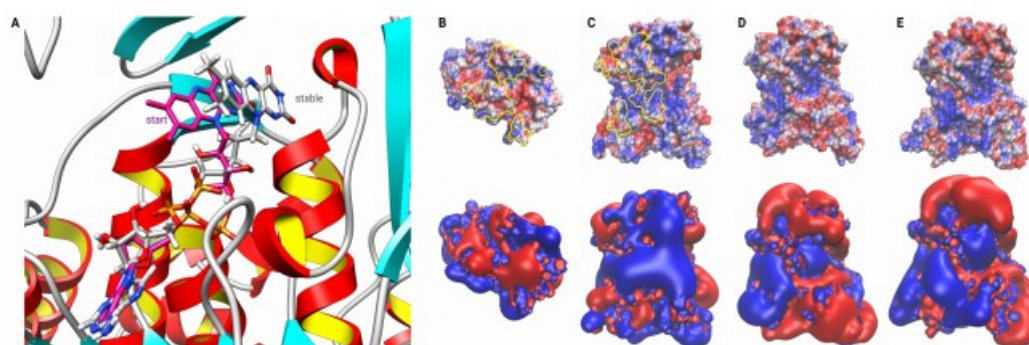


### Figure S8 – Further structural insights into the MICAL-Prx interactions

(A) Position of the FAD at the start of the MD simulation (pink) and the stable conformation over the time course of the simulation (gray, colored by element). (B-E) Electrostatic properties of Prx1 (B) and MICAL1-MO (C) in the area of contacts (circled by yellow lines, see Fig. 4 in the main text). The properties of MICAL2-MO (D) and MICAL3-MO (E) were added for comparison. The pictures show the isosurfaces of the electrostatic potential at +/- 25 mV, see ref. (46) for further details.



## 8 Declaration of originality

I hereby declare that I have submitted this work, so far, neither at the Faculty of Mathematics and Natural sciences at the University of Greifswald nor at any other university with the purpose to earn a PhD degree.

Furthermore I declare that I have written this work as an independent effort and did not use any other sources and guides than those cited in the work. I did not copy any paragraphs of a third author without marking them as citation.

## Eigenständigkeitserklärung

Hiermit erkläre ich, dass diese Arbeit bisher von mir weder an der Mathematisch-Naturwissenschaftlichen Fakultät der Universität Greifswald noch einer anderen wissenschaftlichen Einrichtung zum Zwecke der Promotion eingereicht wurde.

Ferner erkläre ich, dass ich diese Arbeit selbständig verfasst und keine anderen als die darin angegebenen Hilfsmittel und Hilfen benutzt und keine Textabschnitte eines Dritten ohne Kennzeichnung übernommen habe.

## 9 Curriculum vitae

---

### Personal information

Name Clara Ortegón Salas  
 Place of birth Jerez de la Frontera, Spain  
 Date of birth 03.12.1989  
 Contact (+34)651146752  
 clara.ortegon89@gmail.com

---

### Education

10/2017 – current PhD thesis: Receptor-induced redox relay reactions control cytoskeletal dynamics  
 Thesis supervisors: Prof. Dr. Christiane A. Helm, from the Institute of Physics, University of Greifswald, Germany, and PD Dr. Dr. Christopher Horst Lillig, from the Institute of Medical Biochemistry and Molecular Biology, University Medicine Greifswald, Germany  
 10/2013 – 09/2014 ERASMUS scholarship – MSc Molecular Life Science  
 Humboldt Universität zu Berlin, Germany  
 09/2012 – 07/2014 Lic. Biochemistry (equivalent to MSc)  
 Universidad Complutense de Madrid, Spain  
 09/2007 – 07/2012 Lic. Pharmacy (equivalent to BSc and MSc)  
 Universidad Complutense de Madrid, Madrid, Spain  
 09/2005 – 06/2007 Upper Secondary Education  
 Ntra. Sra. del Pilar, Jerez de la Frontera, Spain

---

### Work experience

06/2015 – 06/2016 Research assistant at Pensatech Pharma GmbH, Berlin, Germany  
 04/2014 – 07/2014 Internship at Max-Delbrück Center for Molecular Medicine, Berlin, Germany. Research Team: Molecular muscle physiology  
 Head of the group: Prof. Dr. Ingo Morano  
 06/2013 – 09/2013 Pharmacist at Paz Sánchez Pharmacy's, Madrid, Spain  
 02/2012 – 05/2012 Internship at Paz Sánchez Pharmacy's, Madrid, Spain

---

### Languages

Spanish (mother tongue)  
 English (fluent)  
 German (advanced)

---

---

<b>Skills</b>	Experience in cell culture, basis of protein biochemistry and molecular biology, <i>e.g.</i> electrophoresis, Western Blot, spectrophotometers, cloning, mutagenesis, RT-qPCR, FPLC, enzyme kinetics, as well as bacteriological techniques including recombinant protein expression. Analysis of redox-regulated proteins FELASA category B certification Supervision of Bachelor and Master students' theses
---------------	--

---

<b>Distinctions</b>	
03/2021	Grant for a start-up funding of a junior research project from the Community Medicine and Molecular Medicine (FVMM), University Medicine Greifswald
09/2019	Research project: Regulation of ferroptosis by FeS glutaredoxins Invitation from the Associate Editors of Biochemical Society Transactions to contribute a review article for the Biochemical Society journal
06/2019	Award to the best elevator talk at the international conference "Redox signalling in physiology, ageing and disease", Newcastle, UK
05/2019	Travel grant from the Research Association Molecular Medicine of the University Medicine Greifswald
03/2019	Award to the best poster at the international conference "Dynamics of Thiol-based Redox Switches in Cellular Physiology", Rauschholzhausen, Germany
11/2015	Award with Special Distinction in Lic. Biochemistry
11/2014	Award to the best academic record of Lic. Biochemistry
04/2013	Award to the best oral communication at the Complutense national conference, Madrid, Spain

---

**Publications**

1. Hossain MD, Bodnar Y, Klein K, Ortegón Salas C, Arnér ESJ, Gellert M, Lillig CH. Molecular basis for the interactions of human thioredoxins with their respective reductases. *Oxid Med Cell Longev* (2021). doi: [10.1155/2021/6621292](https://doi.org/10.1155/2021/6621292)

2. Ortegón Salas C, Gellert M, Lillig CH. Redox regulation of cytoskeletal dynamics. Chapter in book Redox regulation of differentiation and de-differentiation. CRC Press Taylor & Francis Group, in press (2021) ISBN 9780367895662
3. Ortegón Salas C, Knaup LK, Schneider K, Scharf C, Berndt C, Deponte M, Lillig CH, Gellert M. Receptor-induced Redox Signalling Relay - From Signal to Effector. *Free Radical Biology and Medicine*, 159 (1), S118 (2020). doi: [10.1016/j.freeradbiomed.2020.10.298](https://doi.org/10.1016/j.freeradbiomed.2020.10.298)
4. Ortegón Salas C, Schneider K, Lillig CH, Gellert M. Signal-regulated oxidation of proteins via MICAL. *Biochem Soc Trans* (2020). doi: [10.1042/BST20190866](https://doi.org/10.1042/BST20190866)
5. García Hernández M, Ortegón Salas C, Oset Gasque MJ. Protein etiology of Alzheimer's disease. *Reduca*, 6 (1), 312-316 (2014). [reduca/article1719/1736](https://reduca/article1719/1736)

## 10 Acknowledgments

I would like to express my sincere gratitude to Christopher Horst Lillig and Manuela Gellert, without your support this work wouldn't have been possible. Horst, your email was the fresh air I was missing for quite a long time. For taking me on board, for your trust, your encouragement, your leadership and supervision, your craziness, your German and Latin words... thanks for everything. I learned a lot and had so much fun in your group. Manu, you were the first person I met in Greifswald. I didn't know where I had to go. You just came to pick me up and drove me to the right place. And ever since you have done the same thing during my PhD thesis. Thanks for being always there, even in the middle of the night in some very old university building in Kaiserslautern. I'd also like to thank all former and current members from Lillig's group that I met during this time: Faruq, Daggi, Daniel, Claudia, Laura, Michel, Calvin, Katha, Willy, Lara, Yana, Tim, Tom, the other Tom, Anastasia, Hannah... Some of you might have made my days a bit longer and/or harder, but still, thanks for the great working atmosphere, the laughs, and the most important, the food. To my project ancestors, hats off. I don't know all of you, but your input allowed the project to turn into this thesis.

I also want to acknowledge Prof. Dr. Elke Krüger and Prof. Dr. Uwe Lendeckel for giving me the opportunity to be part of the Institute of Medical Biochemistry and Molecular Biology. Thanks for the help and discussions to all other members of the institute. Especially to Elmer, thanks a lot for our relieving chats, your jokes and your good advice.

Many thanks to Prof. Dr. Christiane Helm. I appreciate your help as co-supervisor as well as speaker of the RTG1947, where you have organized many valuable workshops and seminars. At this point I would also like to thank all members from the RTG1947. As part of this program, this thesis was financially supported by the German Research Foundation (DFG).

To my collaborators, Carsten Berndt, Marcel Deponte, Elias Arnér, Markus Schwarzländer, Christian Scharf, Gereon Poschmann, thank you so much for the new ideas, discussions and time that you contributed to this work.

Finally, I want to thank my friends in Jerez and in Madrid, every moment spent with you has cheered me up. Above all, I must thank my parents and my brother. No words can ever be strong enough to express how grateful I am for your unconditional love and support. Thank you for always being there for me. Same to Fran, I can't think of any other better journey companion. This achievement is also yours. Thanks for never letting me down.